THE ANALYTICAL GEOCHEMISTRY OF PLATINUM GROUP METALS IN CRETACEOUS/TERTIARY BOUNDARY CLAYS

A Thesis Presented in Partial Fulfilment of the Requirements for the Degree of Doctor of Philosophy in Chemistry at Massey University

Shane Malcolm Wilson

1991

Massey University Library
Thesis Copyright Form

Title of thesis:

(1) (a) I give permission for my thesis to be made available to readers in Massey University Library under conditions determined by the Librarian.

(b) I do not wish my thesis to be made available to readers without my written consent for ... months.

(2) (a) I agree that my thesis, or a copy, may be sent to another institution under conditions determined by the Librarian.

(b) I do not wish my thesis, or a copy, to be sent to another institution without my written consent for ... months.

(3) (a) I agree that my thesis may be copied for Library use.

(b) I do not wish my thesis to be copied for Library use for ... months.

Signed Shane Wilson

Date 15/3/91

The copyright of this thesis belongs to the author. Readers must sign their name in the space below to show that they recognise this. They are asked to add their permanent address.

NAME AND ADDRESS DATE

ABSTRACT

The Cretaceous/Tertiary boundary controversy is discussed. The importance of the platinum group metals (PGM) as markers of extraterrestrial material in sediments is explained.

The use of inductively coupled plasma source mass spectroscopy (ICP-MS), and graphite furnace atomic absorption spectroscopy (GF-AAS), to determine PGM in geological materials, was investigated. Both techniques require the analyte to be substantially separated from the geological matrix before instrumental analysis is performed. Separation schemes involving fire-assay, ion exchange chromatography, solvent extraction, and coprecipitation, were investigated.

A standard ore (PTC-1) was successfully analysed for Rh and Pd using a separation scheme involving Te coprecipitation followed by dissolution and determination by ICP-MS. The same ore was successfully analysed for Pd using GF-AAS after a separation procedure involving solvent extraction of a Pd- ammonium pyrrolidine dithiocarbamate complex.

Sedimentary rock samples were collected from a newly discovered K/T boundary site (Flaxbourne River) in New Zealand. Determinations of Pd in Flaxbourne River sediments were made using GF-AAS after matrix separation using solvent extraction.

Elevated levels of Pd at the K/T boundary were found contiguous with elevated levels of Ir. Besides these PGM, a further twenty elements were determined in Flaxbourne River K/T boundary sediments. The results of this geochemical survey are discussed with respect to the impact and volcanism theories (theories which seek to explain the palaeontological, geochemical, and geological changes occurring at the K/T boundary).

ACKNOWLEDGEMENTS

I would like to express my gratitude to my supervisors, Professor R. R. Brooks and Doctor R. D. Reeves, for their advice, assistance, and encouragement during the course of this work. Also I must express my gratitude to my parents for their wonderful support over the years.

I acknowledge the receipt of a New Zealand University Grants Committee Scholarship.

Finally I would like to thank all the people I have worked with for their friendship and encouragement.

TABLE OF CONTENTS

Abstract		(i)
Acknowledgements		(ii)
Table of Contents		(iii)
List of Figures		(v)
List of Tables		(vi)

Chapter One Introduction

1.0	Meteorite Impacts	2
1.1	The Impact Theory	2
1.2	Size of the Impact	3
1.3	Environmental Effects	4
1.4	Criticisms of the Impact Theory	6
1.5	Elemental Impact Markers	6
1.6	Research Areas	8

Chapter Two Instrumental Techniques, Separation Techniques, and Materials

2.0	Atomic Absorption Spectroscopy	11
2.1	Inductively Coupled Plasma Atomic Emission Spectroscopy	29
2.2	Inductively Coupled Plasma Source Mass Spectrometry	29
2.3	Neutron Activation Analysis	30
2.4	Ultraviolet-Visible Molecular Absorption Spectroscopy	32
2.5	Solvent Extraction	32
2.6	Ion Exchange Chromatography	37
2.7	Materials	38

Chapter Three Investigation of Methods for the Separation of the Platinum Group Metals from a Geological Matrix

3.0	Nickel Sulphide Fire Assay/ICP-MS Determinations	41
3.1	Iodide Complex Anion Exchange	52
3.2	Solvent Extraction of a Rhodium Chelate Complex	58
3.3	The DDTU/MIBK Solvent Extraction System	62
3.4	The APDC/MIBK Solvent Extraction System	63

Chapter Four The Quantification of Palladium in Geological Materials

4.0	Introduction	69
4.1	Determination of Palladium in PTC-1	70
4.2	Palladium in the K/T Boundary	71
4.3	The Extractable Palladium Complex	74
4.4	Method Used to Quantify Palladium in Sediments	75

Chapter Five The Flaxbourne River K/T Boundary Sequence: A Case Study

5.0	Introduction	77
5.1	Site Location	77
5.2	Lithology	78
5.3	Biostratigraphy	82
5.4	Geochemistry	84
5.5	Conclusion	95

Final Discussion 97

List of References 100

Appendix One: Thermodynamic Derivation of the Distribution Law 110

Appendix Two: Limits of Detection (Theory) 111

Appendix Three: Abbreviations 115

Publications Arising from this Thesis 116

LIST OF FIGURES

2.0	AAS Processes	11
2.1	Hollow Cathode Lamp	12
2.2	Graphite Furnace and Electrodes	15
2.3	GBC System 1000 Workhead	16
2.4	A Typical Furnace Cycle	17
2.5	Absorption Signals (for Palladium)	17
2.6	Furnace/Probe Geometries for Palladium	18
2.7	Optimization of Hollow Cathode Lamp (Palladium Lamp) Current	19
2.8	Optimization of Atomisation Temperature (for Palladium)	22
2.9	Calibration Curve for the Determination of Palladium in MIBK by GF-AAS	22
2.10	Optimization of Atomisation Temperature (for Rhodium)	26
2.11	Calibration Curve for the Determination of Rhodium in HCl by GF-AAS	26
2.12	Absorption Signals (for Rhodium)	27
2.13	Diagram of an ICP Mass Spectrometer	30
2.14	Detection Limits for Elemental Determinations by ICP-MS	31
3.0	Fire Assay Pots	44
3.1	Moulding an Assay Pot	44
3.2	Distillation Apparatus	50
3.3	Molecular Absorption Spectrum	53
3.4	Calibration Curve for the Determination of Ruthenium in Chloroform	53
3.5	Curves for the Elution of PTC-1 Constituents from Anion Exchange Resin	55
3.6	Optimization of Acid Concentration for Rhodium Extraction	59
3.7	Curves for the Extraction of PGM Complexes into MIBK	65
4.0	Effect of APDC Levels on Extraction	70
5.0	Location Map Showing the Flaxbourne River K/T Boundary Site in Relation to Other Sites in the Area	78
5.1	The Flaxbourne River K/T Boundary Section	79
5.2	The Boundary Clay and Surrounding Sediments	79
5.3	The Stratigraphic Column	81
5.4	Analytical Scheme for The Determination of Iridium by Neutron Activation Analysis	86

5.5 Iridium and Palladium Abundances in the Vicinity of the K/T Boundary 88
5.6 Mean Elemental Abundances in Lithological Units of the Flaxbourne River K/T Boundary Sequence 89
5.7 Chondrite Factors for Eight Elements in boundary Clays and Volcanic Emissions 91

LIST OF TABLES

1.0 Asteriod Impact Environmental Stresses 5
1.1 Arguments Against and in Defense of the Impact Theory 7
2.0 Heating Cycle Conditions for MIBK 20
2.1 Heating Cycle Conditions for Aqueous Solutions 21
2.2 Palladium Standard-Solution Absorbances 23
2.3 Rhodium Standard-Solution Absorbances 28
3.0 Replicate Determinations of Platinum and Palladium in PTC-1 by GF-AAS 57
3.1 Distribution Coefficients for the Extraction of Rhodium (3+), Palladium (2+), and Platinum (4+) from HCl Solutions into a DDTU/MIBK Solution 63
3.2 Values of K_D for the Extraction of PGM Ions into MIBK from Acid Solutions 66
4.0 Palladium Abundances Across the Flaxbourne River Sequence 72
4.1 Boundary Clay Iridium and Palladium Abundances 73
5.0 Biostratigraphic Zones Resolved From the Flaxbourne River K/T Boundary Sequence 83
5.1 Elemental Abundances at the Flaxbourne River K/T Boundary Sequence 87
5.2 Elements Enriched at the K/T Boundary: Abundances (decalcified basis) and Ratios 92
5.3 Mass Balance for the chalcophiles in the Flaxbourne River K/T Boundary Clay 93

CHAPTER ONE

INTRODUCTION

1.0 METEORITE IMPACTS

Both the Earth and its moon have been subjected to repeated bombardment during the course of geological history. The Moon's heavily cratered surface bears testament to this. The relative paucity of detectable terrestrial impact features is due to tectonic erasure and weathering. So, although the Earth is over 4,000 million years old, only 5% of its visible impact features are older than 600 million years [1].

The frequency of impacts decreases with increasing size of impacting objects [2]. So, while small objects hit the Earth every day, impacts involving objects with diameters of greater than 10 km occur only every 100 million years or so, on average [3].

Until 1980 little study had been made of the effects very large impacts would have on the global biosphere. In that year Alvarez *et al* published their benchmark paper suggesting the Cretaceous geological period had been terminated by a large asteroid impact [4].

1.1 THE IMPACT THEORY

The boundary between the Cretaceous and Tertiary geological periods can be identified in the sedimentary record by the rapid disappearance of typical Cretaceous fossils followed by the appearance of typical Tertiary forms. The precise palaeontological boundary usually corresponds to a clay layer almost devoid of fossils [3]. Alvarez *et al* suggested that the extinctions occurring at the boundary resulted from environmental stresses caused by a large asteroid impact [4]. This idea is the basis for what has become known as the 'impact theory'. The authors also concluded that the distinctive boundary layer consists mainly of impact ejecta [4].

The impact theory was proposed after the discovery of anomalously high levels of Ir in Cretaceous/Tertiary (K/T) boundary sites in Italy, Denmark, and New Zealand [5][4]. This element is found in much higher levels in meteorites than in terrestrial rocks [6]. Since 1980, anomalous Ir concentrations have been found in K/T boundary sediments from over 80 sites world-wide.

Public interest in the impact theory has focussed on the extinction of the dinosaurs, this being due to the exotic nature of those creatures. However, their contribution to the total biomass mortality was tiny. About 70% of all lifeforms perished in the K/T holocaust [7].

1.2 SIZE OF THE IMPACT

Simple calculations can be performed to obtain an estimate for the size of the proposed asteroid, and the energy involved in the impact explosion.

1.2 (a) The Asteroid Diameter

Studies of K/T boundary materials indicate that about $1x10^{-7}$ g of Ir was deposited for every square centimetre of the Earths surface [8]. The surface area of the globe is about $5x10^{18}$ cm^2 [9]. Therefore the mass of Ir deposited at the boundary (M_{Ir}) is given by:

$$M_{Ir} = (1x10^{-7}\ g/cm^2)\ x\ (5x10^{18}\ cm^2) = 5x10^{11}\ g$$

If the proposed asteroid were a C1 chondrite (i.e. undifferentiated solar system material), its Ir content would have been about $0.5x10^{-6}$ g/g, and its density would have been about 2.2 g/cm^3 [4]. Assuming all the asteroid's Ir was deposited at the boundary, the total mass (M_{ast}) of the asteroid is given by :

$$M_{ast} = \frac{5x10^{11}\ g}{0.5x10^{-6}\ g/g} = 1x10^{18}\ g$$

Therefore the the volume of the asteroid (V_{ast}) is given by:

$$V_{ast} = \frac{1x10^{18}\ g}{2.2\ g/cm3} = 5x10^{17}\ cm^3$$

For a spherical asteroid, the diameter (D_{ast}) is given by:

$$D_{ast} = \sqrt[3]{\frac{6\ x.V_{ast}}{\pi}} = \sqrt[3]{\frac{6\ x\ (5x10^{17}\ cm^3)}{\pi}}$$

$$= 1x10^6\ cm = \underline{10\ km}$$

1.2 (b) Impact Energy Yield

Assuming the proposed impactor had the mass of $1x10^{15}$ kg derived above, and had a typical velocity of $2.5x10^4$ m/s [10], its kinetic energy (E_{ast}) would be given by:

$$E_{ast} = 0.5 \times (1x10^{15} \text{ kg}) \times (2.5x10^4 \text{ m/s})^2 = \underline{3x10^{23}} \text{ J}$$

This energy is available to be released into the terrestrial environment on impact. A one megaton T.N.T. detonation releases $4.2x10^{15}$ J of energy [10]. So, a $3x10^{23}$ J impact explosion would be equivalent to the detonation of about $7x10^7$ megaTons of T.N.T. explosive. This is around 10^4 times greater than the combined energy yield of the world's nuclear arsenals [3].

1.3 ENVIRONMENTAL EFFECTS

As most of the ejected impact material would not reach escape velocity [11], the impact energy would be largely retained by the terrestrial environment. Of course, some of the energy would be lost to space as electromagnetic radiation.

1.3 (a) Atmosphere, Hydrosphere, and Geosphere Effects

Impact energy coupled to the atmosphere would overcome activation energy barriers and allow the formation of nitrogen oxides from O_2 and relatively inert N_2 [12]. Also, winds of up to 500 km/h would be generated [13].

There is a 70% probability the asteroid would have struck the ocean. If so, an enormous quantity of seawater would have been vaporised, adding water to the atmosphere [13]. Tsunamis would have flooded coastal areas [13]. The asteroid would penetrate the ocean floor leaving a crater of 100 to 150 km in diameter [13]. Vaporised rock would be expelled and lead to the formation of fine dust

particles in the stratosphere [13]. Under the ocean basins the Earth's crust is quite thin, perhaps allowing the asteroid to penetrate the crust, thereby causing volcanic activity [14].

A continental impact would generate impact dust in a similar manner to a marine impact. Wolbach *et al* suggested a continental impact would be more likely to cause world-wide wildfires [15].

1.3 (b) Biosphere Effects

The influx of $>10^{23}$ J of impact energy into the terrestrial environment would be catastrophic for the biosphere. Wolbach *et al* mentioned twelve impact-imposed environmental stresses that could disturb the biosphere. Table 1.0 lists these stresses

TABLE 1.0 ASTEROID IMPACT ENVIRONMENTAL STRESSES

STRESS	TIME SCALE	REFERENCE
Tsunamis	Hours	[13] [16]
Winds (500 km/h)	Hours	[13]
Cold	Months	[4] [17]
Darkness	Months	[4] [17]
Fires	Months	[18] [19]
H_2O-Greenhouse	Months	[13]
Acid Rain	Years	[12]
Pyrotoxins	Years	[20] [18]
CO_2-Greenhouse	Decades	[21] [22]
Destruction of Ozone Layer	Decades	[12] [23]
Impact-Triggered Volcanism	Millenia?	[14]
Mutagens	Millenia	[24]

Dust ejected into the stratosphere by a $>10^{23}$ J impact would block out sunlight. This would cause the cessation of photosynthesis and extreme cold. Enormous quantities of HNO_3 would be created from the nitrogen oxides formed in the impact blast [12]. The resulting decrease in the marine pH would dissolve carbonates in sediments, and in the shells of marine animals [12]. This would add CO_2 to the atmosphere. The 500 km/h winds would flatten the Earth's forests and effectively freeze-dry the remains [13]. These remains could be set

alight by electrical storms generated by static electricity build-up in the dust clouds, resulting in world-wide wildfires [15]. Such a conflagration would add substantial amounts of CO_2 to the atmosphere.

The cessation of photosynthesis would disrupt food chains and therefore affect all life on Earth. The extreme cold of the dust-induced winter would kill species not suitably adapted. This period may have been followed by an impact-induced swelter; water vapour from a marine impact, and CO_2 emissions, would cause greenhouse warming [13] [21]. High NO levels in the stratosphere would affect the ozone layer [12]. Wildfires would generate chemicals (pyrotoxins) which are harmful to biota [20]. A sub-class of the pyrotoxins, the mutagens, would cause genetic defects [24].

1.4 CRITICISM OF THE IMPACT THEORY

Table 1.1 presents arguments that have been propounded by critics of the impact theory. The table also gives rebuttals (extracted from the literature) of these arguments from supporters of the theory.

The final anti-impact argument in the table suggests the K/T changes were due to a pulse of intense volcanism. This suggestion was given credence by the work of Zoller *et al* , who found high levels of Ir in aerosols emanating from volcanic vents in Hawaii. Since 1985 the debate about the K/T events has been characterised by comparative scrutiny of the impact and volcanism proposals.

1.5 ELEMENTAL IMPACT MARKERS

The elements Ru, Os, Rh, Ir, Pd, and Pt are known collectively as the platinum group metals (PGM). These elements are useful markers of extraterrestrial material in sediments. This is because they are depleted in crustal rocks relative to their mean solar system abundances.

TABLE 1.1 ARGUMENTS AGAINST, AND IN DEFENSE OF, THE IMPACT THEORY

ARGUMENTS AGAINST THE IMPACT THEORY	REBUTTALS
K/T boundaries are not synchronous . The impact theory predicts that there was synchronous formation of the K/T boundary, at all sites world-wide. Officer and Drake [25] claim that some boundaries are diachronous by as much as 8.4×10^5 years.	Alvarez *et al* [26] suggested that the palaeomagnetic data used by Officer and Drake [25] was unreliable, due to sediment mixing. They reported analyses of the same sediments with results at variance with those of Officer and Drake.
Elemental anomalies at the boundary could be due to carbonate dissolution . During periods of low marine pH, the carbonates in a segment of limestone can dissolve, leaving trace elements such as Ir concentrated in residual insoluble material [27].	Trace element concentrations across boundary sequences can be calculated on a carbonate free basis. When this is done boundary materials still show anomalously high levels of Ir [28][8].
The PGM in boundary sediments may have precipitated from seawater. Anoxic ocean conditions may have led to the precipitation of Ir from seawater [29].	The discovery of an Ir anomaly in non-marine K/T boundary shales [30] negated this argument, as did studies of Os isotope abundances in boundary materials [31][32].
Extinctions attributed to an asteroid impact are not synchronous with the Ir anomaly. Some Cretaceous nannoplanckton species survived for thousands of years after the boundary Ir was deposited [25].	Several impact stresses would occur over thousands of years (Table 1.0). Some Cretaceous species would survive into the Tertiary period only to succumb to competition from new Tertiary forms [33].
No impact crater has been found. Despite satellite searches, no impact features have been found which are of the right age, and size, to have been formed by the K/T asteroid [34].	About 20% of the Earths surface has been subducted into the mantle in the last 65 million years. If the impact had struck a region that has since been subducted, no crater would remain. Also, the impact may have triggered Deccan Traps volcanism; the basaltic outpouring would have obscured any crater [35].
The K/T boundary Ir could be derived from the mantle. Orthodox cosmochemical theories suggest that Ir should be depleted in the Earths crust relative to the mantle and the core [36]. Officer and Drake [36] have suggested that volcanism on an enormous scale could have deposited the K/T boundary Ir.	Arguments which refute a mantle origin for the K/T boundary Ir are presented in detail elsewhere in this thesis.

About $4.5x10^3$ million years ago, the Earth accreted, forming a molten planet. As it cooled, by radiating energy into space, chemical fractionation occurred. Three phases were formed: the core, the mantle, and the crust. The PGM are siderophile elements (they have an affinity for iron), and were retained mainly in the core and to a lesser extent the mantle. This left the PGM severely depleted in the Earth's crust relative to meteorites, which tend to have similar compositions to the mantle and the core [3].

1.6 RESEARCH AREAS

The role of chemical analysis in the K/T boundary controversy has been pivotal to the formulation of both the impact and volcanism proposals [37]. Chemical analysis also has a part to play in the scrutiny of the proposals.

The most common elemental marker of an extraterrestrial component in sediments has been Ir, as it is more easily determined by neutron activation analysis (NAA) than the other PGM. Unfortunately the use of this technique is dependant on the availability of nuclear reactor facilities. The technique is also relatively expensive. Therefore, it would be an advantage to be able to determine the PGM in sediments by other techniques. This capability would also show whether other PGM anomalies coincide with the Ir anomalies in boundary sediments, as predicted by the impact theory.

Part of this thesis reports a geochemical survey carried out on the Flaxbourne river K/T boundary sequence. This sequence had not been previously sampled. Palaeontological studies showed that the sequence is exceptionally complete and therefore provides an excellent record of late Cretaceous to early Tertiary environmental changes. Detailed sampling of this sequence was carried out.

The following research goals were set:

(1) To investigate alternative methods to neutron activation analysis for detemining PGM in sediments.
(2) To apply these methods to Flaxbourne River boundary sediments as well as determining the levels of other elements in the sediments.

(3) To analyse the elemental data and draw conclusions from the data with respect to the impact and volcanism proposals.

CHAPTER TWO

INSTRUMENTAL TECHNIQUES, SEPARATION TECHNIQUES, AND MATERIALS

2.0 ATOMIC ABSORPTION SPECTROSCOPY

2.1 (a) Principles

Atomic absorption spectroscopy (AAS), is an analytical method for the determination of elemental concentrations in samples, based on the absorption of radiation by free atoms. Sir Alan Walsh pioneered the development of the technique for routine analysis, and published a report on the subject in 1955 [38]. The technique was used extensively in research reported in this thesis. All the AAS analyses were performed on solution samples.

Figure 2.0 illustrates the basic principles of AAS. When a solution sample is analysed by AAS, atomic vapour is formed from the solution. Spectral line radiation is passed through the vapour; the line used, corresponds to a resonance transition for the analyte atoms. Although the source emits a spectrum of lines, the line chosen for detection is isolated with a monochromator. Analyte atoms in the light path absorb the radiation, and the level of absorbance (A_Z) is determined.

$$A_Z = \log \left(\frac{P_0}{P}\right)$$

P_0, is the radiant power of the incident radiation.
P, is the radiant power of the transmitted radiation.

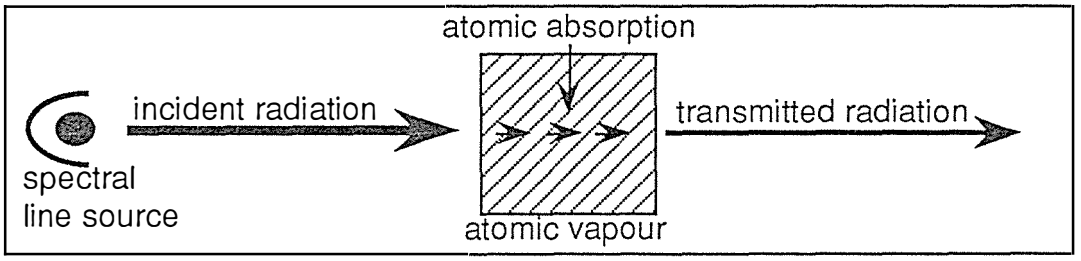

Figure 2.0 AAS Processes
Spectral line radiation is emitted from the source. Analyte atoms in the atomic vapour absorb the radiation. The level of absorbance is measured. This is related to the concentration of analyte atoms in the atomic vapour.

Solution standards are used to calibrate the system. This allows the relationship between absorbance readings (A_Z), and element concentrations in solution (C_Z), to be determined. Within the dynamic range for the technique, this relationship has the form:

$$A_Z = s \times C_Z + i.$$

The letters s and i, represent constants which can be determined graphically, or with least squares analysis. Once this relationship has been determined for a particular element, the element's concentration in a sample can be determined from the absorbance reading.

2.1 (b) Hollow Cathode Lamps

Source radiation for AAS is most commonly supplied by a hollow cathode lamp. This was the only type of source used for work reported in this thesis.

Figure 2.1 gives a schematic representation of a hollow cathode lamp. In the back of the lamp is a hollow cathode made of the element to be analysed, or an alloy containing that element. The window of the lamp can be constructed of borosilicate glass, or if ultraviolet radiation is required, quartz. The lamp is filled with an inert gas under reduced pressure. A potential is applied between the electrodes to cause a current to flow. The potential ionises the inert gas at the anode and accelerates the inert gas ions towards the cathode. These ions

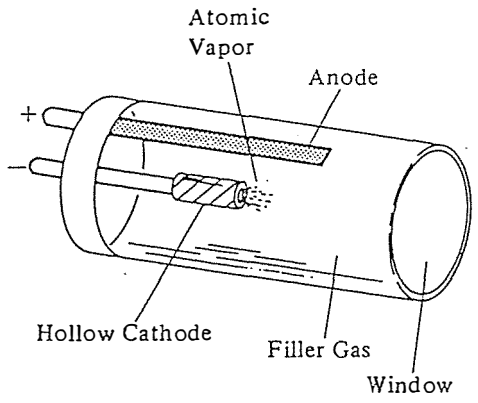

Figure 2.1 Hollow Cathode Lamp

collide with the cathode causing free metal atoms to be removed which then undergo collisional excitation due to collisions with fast moving inert gas ions. The excited atoms lose energy and produce their characteristic emission line spectrum.

2.0 (c) Flame Atomic Absorption Spectroscopy

Flame atomic absorption spectroscopy (F-AAS), utilises a combustion flame to produce atomic vapour from solutions. A variety of flames can be used for this purpose. The choice of flame is dependent on the flame temperature, and the oxidising or reducing conditions required. Air acetylene, and nitrous oxide acetylene flames were used in work reported in this thesis. The air acetylene flame produces temperatures of around 2,400 K, while the hotter nitrous oxide acetylene flame produces temperatures of around 3,200 K [39].

All F-AAS analyses reported in this thesis were made using an IL 457 double-beam AA/AE spectrometer. This system uses deuterium background correction.

2.0 (d) Graphite Furnace Atomic Absorption Spectroscopy

(i) Background Information

Atomic vapour can be produced from solutions by electrothermal means. For example, a solution can be dried onto the surface of a material like tungsten, tantalum, or graphite; atomic vapour can then be produced by resistive heating of the material.

The electrothermal atomiser which has gained the most acceptance, has been the graphite furnace. L'vov introduced graphite furnace atomic absorption spectroscopy (GF-AAS) [40]. In his original design, heating of the sample was achieved by striking an arc between a sample electrode and the furnace [41].

It was Massman who paved the way for the widespread acceptance of GF-AAS as an analytical technique. In 1968 he reported the use of resistively heated

graphite tubes (furnaces) to produce atomic vapour [41]. During heating, these tubes were immersed in a stream of argon gas to prevent oxidation of the graphite. Massman introduced step-wise heating cycles for GF-AAS analyses [41]. The use of these cycles has become a standard procedure with this technique.

Each cycle consists of three principal stages:
(1) The drying stage. After the injection of sample solution onto the inner surface of the tube, the tube is heated to around 100 °C (depending on the solvent) to evaporate the solvent. This leaves the analyte deposited on the tube.
(2) The ashing stage. The tube is further heated to a temperature which is hot enough to pyrolyse any organic material deposited on its surface, but not so hot as to allow the formation of atomic vapour from the analyte.
(3) The atomisation stage. Finally, the tube is heated rapidly to a temperature which causes the analyte to be vaporised.

(ii) GF-AAS Instrumentation Used.

All GF-AAS determinations reported in this thesis were performed using a GBC (System 1000) furnace unit, coupled to a GBC 902 atomic absorption spectrometer. Sample injections were made using a PAL 1000 automatic sampler.
The System 1000, uses a 'mini-Massman' type of furnace which is 9 mm long and has an internal diameter of 3 mm. Figure 2.2 shows the furnace tube between two

electrodes. The hole in the wall of the tube allows sample solution to be injected into it. When operational, the furnace is aligned so that light from the hollow cathode lamp passes through the tube.

Figure 2.3, shows a diagram of the system 1000 workhead. When the furnace is heated, oxygen free nitrogen flows out of the diffuser to prevent oxidation of the graphite. The workhead is water cooled to keep 'down time' between heating cycles to a minimum. The furnace is not enclosed, so it is readily accessible. Setting the furnace clamp to load draws the support rods apart which allows the furnace to be removed and replaced.

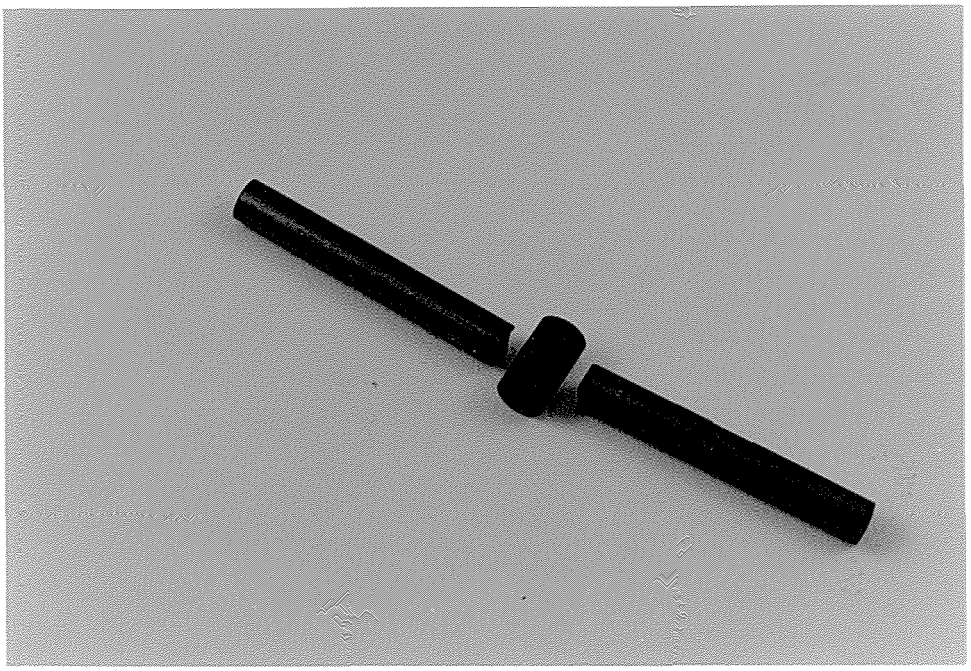

Figure 2.2 Graphite Furnace and Electrodes

(iii) GBC System 1000 Capabilities

Figure 2.4 illustrates a step-wise heating cycle used, with the GBC system 1000, to determine Pd in a 1 mol/l HCl solution. With this system, the furnace temperature increases at a constant rate. This is known as the 'ramp' rate, which is specified as part of the furnace program. Each heating stage consists of a temperature ramp, followed by a temperature hold; the hold keeps the furnace temperature constant for a specified period. Low ramp rates are used at the drying and ashing stages to prevent spitting of the sample material. A high ramp rate is needed at the atomisation stage to rapidly vaporise all the analyte.

Up to 5 µl of solution can be dryed in a furnace at a time. Ten dryings can be done before the ashing and atomisation stages are carried out. So, the absorbance signal due to analyte from 50 µl of solution can be obtained. A range of volumes from 1 to 50 µl can be chosen to be dryed onto the tube, prior to atomisation.

Figure 2.5, shows two absorption signals. Signal A was obtained from 3 µl of a 0.1 µg/ml Pd solution. Signal B was obtained using a 0.01 µg/ml Pd solution using ten, 3 µl dryings. The signals are practically identical. This shows the potential of multiple dryings to effectively increase the sensitivity of the technique.

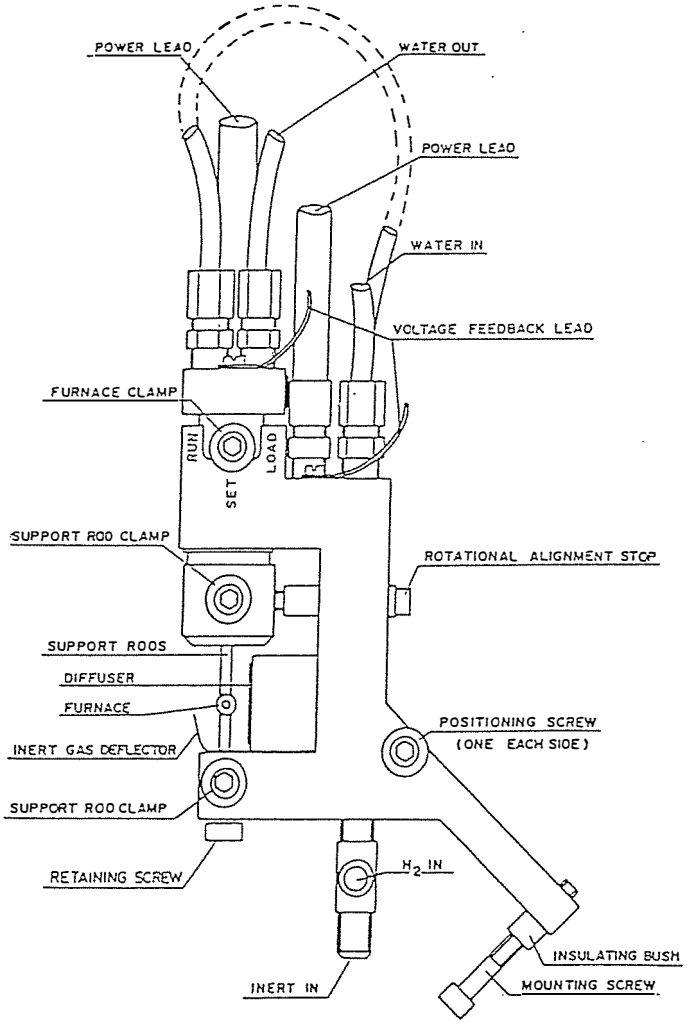

Figure 2.3 GBC System 1000 workhead

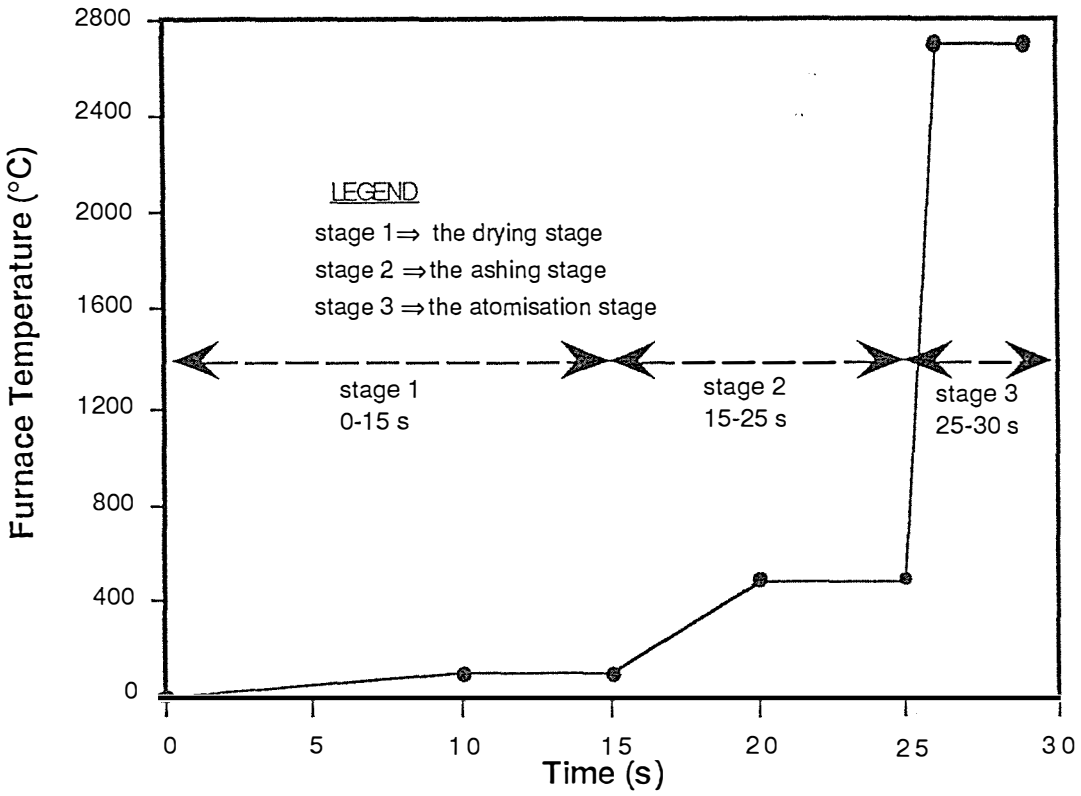

Figure 2.4 A Typical Furnace Cycle

Graph showing variation of graphite furnace temperature with time elapsed during a furnace heating cycle. The cycle shown, is used to determine Pd in aqueous solutions.

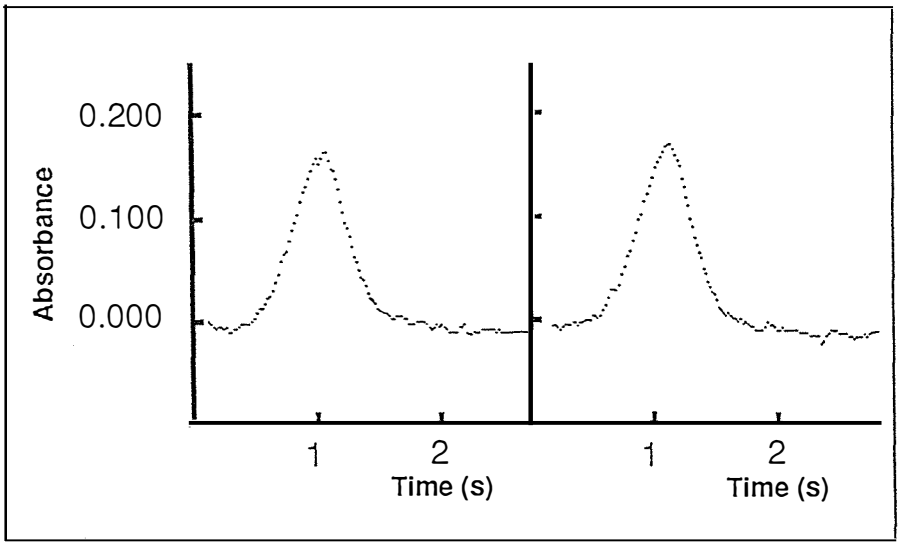

Figure 2.5 Absorption Signals

Two absorption signals obtained using GF-AAS. Signal A was obtained from 3 µl of a 0.1 µg/ml Pd solution. Signal B was obtained from 30 µl of a 0.01 µg/ml Pd solution, using the multiple drying facility.

2.0 (e) GF-AAS Optimization for Palladium Determination

(i) Spectral line selection

All Pd analyses were performed using the 247.6 nm line . The 244.8 nm line gives better sensitivity, however this line gives a considerably less stable lamp signal.

(iv) Injection Tip Alignment

The PAL 1000 auto-sampler uses a robot arm to manoeuvre the sample injection tip. Sample solution is drawn up into a plastic tube through the tip. The robot arm then places the tip through the sample injection port, and the sample solution is injected into the furnace tube.

The furnace/tip geometry, at the moment of injection, is a critical factor in the optimization of perfomance for GF-AAS.

The injection probe, as supplied, has a flat tip. If the tip is touching the tube (as in geometry (A), Figure 2.6), the injected solution tends to be deposited

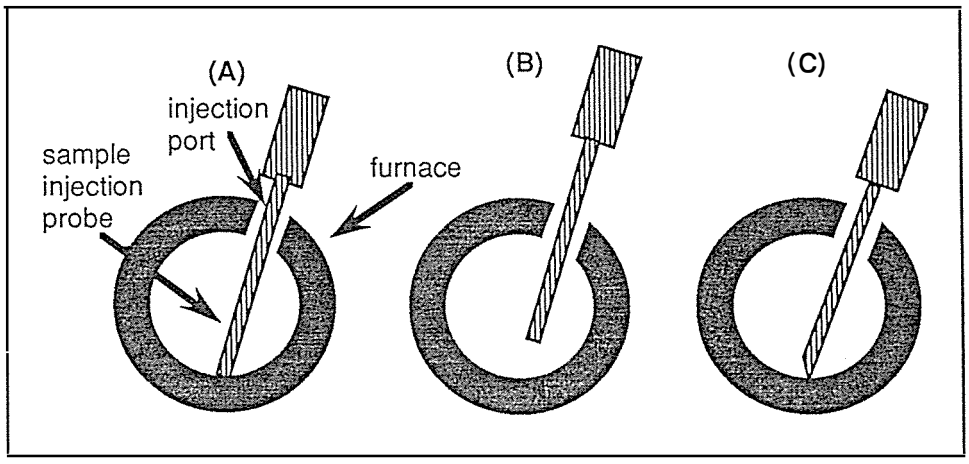

Figure 2.6 Furnace/Probe Geometries
Diagram of three possible geometries for the sample injection probe, at the moment of sample injection. Geometry (A) shows the probe with a flat tip that is touching the bottom of the furnace. Geometry (B) shows the probe with a flat tip that is positioned above the furnace bottom. Position (C) shows the probe with a pointed tip that is touching the bottom of the furnace.

unevenly, and some may be lost through the injection port, or over the sides of the tube. If the tip is not touching the tube (see geometry(B)), some of the solution tends to migrate up the probe and is lost through the injection port. The best results are obtained if the tip is cut, to give it a point, and if it is touching the tube (see geometry (C)). With this geometry a drop of solution is deposited to one side, in the tube. This provides good reproducibility of drop deposition.

(ii) Lamp current selection.

The lamp current influences the fluctuation in the lamp signal. A large fluctuation leads to a large background absorption signal. When lamp currents of less than 5 mA are used, the background absorption signal is unacceptably large. Figure 2.7 shows that the lamp is most stable when a current of 13 mA is used.

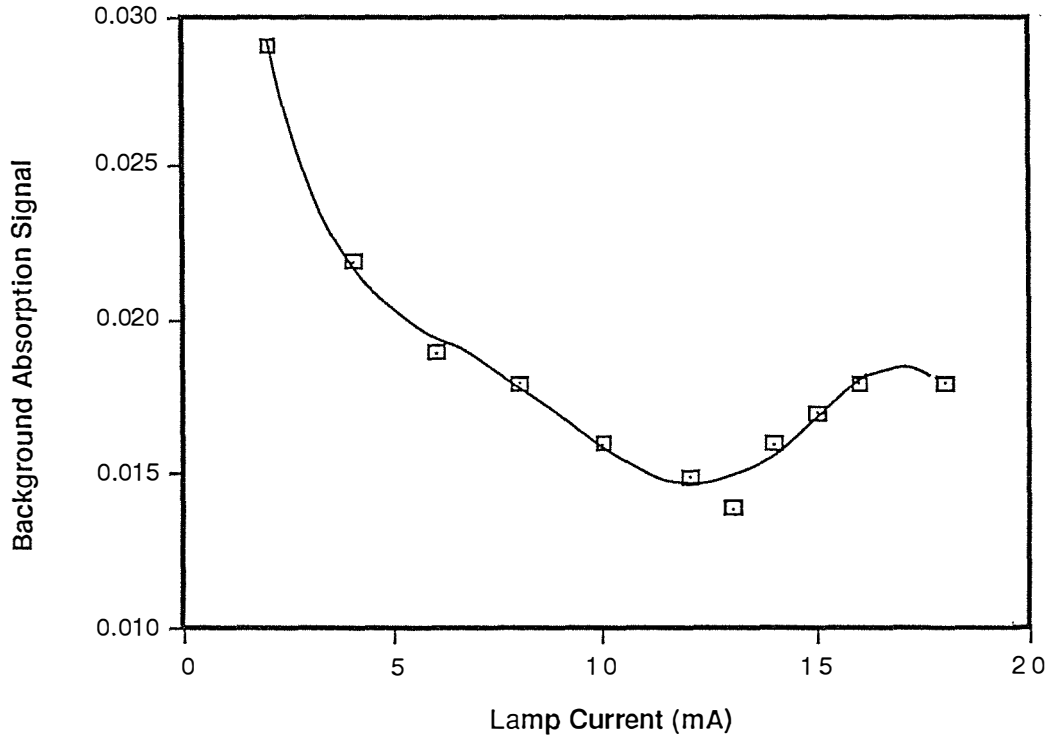

Figure 2.7 Optimization of Hollow Cathode Lamp Current
Variation of the background absorption signal with the hollow cathode lamp current.

Unfortunately, the life-span of a hollow cathode lamp shortens when high operating currents are used. With this in mind, a compromise lamp current of 10 mA was used for all Pd determinations.

(iii) Furnace heating programs.

The GBC System 1000 instrument, allows up to ten heating stages with each heating cycle. When organic solvents are analysed, it is common to include a pre-heating stage with the three principal heating stages (see sub-section 2.0 (d)(i)). Pre-heating the tube before sample injection can increase sensitivity. This was observed when MIBK solutions were analysed. When preheating was not employed, the MIBK had a tendency to creep along the tube and flow over the sides before drying could be completed. With judicious choice of the pre-heat temperature, the MIBK can be made to dry evenly before it has a chance to move towards the tube extremities.

All determinations of Pd in MIBK were performed using the conditions given in Table 2.0. The conditions used to analyse aqueous solutions are given in Table 2.1. The pre-heat stage is not required for these solutions.

Table 2.0 Heating Cycle Conditions for MIBK

Heating Stage	Pre-heat	Dry	Ash	Atomise
Final Temp. (°C)	75	100	500	2500
Ramp Time (s)	3.0	10.0	5.0	1.0
Hold Time (s)	1.0	5.0	5.0	3.0
Inert Gas	No	No	No	Yes

Table 2.1 Heating Cycle Conditions for Aqueous Solutions

Heating Stage	Pre-heat	Dry	Ash	Atomise
Final Temp. (°C)	—	120	500	2500
Ramp Time (s)	—	10.0	5.0	1.0
Hold Time (s)	—	5.0	5.0	3.0
Inert Gas	—	No	No	Yes

For the drying stage, a ramp time of at least 10 seconds is needed to prevent sudden boiling and 'spitting' of the MIBK. An atomisation temperature of 2500 °C was chosen after an optmization study. The results of this study are plotted in Figure 2.8. This figure shows that no large increase in signal would be achieved by using an atomisation temperature of greater than 2500 °C. Atomising at greater than this temperature would cause unnecessary furnace wear.

(iv) Calibration curve

Figure 2.9 shows a calibration curve for the determination of Pd in MIBK. Due to the mediocre precision possible with this technique, each standard solution was analysed five times and the mean absorption was obtained. When this is done the calibration curve is reasonably smooth. The curve is linear up to a Pd concentration of 0.16 μg/ml. At higher concentrations there is a negative deviation from Beer's Law.

(v) Absorption Signal

Figure 2.5 shows typical absorption signals for Pd. All signals observed for Pd, where an atomisation temperature of 2500 °C was used, show an absorption maximum at just over one second after the atomisation stage begins. The signals shown in Figure 2.5 were recorded when the hollow cathode lamp was relatively new, and when the lamp signal fluctuation was small. The fluctuation increased with the use of the lamp.

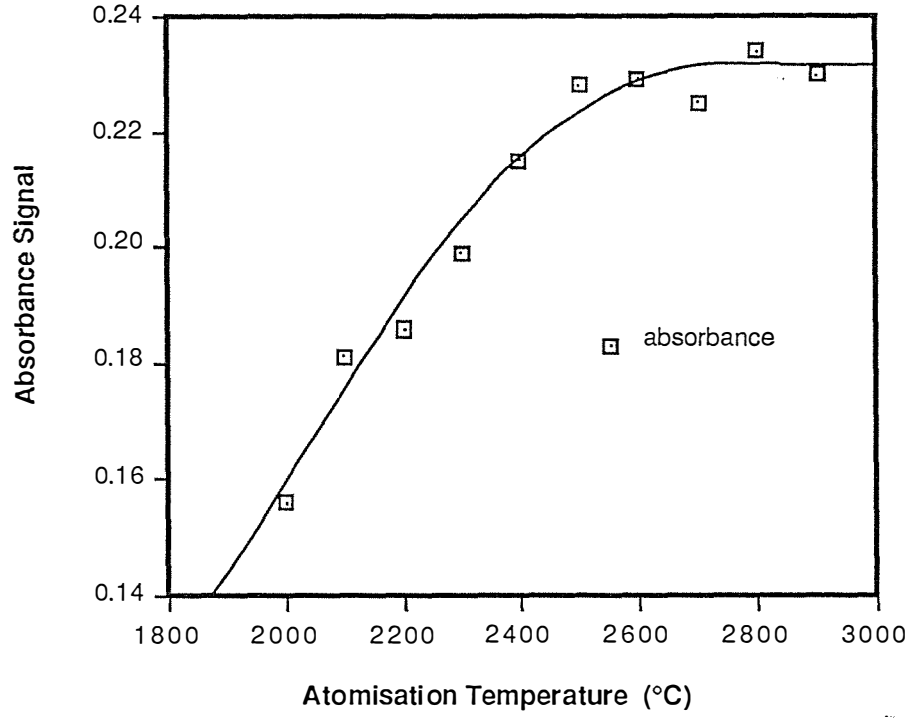

Figure 2.8 Optimization of Atomisation Temperature

The effect of atomisation temperature on the absorption signal for Pd. Each point represents the mean signal of five atomisations. One drying of 3 µl, of a 0.2 µg/ml solution of Pd in MIBK, was performed before each atomisation. The heating cycle given in Table 2.1 was used for the determinations.

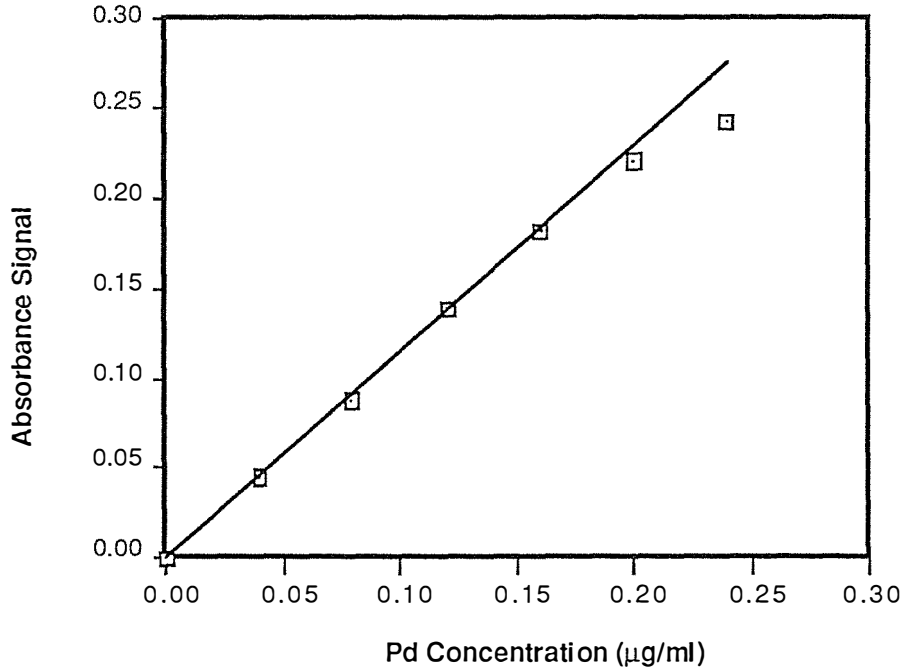

Figure 2.9 Calibration Curve for the Determination of Palladium in MIBK by GF-AAS

The variation of absorbance with the concentration of Pd in MIBK, when this solution is analysed by GF-AAS. Each absorbance point represents the mean value of five analyses. One drying of 3 µl of MIBK occurred before each atomisation.

(vi) Limits of Detection

The IUPAC and propagation of errors (POEM) methods for determining limits of detection (c_L) are fully described in Appendix II. GF-AAS absorbance signals were obtained for four MIBK solutions. Table 2.2 shows the absorbances obtained. Three of the solutions contained known concentrations of Pd, and the other was a reagent blank.

Table 2.2 Palladium Standard-Solution Absorbances

	Pd Concentration in MIBK (µg/ml)			
	0.00	0.02	0.04	0.06
GF-AAS Absorbance Signals	-0.009	0.057	0.125	0.185
	-0.003	0.054	0.115	0.162
	0.003	0.068	0.111	0.174
	-0.005	0.049	0.112	0.178
	-0.013	0.049	0.108	0.182
	0.008	0.058	0.128	0.180
	0.031	0.056	0.117	0.156
	0.008	0.071	0.126	0.167
	-0.008	0.051	0.116	0.172
	0.004	0.055	0.111	0.177
	0.003	0.067	0.125	0.172
	0.005	0.061	0.119	0.186
	0.006	0.062	0.099	0.163
	-0.006	0.048	0.121	0.153
	-0.008	0.045	0.114	0.180
	-0.002	0.065	0.129	0.178
	0.001	0.065	0.124	0.193
	-0.006	0.068	0.103	0.169
	-0.010	0.047	0.124	0.158
	0.003	0.043	0.118	0.186

Using the data from Table 2.2, the IUPAC and POEM limits of detection can be calculated as follows (see Appendix II for details of the formulae used):

$$c_L(\text{IUPAC, k=3}) = \frac{3 \times s_B}{m}$$

$$= \frac{3 \times 0.010}{2.90} = \underline{0.010\ \mu g/ml}$$

$$c_L(\text{POEM, k=3}) = \frac{3[s_B^2 + s_i^2 + \left(\frac{i}{m}\right)^2 \times s_m^2]^{1/2}}{m}$$

$$= \frac{3[(0.010)^2 + (0.012)^2 + \left(\frac{0.000}{2.90}\right)^2 \times (0.332)^2]^{1/2}}{2.90}$$

$$= \underline{0.016\ \mu g/ml}$$

The limit of detection obtained with the POEM method is greater than that obtained with the IUPAC method. This is because the former method takes account of the uncertainty in the slope and intercept of the calibration curve. The data in Table 2.2 were collected using two 3 µl dryings before each atomisation. With ten 3 µl dryings the effective limit of detection (POEM) is 0.003 µg/ml. The data in Table 2.2 were collected using a hollow cathode lamp which was near the end of its useful life. The background fluctuation observed should be seen as the worse possible case.

(vii) Memory Effect

An unusual memory effect was observed following the analysis of a Pd (MIBK) standard, by GF-AAS, when worn furnaces were used. Under these circumstances Pd adhered to the furnace. Subsequent MIBK blank determinations gave large Pd signals, even though a 'furnace clean' program (rapid heating to 3000 °C) was run between each determination. The signals decreased with each successive blank/clean cycle. Many cycles were required before the memory signal ceased to be observed. This indicates that the memory effect was due to chemisorption rather than the weaker physisorption.

MIBK would appear to play an important role in the desorption of Pd from the furnace; no memory signal was observed when an aqueous-blank solution was analysed.

It is possible Pd is adsorbed by amorphous carbon deposits on worn furnaces. Pd is known to be strongly adsorbed by amorphous carbon [42], which is well suited as an adsorbent because of its porous microcrystalline structure (composed of graphite packets) [43].

2.0 (f) GF-AAS Optimization for Rhodium Determination

(i) Spectral line selection.

The most sensitive AAS line for Rh is the 343.5 nm line. Unfortunately deuterium lamp background correction cannot be used at this wavelength because the output of the deuterium lamp is poor at wavelengths over 300 nm. However, most common molecular absorption interferants do not significantly absorb at wavelengths as high as 343 nm.

(ii) Lamp current selection.

Lamp currents between 3 mA and 15 mA gave very stable background signals. A lamp current of 5 mA was used for all Rh determinations.

(iii) Furnace heating programs.

The furnace heating programs used for Rh are the same as those used for Pd except for the atomisation temperature. An atomisation temperature of 2600 °C was used for all Rh determinations. The decision to use this temperature was based on an optimization study. The results of this study are plotted in Figure 2.10. This figure shows no large increase in signal would be achieved by using an atomisation temperature of greater than 2600 °C. Atomising at greater than this temperature would cause unnecessary furnace wear.

(iv) Calibration Curve

Figure 2.11 shows a calibration curve for the determination of Rh in 2 mol/l HCl. Each solution was analysed five times and the mean absorption was obtained.

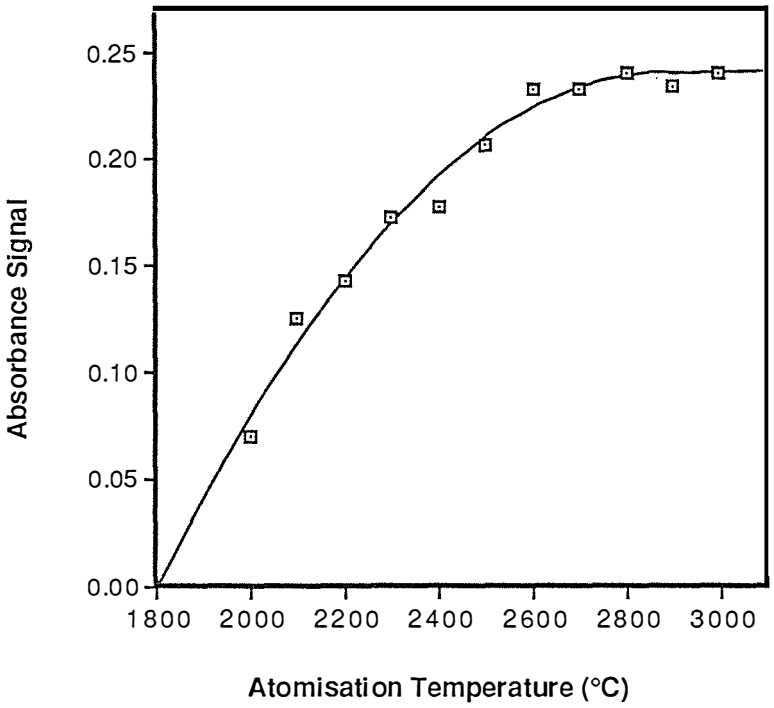

Figure 2.10 Optimization of Atomisation Temperature

The effect of atomisation temperature on the absorption signal for Rh. Each point represents the mean signal of five atomisations. One drying of 3 µl, of a 0.2 µg/ml solution of Rh in HCl (2 mol/l), was performed before each atomisation. The heating cycle given in Table 2.0 was used for the determinations.

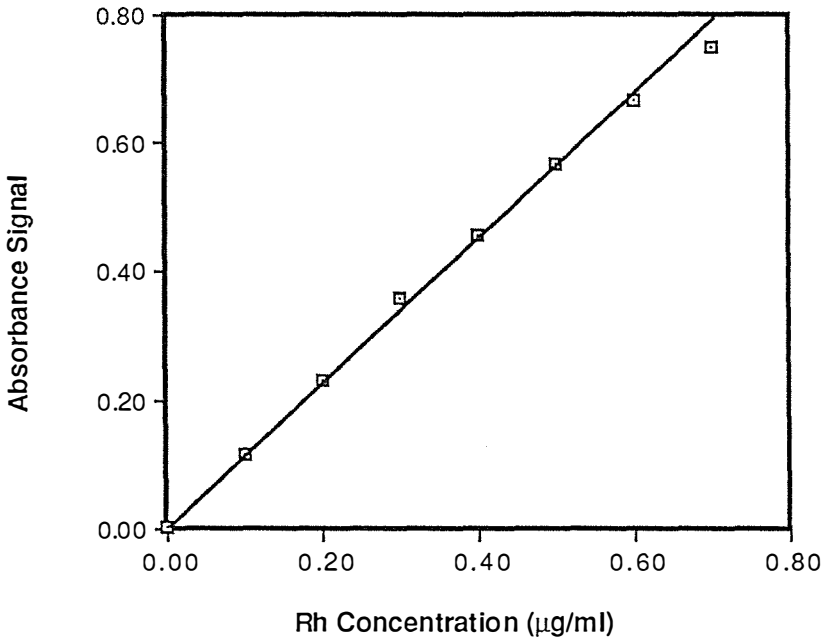

Figure 2.11 Calibration Curve for the Determination of Rh in HCl by GF-AAS

The variation of absorbance with the concentration of Rh in HCl (2 mol/l), when this solution is analysed by GF-AAS. Each absorbance point represents the mean value of five analyses. One drying of 3 µl of MIBK occurred before each atomisation.

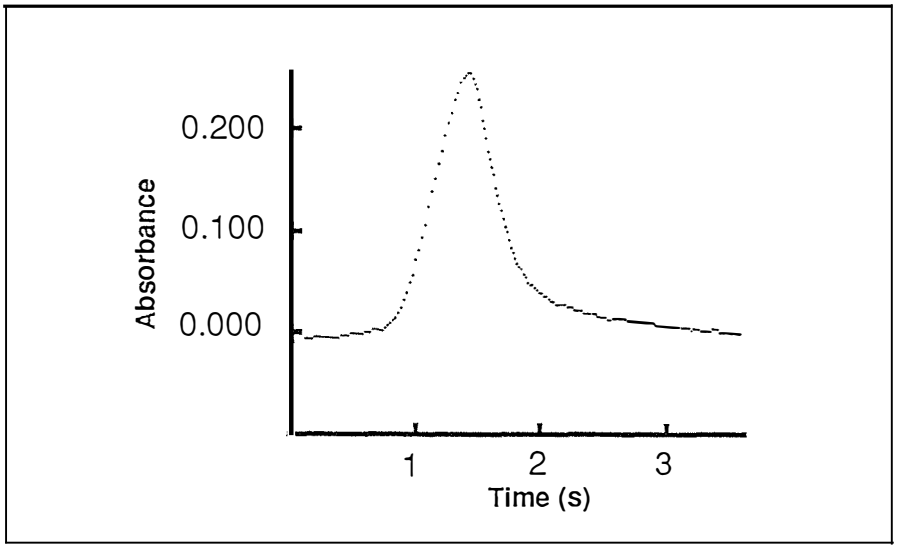

Figure 2.12 Absorption Signal for Rhodium

(v) Absorption Signal.

Figure 2.12 shows a typical absorption signal for Rh. All signals observed for Rh, where an atomisation temperature of 2600 °C was used, show an absorption maximum at just over one second after the atomisation stage begins. The signal shown was produced using a relatively new hollow cathode lamp, hence the low noise level for the signal.

(vi) Limits of Detection

The IUPAC and POEM limits of detection (k=3) were calculated in the same manner for Rh as for Pd. GF-AAS absorbance signals were obtained for four 2 mol/l HCl solutions. Table 2.3 shows the absorbances obtained. Three of the solutions contained known concentrations of Rh, and the other was a blank. Using the data from Table 2.2, the IUPAC and POEM limits of detection can be calculated as follows (see Appendix II for details of the formulae used):

$$c_L(\text{IUPAC, k=3}) = \frac{3 \times s_B}{m}$$

$$= \frac{3 \times 0.001}{1.07} = \underline{0.003\ \mu g/ml}$$

$$c_L(\text{POEM, k=3}) = \frac{3[s_B^2 + s_i^2 + \left(\frac{i}{m}\right)^2 \times s_m^2]^{1/2}}{m}$$

$$= \frac{3[(0.001)^2 + (0.011)^2 + \left(\frac{-0.000}{1.07}\right)^2 \times (0.121)^2]^{1/2}}{1.07}$$

$$= \underline{0.031\ \mu g/ml}$$

The data in Table 2.3 were collected using one 3 µl drying before each atomisation. With ten 3 µl dryings the effective limit of detection (POEM) is 0.003 µg/ml. This is the same value that was obtained for Pd. While the sensitivity of GF-AAS is better for Pd than for Rh, Pd has a more noisy background signal.

Table 2.3 Rhodium Standard-Solution Absorbances

	Rh Concentration in 2 mol/l HCl (µg/ml)			
	0.00	0.05	0.10	0.15
GF-AAS Absorbance Signals	-0.001	0.040	0.081	0.172
	0.000	0.044	0.102	0.154
	-0.002	0.046	0.091	0.168
	0.000	0.050	0.094	0.165
	0.001	0.045	0.095	0.154
	0.001	0.042	0.100	0.158
	-0.001	0.041	0.103	0.161
	0.001	0.041	0.090	0.163
	-0.002	0.046	0.091	0.152
	0.001	0.046	0.102	0.168
	0.000	0.044	0.101	0.167
	-0.001	0.050	0.097	0.151
	0.000	0.045	0.091	0.164
	0.000	0.046	0.102	0.162
	-0.001	0.044	0.099	0.157
	0.000	0.045	0.096	0.153
	0.001	0.041	0.095	0.166
	-0.001	0.043	0.090	0.169
	0.002	0.046	0.101	0.153
	0.000	0.047	0.085	0.171

2.1 INDUCTIVELY COUPLED PLASMA ATOMIC EMISSION SPECTROSCOPY (ICP-AES)

The development of ICP-AES as an analytical technique, began in early 1962 with two research groups independently pursuing the same concept [44]. The first commercial instrumentation became available in 1974.

ICP-AES allows multi-element determinations to be determined for solution samples. Sample solution is nebulised into an inductively coupled plasma where the solution constituents are thermally excited. Electronic deactivation of the thermally excited atoms occurs with the emission of radiation that is characteristic (in energy) of the particular element and electronic transition involved. The emission signals for a range of elements from the sample solution can be isolated and recorded simultaneously using a multichannel spectrometer. The intensity of an emission signal can be related to an analyte concentration in solution.

All ICP-AES determinations reported in this thesis were performed using an ARL 34000 vacuum polychromator system that is configured for 23 elements.

2.2 INDUCTIVELY COUPLED PLASMA SOURCE MASS SPECTROMETRY (ICP-MS)

ICP-MS allows simultaneous multielement determinations to be performed on solution samples. The technique also allows isotope ratios for analyte elements in solution to be determined.

The principles of the technique are as follows: The analyte solution is nebulized and the resulting aerosol is injected into an inductively coupled plasma where temperatures reach up to 10,000 K. A proportion of the solution constituents is ionised. A small proportion of these ions is extracted through a sampling orifice into a vacuum system. An ion lens directs the ions to another vacuum stage housing a quadrupole mass spectrometer.The spectrometer gives a reading of ion count versus charge/mass ratio for the ions. Figure 2.13 shows a schematic diagram of a typical ICP mass spectrometer.

The technique is extremely sensitive for most metals. All the PGM can be determined in aqueous solutions at ng/ml levels or lower. This is shown in Figure 2.14. A useful introduction to this technique has been published by Date [45]. All ICP-MS determinations reported in this thesis were performed using a Sciex Elan instrument.

2.3 NEUTRON ACTIVATION ANALYSIS (NAA)

Instumental neutron activation analysis involves irradiation of the sample followed by measurement of the radiation emitted from analyte atoms. Irradiation is accomplished by placing the sample in a neutron flux (in a nuclear reactor). The analyte atoms absorb neutrons to form radioactive isotopes which emit gamma radiation and sometimes beta radiation. The level of radiation is measured and is used to calculate the abundance of the analyte in the sample. A sample with a complex matrix may contain many elements which become radioactive in the reactor and subsequently emit gamma radiation. In this instance the gamma ray spectrometer used, may be unable to resolve the analyte signal from other signals emanating from the sample. Radiochemical neutron activation analysis (RNAA) may be used to overcome this difficulty.

RNAA involves the irradiation of the sample in the same manner as is performed for INAA. Then the sample is dissolved and a known amount of carrier (analyte element) is added to the solution. Separation techniques are used to separate the analyte element (sample + carrier) from the other elements of the sample matrix. The level of radiation emitted by the irradiated analyte atoms can then be determined free from interferences.

Data from neutron activation analyses are recorded in this thesis. The analyses were performed at two research centres: the Los Alamos National Laboratory, Los Alamos, U.S.A.; and the Trace Analysis Research Centre, Department of Chemistry, Dalhousie University, Halifax, Nova Scotia, Canada.

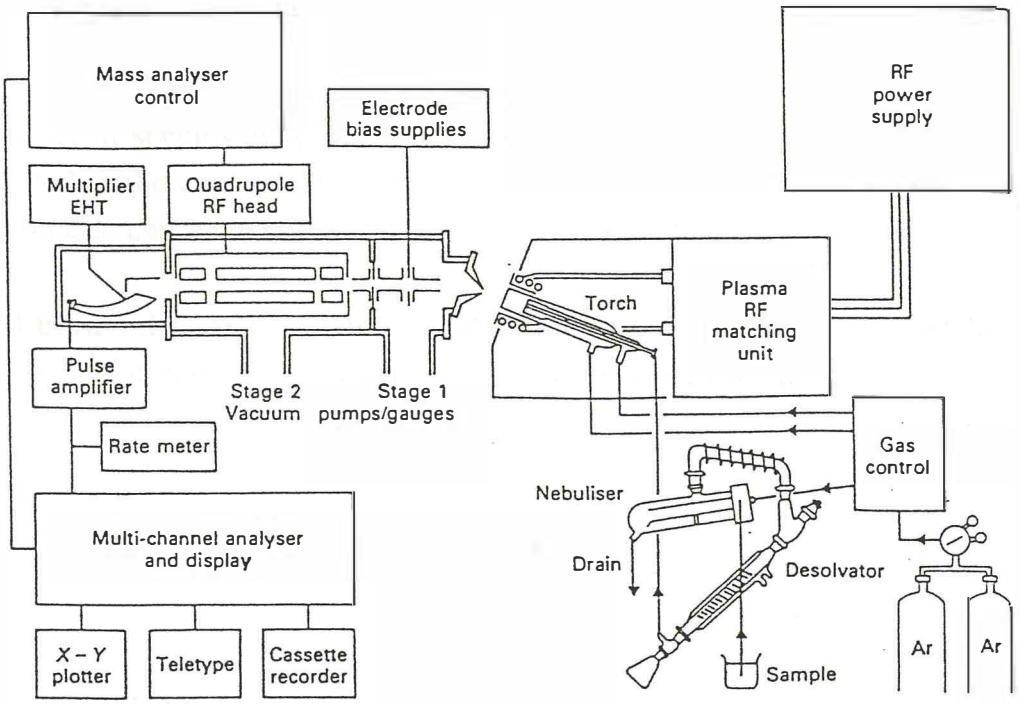

Figure 2.13 Schematic Diagram of an ICP Mass Spectrometer

The inductively coupled plasma forms at the upper end of the plasma torch. Samples are introduced to the ICP by conventional solution nebulisation. A portion of the ionized gas is extracted from the tail flame of the ICP into the mass spectrometer through a small hole drilled in a water-cooled Cu, Ni, or Ni alloy cone (into stage 1). The ions are focussed through a differential pumping aperture into stage 2, containing the quadrupole mass filter and detector.

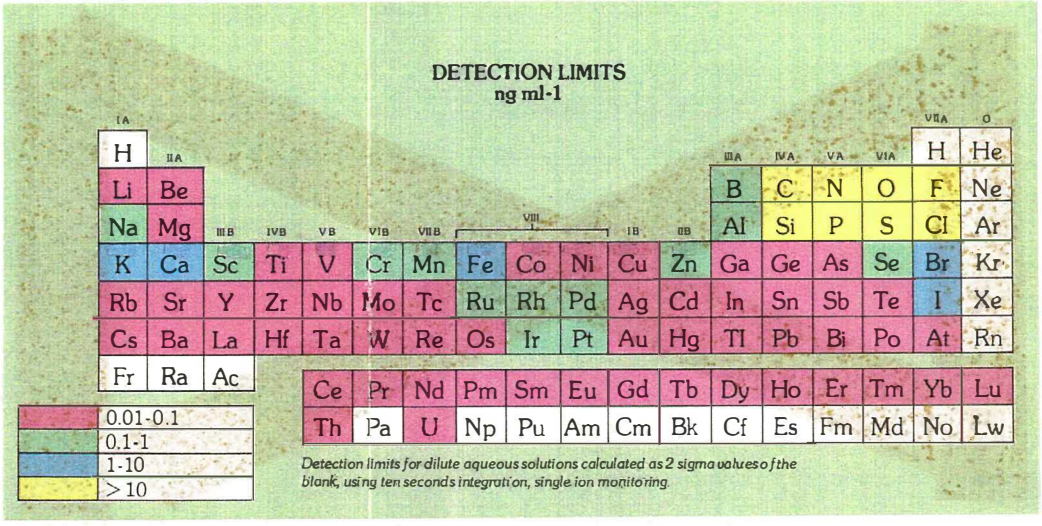

2.14 Detection Limits for Elemental Determinations by ICP-MS

The figure is supplied by VG Isotopes to illustrate the performance of their Plasmaquad instrument. The detection limits are for dilute aqueous solutions calculated as 2 sigma values of the blank, using ten seconds integration, single ion monitoring.

2.4 ULTRAVIOLET-VISIBLE MOLECULAR ABSORPTION SPECTROSCOPY

This technique measures the absorption of ultraviolet or visible radiation by molecular species in solution. Absorbance values are obtained which can be related to the concentration of the species of interest in solution. So, this technique can be used for quantitative analyses of solution samples.

All ultraviolet-visible molecular absorption analyses reported in this thesis were performed using a Shimadzu UV-160A instrument.

2.5 SOLVENT EXTRACTION

2.5 (a) Introduction

Like ion exchange and liquid chromatography, the technique of solvent extraction uses phase distribution as a separation principle. In trace metals analysis, solvent extraction is used to perform two tasks: The separation of the analyte element from chemical species which interfere with instrumental analysis, and the enrichment of the analyte concentration in solution. The analyte can be separated from interferants by solvent extraction of the analyte, or by solvent extraction of the interferants. Clearly, an extraction system must be used in which the analyte and the interferants are not significantly coextracted. Concentration enrichment may be required so that the concentration of the analyte in solution is sufficient to permit quantitative determinations to be made.

2.5 (b) Principles of Solvent Extraction

Solvent extraction requires the use of a pair of solvents which are essentially immiscible. For a solute to extract, it must distribute between two solvents when they are brought into contact as a two phase system. The mixing of two solvents, in order to allow a solute to reach an equilibrium distribution between them is termed 'equilibration'. If initially, all of the solvent is present

in one solvent phase, after equilibration, some of the solute will be distributed in the other phase. In this way extraction is achieved.

For a solute distributing between two phases, the equilibrium distribution can be expressed in terms of the distribution coefficient (K_D).

$$K_D = \frac{[x]2}{[x]1} \quad (E2.0)$$

[x]2 is the concentration of solute x in phase 2.
[x]1 is the concentration of solute x in phase 1.

The Nernst distribution law states that K_D is a constant at a particular temperature, for any total concentration of solute [46]. However, this law is not thermodynamically rigo rous. In Appendix I it is shown using a more rigo rous treatment that,

$$K_D \equiv \frac{\gamma 1}{\gamma 2} \text{ x } K'$$

$\gamma 1$ is the activity coefficient for phase 1.
$\gamma 2$ is the activity coefficient for phase 2.

Variation of the distribution coefficient will result from variations in the activity coefficients for each of the phases. When the solute concentration is very low, as is the case for trace metal extractions, the activity coefficients approach unity and K_D can be regarded as constant.

Most solvent extractions involve an aqueous/organic solvent pair. Usually the component of interest is extracted from the aqueous phase into the organic phase. It is common for the component of interest to exist as a number of chemical forms in the solvent phases. In this instance K_D does not adequately describe the distribution of the component between the two phases; the distribution is then described by the distribution ratio (D).

$$D = \frac{C_o}{C_a}$$

C_o is the total concentration of the component of interest in the organic phase.
C_a is the total concentration of the component of interest in the aqueous phase.

For the extraction of a component from an aqueous to an organic phase, the fraction of the component extracted (F) is given by:

$$F = \frac{D}{D + (V_a/V_o)}$$

V_a is the volume of the aqueous phase.
V_o is the volume of the organic phase.
Enrichment of the analyte concentration in solution can be achieved using a high V_o/V_a ratio. This equation can be used to determine if the ratio chosen will give an acceptable value of F.

2.5 (c) Factors Affecting the Distribution

It is important to understand the factors which cause the solute to have a greater affinity for one phase than the other. Once these factors are understood conditions can be chosen which are likely to maximise the extraction of the component of interest.

The following generalisations can be made with respect to solvent extraction processes: Electrolytes will distribute mainly in the aqueous phase of a solvent pair; a solute will have the greatest affinity for the solvent which it most strongly resembles in terms of chemical properties.

Can these generalisations be rationalised in terms of physical interactions at the atomic level? The position of equilibrium is determined by the free energy properties of the non-equilibrium standard state (ΔG°). For a solvent extraction system at equilibrium,

$$\Delta G^\circ = -RT\ln K_D$$

R is the gas constant.
T is the temperature of the system (degrees K).
ΔG° is the free energy change for the extraction when all the solute is transferred from phase 1 to phase 2, where all substances are in their standard states.

K_D (distribution coefficient) gives the position of equilibrium for the solvent extraction system (not necessarily in the standard state).

$$\Delta G^\circ = \Delta H^\circ - T\Delta S^\circ$$

ΔH° is the enthalpy change for the extraction when all the solute is transferred from phase 1 to phase 2, where all substances are in their standard states.
ΔS° is the entropy change for the extraction when all the solute is transferred from phase 1 to phase 2, where all substances are in their standard states.

For many processes at room temperature, ΔH° rather than $T\Delta S^\circ$ makes the major contribution to ΔG°. The following discussion assumes that this is the case for most solvent extraction processes.

For solvent extraction ΔH° is a function of the intermolecular forces which are disrupted and formed in the process of extraction. The disruption of these electrostatic forces requires absorption of heat from the surroundings; therefore it is an endothermic process. The formation of new forces is exothermic. If stronger forces are disrupted than formed, the overall process is endothermic; if the reverse is true the process is exothermic.

Electrolytes are generally well solvated in highly polar aqueous solution. A solvation shell of water molecules surrounds both cations and anions. This is due to the strong electrostatic attraction between polar water molecules and charged species in solution. In order for charged species to transfer from an aqueous to an organic phase, these strong attractive forces have to be disrupted to be replaced by weak interactions with the organic solvent. So, ΔH° for the transfer will be very large and positive, leading to a large positive value for ΔG°. In this case, K_D will be very low and almost all the charged solute will be present in the aqueous phase at equilibrium. In order for a species to extract significantly into an aqueous phase, it must be uncharged.

It was suggested that a solute will be present mainly in the phase it most closely resembles in physical properties. Is there a thermodynamic rationale for this suggestion? Generally intermolecular forces are strongest between species which are closest in structure and physical properties. For example methanol interacts strongly with water by participating in hydrogen bonding. Larger alcohols bear less resemblance to water because they have large non-polar sections, which do not interact strongly with water. Nonpolar organic

molecules have strongest interaction with other non-polar organic molecules with similar structures. This allows good structural alignment thereby maximising the Van de Waals forces.

Consider a theoretical experiment involving two phases, p1 and p2, and a solute s1. If s1 is closest in physical properties to p1, the transfer of s1 from p1 to p2 will involve endothermic enthalpy change. For the reverse process the enthalpy change has the same magnitude but is exothermic. ΔG° for the forward process will be positive (assuming $|\Delta H^\circ| >> |T\Delta S^\circ|$), therefore at equilibrium the solute (s1) will be present mainly in p1. This conclusion is based on looking at solute-solvent intermolecular forces.

It should be noted that enthalpy change can arise from changes in the level of disruption of solvent-solvent intermolecular forces caused by solute molecules. An increase in disruption will occur when a solute transfers to the solvent it least 'resembles'. So, enthalpy change from this source is in the same direction as enthalpy change caused by changes in solvent-solute interactions.

2.5 (d) The Application of Solvent Extraction to Trace Metals Analysis

Often in trace metals analysis the initial step is to get the analyte elements into solution. Acid digestion of the sample material is commonly used to achieve this. This provides an aqueous solution which will suffice as the aqueous phase in a solvent extraction system.

As metal ions in aqueous solution will not extract significantly into an organic phase, it is necessary to form a metal species which is uncharged, in order to facilitate extraction. Any water molecules coordinated to the metal must be replaced so that the metal species does not resemble the aqueous solvent. Strong extraction can be encouraged by producing a metal species which 'resembles' the organic phase.

Complex formation and ion association are used to form metal species which meet the requirements for good extraction. Complex formation can be achieved by simple monocoordination or by using organic chelating agents. A mixture of these two approaches is also possible. In forming a complex, water

molecules in the coordination sphere of the metal ion are replaced. Organic chelate complexes 'resemble' the organic phase making good extraction likely.

The formation of coordination complexes with negatively charged ligands, can lead to charge neutral complexes being formed. Complexes of this type can be readily extracted into organic solvents. For example, Ge^{4+} extracts as $GeCl_4$ from strong HCl solutions into organic solvents [47][48].

Charged complexes will only be strongly extracted as ion association compounds; the charged complex associates with counter ions to form an ion association compound. For example, the species $[Fe^{II}(1,10\text{-phenanthroline})_3{}^{2+}, (ClO_4^-)_2]$ will extract into nitrobenzene from aqueous solution [49].

2.6 ION EXCHANGE CHROMATOGRAPHY

Ion exchange chromatography allows the separation of metal ions in a sample solution. Anion exchange resin is used as a stationary phase with aqueous (usually) sample solution providing a mobile phase. The resins consist of synthetic cross-linked polymers with attached ionisable functional groups [50].

Cation exchange resins have negatively charged functional groups associated with positively charged counter ions. Cation exchange occurs when a sample solution (mobile phase) is passed through the resin. Cations in the solution can replace the resin counterions and therefore be absorbed by the resin. Anions and charge neutral species remain unabsorbed.

Anion exchange resins have positively charged functional groups associated with negatively charged counter ions. Anions in sample solution are absorbed onto the resin in a manner analogous to the absorption of cations by cation exchange resin.

Bio-Rad AG 1-X8 anion exchange resin was used in work reported in this thesis. The resin is made of polymer chains formed by the copolymerisation of styrene and a small proportion of divinyl benzene. The structure of this resin is shown below.

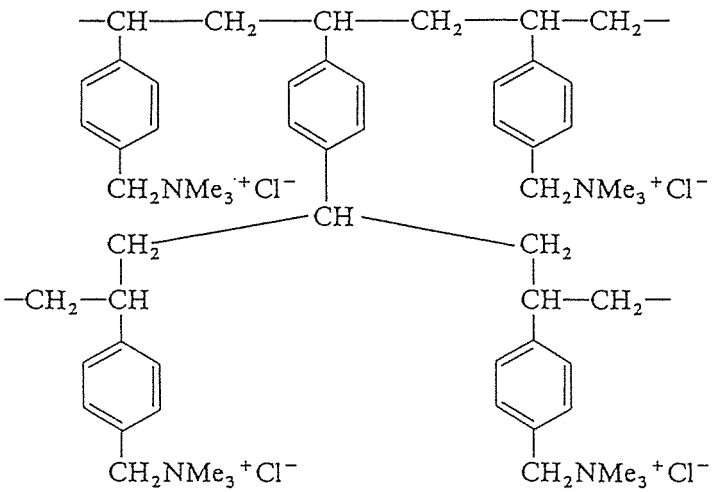

The functional groups are substituted into the ring structure using chloromethylation followed by reaction with trimethylamine [51].

2.7 MATERIALS

(i) Reagents

Ammonium pyrrolidine dithiocarbamate.—BDH Spectrosol.
Concentrated hydrochloric acid.— BDH Analar 35.4% HCl.
Concentrated hydrofluoric acid.—Merck Pro Analysi 40% HF.
Concentrated nitric acid.—BDH Analar 70% HNO_3.
Concentrated perchloric acid.—Baker 'Baker Analysed' reagent, 70% $HClO_4$.
Aqua regia.—Preparation: Mix one part (by volume) concentrated HNO_3 with three parts concentrated HCl.
HNP acid solution.—Preparation: Mix equal volumes of concentrated HF, HNO_3, and $HClO_4$.
2-Mercaptobenzothiazole.—May and Baker Pronalys (AR)
Methyl isobutylketone (MIBK).—May and Baker Laboratory Chemical

PGM complexes (spectrographically pure).—Matthey SPECPURF $(NH_4)_2IrCl_6$, $(NH_4)_2RhCl_6$, $(NH_4)_2Ru(H_2O)Cl_5$,and $(NH_4)_2OsCl_6$

Platinum solution.— BDH 1000 µg/l platinum chloride in 1N HCl

S-(1-decyl)-N,N'-diphenylisothiouronium bromide (DDTU).— Preparation: Reflux 11.6 g of n-decyl bromide with 11.4 g of N,N'-diphenylthiourea in 12 ml 98% ethanol for 6 hours. Transfer the product to a beaker and evaporate the solvent. Dissolve the residue in 75 ml of CCl_4. Treat the solution with activated charcoal (0.1 g). Filter the solution through a Whatman no. 542 filter paper. Evaporate the CCl_4 and dissolve the residue in $CHCl_3$. Filter the solution through a Whatman no. 540 filter paper and evaporate the $CHCl_3$. The residue is DDTU, a characteristic viscous orange coloured liquid.

(ii) Standard

PTC-1 flotation concentrate._ Canadian Certified Reference Materials Project standard ore.

(ii) Stock Solution.

1% (w/v) PTC-1 solution._ Preparation: Add 1 g PTC-1 and 10 ml HNP acid solution to a 25 ml Teflon™ beaker. Heat over a sandbath until fumes of $HClO_4$ have disappeared. Add 16 ml of aqua regia and evaporate the solution down to 5 ml. Wash the solution into a separatory funnel with 5 ml of 6 mol/l HCl and shake for five minutes with 10 ml MIBK. Pour the aqueous phase into a 100 ml volumetric flask containing 10 ml of distilled deionised water. Make the solution up to 100 ml with 3 mol/l HCl.

CHAPTER THREE

INVESTIGATION OF METHODS FOR THE SEPARATION OF THE PLATINUM GROUP METALS FROM A GEOLOGICAL MATRIX

3.0 NICKEL SULPHIDE FIRE ASSAY/ICP-MS DETERMINATIONS

3.0 (a) Introduction

The advent of inductively coupled plasma source mass spectrometry (ICP-MS) has given the analyst increased capabilities in the area of trace metals determinations. The sensitivity of this technique matches or betters that of GF-AAS for many elements, and it has the capability of performing rapid multi-element determinations on solutions. Because the technique determines relative isotopic abundances, isotope dilution can be used to overcome many matrix effect problems.

All the PGM can be determined in solutions at ng/ml levels or lower, using ICP-MS (see Figure 2.14). Such high sensitivities are required if the technique is to be used to determine PGM concentrations in boundary clays. Access to ICP-MS facilities was sought to allow this possibility to be studied. Facilities at Memorial University, Newfoundland, Canada were made available. A collaborative research project was pursued with Professor Henry Longerich of the Earth Science Department, Memorial University.

If ICP-MS is to be used to determine PGM levels in a geological sample, the analyte elements must first be extracted from the material into a suitable solution. Fire assay procedures are commonly used as an initial extraction step.

Three main functions are performed by fire assay fusions:

(1). A breakdown of the sample matrix. Silicates, chromites and other materials which are resistant to attack can be broken down by fire assay fusions. Analyte elements released from these materials then accumulate in the collection material.
(2). A concentration enrichment of the analyte elements. For example, PGM from 20 g of sample material can be concentrated in a silver prill of only a few milligrams in weight, using the lead assay.
(3). Collection of the analyte elements in a simplified matrix of known composition. The collector material is almost always a simpler matrix than the

original sample. As the bulk matrix of the material varies little for different samples, standard chemical treatments of the collector can be used with confidence.

Fire assay procedures have been used since biblical times [52]. Yet the first known comprehensive account of fire assay procedures was not published until 1574 A.D. [53]. Until the beginning of this century little research was carried out into the collection of the PGM using these procedures. Today fire assay procedures are used in conjunction with a wide range of instrumental techniques to determine PGM in geological materials.

In the classical fire assay technique, noble metals are collected in a lead button containing a few mg of silver. Cupellation of the button then gives a silver prill containing the other noble metals [54]. These procedures require specialist furnace equipment and can lead to losses of Os, Ru, and Ir [55].

Other fire assay techniques have been developed because of the losses for some noble metals. These techniques are best classified in terms of their collector materials. The most common alternative collectors are NiS, Fe/Cu/Ni alloy, and Sn.

It was decided to investigate the potential of the NiS fire assay system as a collector of PGM from K/T boundary materials. Because the technique uses a lower fusion temperature (1,000 °C) than the other techniques mentioned, no specialist furnace equipment was required.

3.0 (b) Nickel Sulphide Fire Assay

(i) The Fusion Process

The NiS fire assay procedure involves fusing the geological sample with a mixture containing a flux and elemental Ni and S. During the fusion, Ni is oxidised and sulphur is reduced to form a molten bead of NiS. The PGM collect in the NiS phase of the fusion melt.

Robert *et al* used NiS beads of about 25 g in weight to collect PGM from sample weights of typically 50g [56]. For work with K/T boundary materials, smaller samples and bead weights are desirable. This is because, often only small quantities of sample material are available. All the fusions in this study used 0.5-1.0 g sample weights, and quantities of fusion material that give a bead weight of about 0.9 g.

To perform a fusion, the sample is mixed with about 0.4 g of S, 0.64 g of Ni, 1.2 g of $NaCO_3$, 2.4 g of $Na_2B_4O_7.10H_2O$, and 0.4 g Si. The mixture is then transferred to a fire-clay pot. To begin a fusion the pot is placed in a furnace at 600 °C and the temperature is allowed to rise to 1,000 °C. The pot is then left in the furnace at this temperature for 90 minutes. Then it is removed and allowed to cool. To obtain the NiS bead, the pot is placed inside a cloth and broken with a mallet. The bead does not adhere to the slag and is easily removed.

(ii) Pot Manufacture and Design

Pots of different designs were produced. Each design was tested to see if it afforded easy removal of the bead after fusion and good separation of the bead from the slag. The best pot was found to be one with a conical shaped cavity, slightly rounded at the bottom to allow a spherical bead to form. It was found that the pot base needed to be at least 1 cm thick to prevent cracking of the pot and spillage of the contents. Figure 3.0 shows one of the pots intact, and also a pot that has been broken open after fusion, to reveal a silvery NiS bead.
The fusion pots were produced by the following steps:

(1). Clay (Winstone modelling clay) was placed in a plaster-of-Paris mould.
(2). A moistened pear-shaped flask was rotated down into the clay to form the pot cavity.
(3). The clay was allowed to dry partially and then the pot was removed from the mould.
(4). The pot was further dried in an oven at 100° C for 12 hours.
(5). The pot was fired at 1,000 °C for two hours.
Figure 3.1 shows a pot being shaped, using a plaster-of-Paris mould and a pear-shaped flask.

Figure 3.0 Fire Assay Pots

Figure 3.1 Moulding an Assay Pot

(iii) Nickel Powder Purity

Significant levels of the PGM are often present in Ni ores. For this reason commercially available Ni powders and compounds are often contaminated with PGM. This problem was observed with a nickel powder obtained from a Canadian source (INCO); high blanks were observed when this powder was used to prepare samples for analysis by GF-AAS. Determination of Ir and Rh in the powder by INAA (0.28 and 0.43 μg/g respectively), confirmed that the powder was heavily contaminated. The determination was carried out at Dalhousie University using a Slowpoke research reactor.

Contamination problems were greatly reduced by obtaining high purity nickel powder from INCO, via a New Zealand welding products manufacturer. The powder had been purified by the carbonyl process. ICP-MS analyses of reagent blanks showed only low level contamination.

3.0 (c) Elemental Separations and ICP-MS Analyses

(i) Matrix Constraints for ICP-MS Analyses

The PGM contained in a NiS bead can be taken into solution by dissolving the bead in aqua regia. Unfortunately such a solution is not suitable for ICP-MS analysis. Problems with high acid concentration can be overcome by boiling the solution down to constant boiling HCl and then diluting by a factor of three. Matrix problems associated with the presence of dissolved bead constituents are not easily solved. One such problem is salt buildup when solutions containing more than 1000 μg/ml of dissolved salts are analysed [57]. A problem more specific to bead solutions, involves signal enhancement or suppression (depending on the element being detected) due to the presence of Ni. As little as 50 μg/ml of Ni can cause significant matrix effects [58].

Clearly the PGM need to be separated from the major constituents of the NiS bead before they are determined by ICP-MS.

(ii) Insoluble Sulphide Filtration

Robert *et al* [56] used a simple procedure to separate the PGM in a NiS bead from the major bead constituents . They dissolved a crushed NiS sulphide bead in HCl, and filtered off the residue containing insoluble PGM sulphides. The authors used this separation technique to handle milligram quantities of the PGM. There is however, no guarantee that the metals are insoluble when they are in microgram quantities. An experiment was conducted to check whether PGM in microgram quantities can be filtered off after bead dissolution. The following steps were performed:

(1). An artificial sample containing known amounts of Ir was prepared.
(2). Subsamples of this material were processed by NiS fire assay, thereby producing NiS beads.
(3). The beads were crushed and dissolved in concentrated HCl.
(4). The resulting solutions were filtered by Millipore and Whatman 452 filters.
(5). The filters were ashed in 20 ml beakers.
(6). Aqua regia was added to the beakers and boiled down to constant boiling HCl.
(7). The resulting solutions were diluted to 2 mol/l strength HCl and then analysed by ICP-AES for Ir. In all cases the Ir recoveries were found to be lower than 5%. This indicates the filtering process is an ineffective method for separating the PGM from the base metals of the bead when the metals are in microgram quantities.

(iii) Anion Exchange Separation.

Kraus and Nelson [59] investigated the absorption of metal ions onto an anion exchange resin (Bio-Rad AG 1-X8) from HCl solutions ranging from 0.1 to 12.0 mol/l in concentration . They found that Ni^{2+} was not significantly absorbed by the resin from any of the solutions tested. Yet they found all the PGM can be absorbed depending on the conditions. Thus, their findings indicate anion exchange may offer a means of separating the PGM from the Ni in the bead solution.

The absorption of metal ions from HCl solutions onto Bio-Rad AG 1-X8 resin is due to the formation of their anionic chloro-complexes. The nature of the complexes formed and their stabilities are dependent on the metals involved, their oxidation states and the HCl concentrations. The affinity of the metal for the resin is therefore dependent on these factors.

A scheme was devised to prepare samples for analysis by ICP-MS using Bio-Rad AG 1-X8 resin. The scheme is as follows:

(1). Collect PGM in a NiS bead.
(2). Dissolve the bead in 20 ml of aqua regia and filter off the sulphur precipitate.
(3). Ash the filter paper containing the sulphur in a furnace.
(4). Redissolve the ash in aqua regia.
(5). Combine the aqua regia solutions and boil down to a volume of 5 ml.
(6). Dilute this solution to give 30 ml of approximately 1 mol/l HCl.
(7). Prepare a column of height 6 cm with Bio-Rad AG 1-X8 resin which has been equilibrated with 1 M HCl.
(8). Pass 30 ml of sample solution through the column.
(9). Wash the column with 0.1 mol/l HCl until most of the Ni has been removed.
(10). Remove the resin from the column and allow the resin to dry.
(11). Post the resin to Memorial University for ICP-MS analyses.
Once the resin had been received at Memorial University it was ashed and the ash was dissolved in aqua regia to take the PGM into solution. This solution was then evaporated to low volume, diluted, and analysed for the PGM by ICP-MS.

A 0.5 g sample of PTC-1 was analysed using the scheme outlined above. Eluant fractions were collected when Ni was eluted from the column. Most of the Ni is removed from the column in the first 40 ml of eluant. The 40-45 ml eluant fraction contained only 30 μg/ml of Ni. Washing of the column with 0.1 mol/l HCl was stopped after 45 ml of eluant had been collected. A reagent blank was processed in the same manner as the sample. Analyte concentrations obtained for the reagent blank were subtracted from those obtained for the sample, to give true sample values. The observed PGM abundances in PTC-1 were all well below the recommended values, the best value being for Pt with 42% of the recommended value. No recovery was observed for Ru and Os. This was

expected as the volatile tetroxides of these elements should have been lost from boiling aqua regia.

(iv) Separation by Coprecipitation.

Following the disappointing results obtained using the anion exchange resin separation method, a new procedure was tried. This involved an attempt to co-precipitate the PGM with Te, from an HCl solution in the manner described by Marhenke and Sandell [60].

Steps (1) to (5), of the separation scheme given in subsection 3.2 (c), were used to process a 0.5 g sample of PTC-1. The resulting solution was diluted to give a solution with approximately 2 mol/l strength HCl. The solution was then sealed in a glass vial and sent to Memorial University along with a reagent blank solution. Tellurite was then added to the solutions. This was reduced with $SnCl_2$ to give a Te metal precipitate. The precipitate was then filtered off and dissolved in aqua regia. The resulting solution was diluted fifty times and analysed by ICP-MS. From the results obtained, concentration values for the PGM in PTC-1 material were calculated. For Rh and Pd the values were 0.68 and 11.46 μg/g respectively, which are close to the accepted values of 0.62 and 12.7 μg/g. The calculated value for Pt was 60% of the recommended value. None of the other PGM were significantly recovered. The loss of Os and Ru, as volatile tetroxides, probably occurred when the NiS bead was boiled in aqua regia.

While this avenue of research was promising, especially in terms of determining Pd and Rh in geological materials, changes in funding policy at Memorial University made it impossible for us to continue using the ICP-MS facilities there. It was therefore necessary to seek other methods of determining the PGM in geological materials.

(v) Distillation of Volatile Tetroxides

Dissolution of Os and Ru in boiling aqua regia results in the loss of these elements (as volatile tetroxides) to the atmosphere. In order to try and determine Os and Ru a new approach was tried which did not involve

dissolution in aqua regia. The approach involved distillation of Ru and Os tetroxides from a flask containing a crushed NiS bead and $HClO_4$ (hot perchloric acid readily oxidises Os and Ru to the octavalent state [61]). The volatile tetroxides were distilled over into a separating funnel containing a collection liquid (perchloric acid).

Figure 3.2 shows the equipment used for the distillations. The equipment is the same as that used to determine Os isotope ratios in geological materials (work not reported in this thesis) [31]. In that work, OsO_4 was distilled over into a separating funnel along with perchloric acid. The OsO_4 was then extracted into chloroform and then back-extracted into 0.5 mol/l sulphuric acid containing thiourea. This gave analyte solutions with the same bulk composition for each sample, which could be analysed directly by ICP-MS.

The distribution coefficient (K_D) for the distribution of OsO_4 between chloroform and 70% perchloric acid is 13 [62]. Using lower acid concentrations (down to about 25% $HClO_4$) does not alter the coefficient [62]. For phases of equal volume, a distribution coefficient of 13 equates to a percentage extraction of 93%. Because this value is known, a correction can be made to the final analytical results to allow for the incomplete extraction. The back-extraction of Os into a solution of thiourea in sulphuric acid, occurs because of the reduction of OsO_4 to the charged $[Os(NH_2.CS.NH_2)_6]^{3+}$ species, which is hydrophilic. Complete extraction occurs even when the organic phase volume is five times greater than the aqueous phase volume [62]. Therefore the back-extraction step can be used to give a concentration enrichment.

The separation scheme for Os mentioned above was tested to see if Ru separation occurs in the same manner. This is possible because the elements have similar chemical properties. A trial distillation of Ru showed that more than 99.5% of the element distils over into the collection vessel in the first 5 ml of distillate. When the distillate was equilibrated with an equal volume of chloroform only 81% extraction was observed. These results were obtained by analysing the solutions by ICP-AES.

The 81% extraction of Ru into chloroform was disappointingly low. However this level of extraction was not necessarily a true reflection of the distribution of RuO_4 between the aqueous and organic phases; some of the Ru in the distillate may have been of a lower oxidation state. The RuO_4 compound is

Figure 3.2 Distillation Apparatus

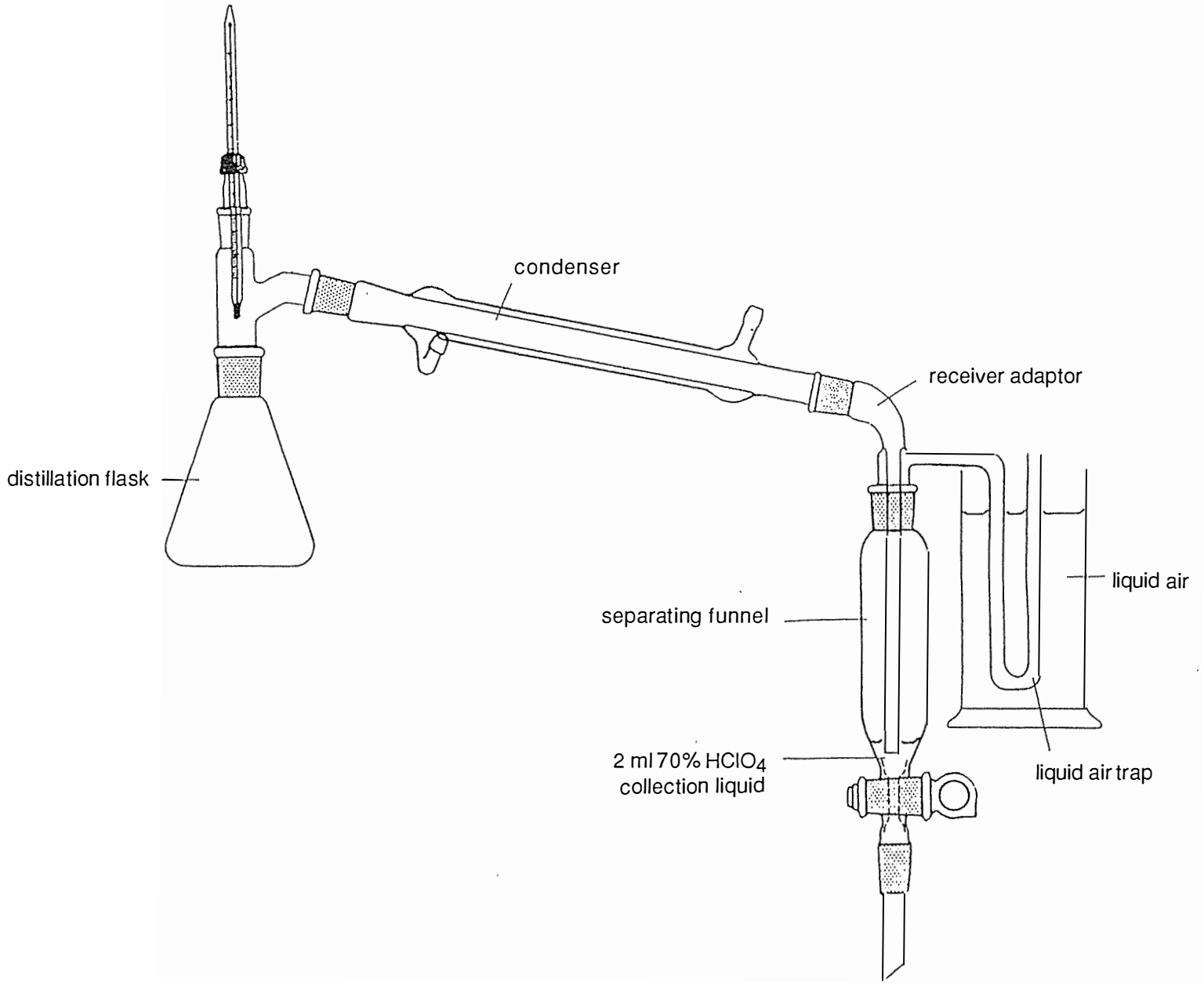

more easily reduced than OsO_4. This factor has been used to separate Os from Ru [63]. Unfortunately organic impurities in chloroform can reduce RuO_4 and thus prevent Ru extraction [64].

A second distillation of RuO_4 was carried out followed, as before, by an extraction into chloroform. This time, redistilled chloroform and oxidising agent ($NaIO_4$) were added to the aqueous phase. From ICP-AES analyses of the aqueous phase before and after extraction, a distribution coefficient of 38 was determined for the system. The distribution coefficient for the previous extraction was only 4.3 (81% extraction).

Unlike Os, Ru does not back extract from chloroform into a sulphuric acid thiourea solution. A Ru compound analogous to $[Os(NH_2.CS.NH_2)_6]^{3+}$ can be formed. However its formation requires prolonged heating in the presence of hydrochloric acid, ethanol, and thiourea [65]. Back extraction can be performed into alkaline solution [66], or solutions containing reducing agents such as sulphurous acid [67]. This promising line of research was abandoned because of funding policy changes for ICP-MS facilities at Memorial University.

(vi) Colorimetric Determination of RuO_4 in Chloroform

During work with chloroform extractions, a colorimetric method was discovered which allows levels of RuO_4 in chloroform to be determined. The discovery occurred when a cu vette containing RuO_4 was washed out with acetone. A dark brown colour developed in the washings.

Mixtures of acetone and chloroform in different proportions, containing RuO_4, were tested in order to find a mixture suitable in colorimetric tests. A mixture containing equal volumes of chloroform and acetone was found to give a good compromise of absorption intensity and stability. Full colour development occurred within two minutes of mixing. Figure 3.3 shows a molecular absorption spectrum for such a solution containing 50 μg/ml Ru (100 μg/ml Ru in the original chloroform). Figure 3.4 shows a calibration curve for the system.

3.1 IODIDE COMPLEX ANION EXCHANGE

The use of anion exchange resin to separate the PGM from a geological matrix was mentioned in subsection 4.0 (c). This relied on the formation of the anionic chloro-complexes of the PGM. The highest recovery obtained was 42% for Pt. The Pd^{2+} ion is classed as a soft acceptor [68]. It forms stronger complexes with I^- than the less polarisable Br^- and Cl^- anions. In the presence of I^-, Pd^{2+} forms the $[PdI_4]^{2-}$ species [69]. Similarly Pt^{2+} is a soft acceptor which readily forms the $[PtI_4]^{2-}$ species in the presence of I^- [69]. The use of HNP mixed acid solution (see Section 2.7) to digest a geological sample is likely to oxidise any Pt to Pt^{4+}. In solution, Pt^{4+} preferentially binds with I^-, rather than with Br^- and Cl^- [70]. The species formed is probably $[PtI_6]^{2-}$. The absorption of $[PdI_4]^{2-}$ and $[PtI_6]^{2-}$ onto anion exchange resin was investigated.

3.1 (a) Distribution Coefficients

Bio-Rad AG 1-X8 resin was found to strongly absorb Pt^{2+} and Pd^{2+} from a solution of 1% KI in 2 mol/l HCl. The distribution coefficients for this process were found to be 320 and 480 respectively. The following steps were used to determine these values:

(1). Take a quantity of Bio-Rad AG 1-X8 resin which has been equilibrated with a 1% solution of KI in 2 mol/l HCl.
(2). To the resin add a known mass of a 1% solution of KI in 2 mol/l containing known masses of Pt^{2+} and Pd^{2+} species.
(3). Shake the solution and resin for half an hour.
(4). Determine the masses of Pt and Pd remaining in the aqueous phase.
(5). Calculate the masses of Pt and Pd which are absorbed on the resin.
(6). Calculate the distribution coefficient using the following formula:

$$K_D = \frac{A_{res} \times M_{soln}}{A_{soln} \times M_{res}}$$

A_{res}, is the mass of analyte in the resin after equilibration.
A_{soln}, is the mass of analyte in the solution after equilibration.
M_{res}, is the mass of the resin.
M_{soln}, is the mass of the solution.

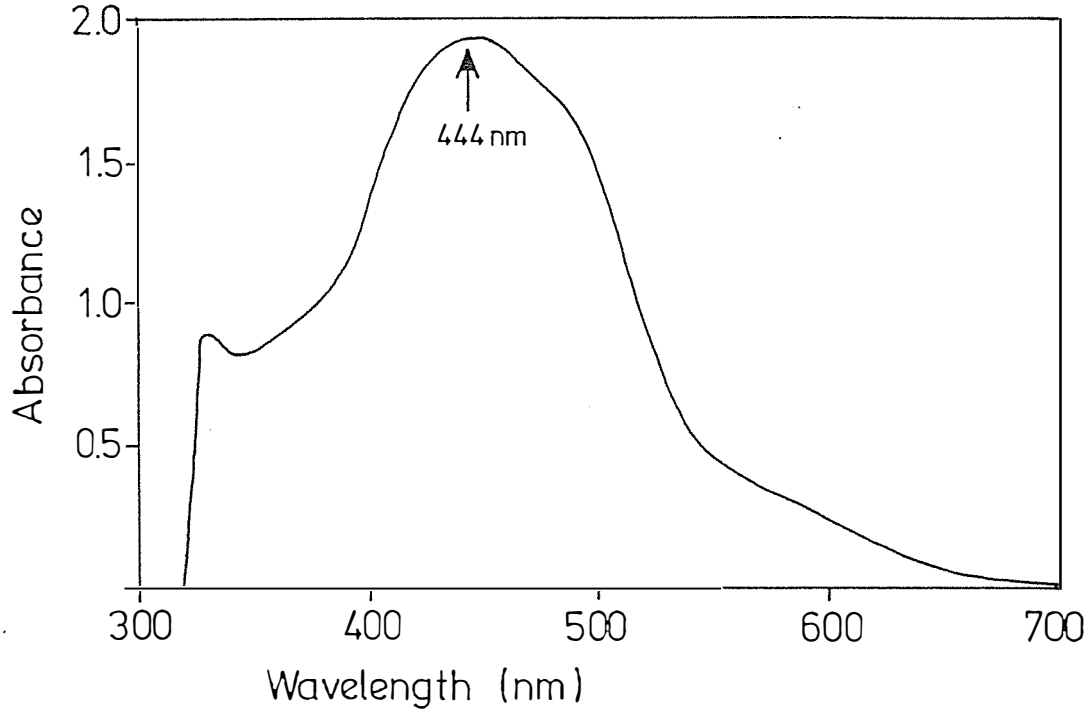

Figure 3.3 Molecular Absorption Spectrum

The molecular absorption spectrum due to a Ru species, formed when acetone was added to a solution containing RuO_4 in chloroform. The volume of acetone added was equal to the volume of chloroform present. The inital chloroform solution contained 100 μg/ml of Ru. Therefore the acetone/chloroform mixture contained 50 μg/ml of Ru. The spectrum was obtained using a Shimadzu UV-160A u.v.-vis. molecular absorption spectrophotometer.

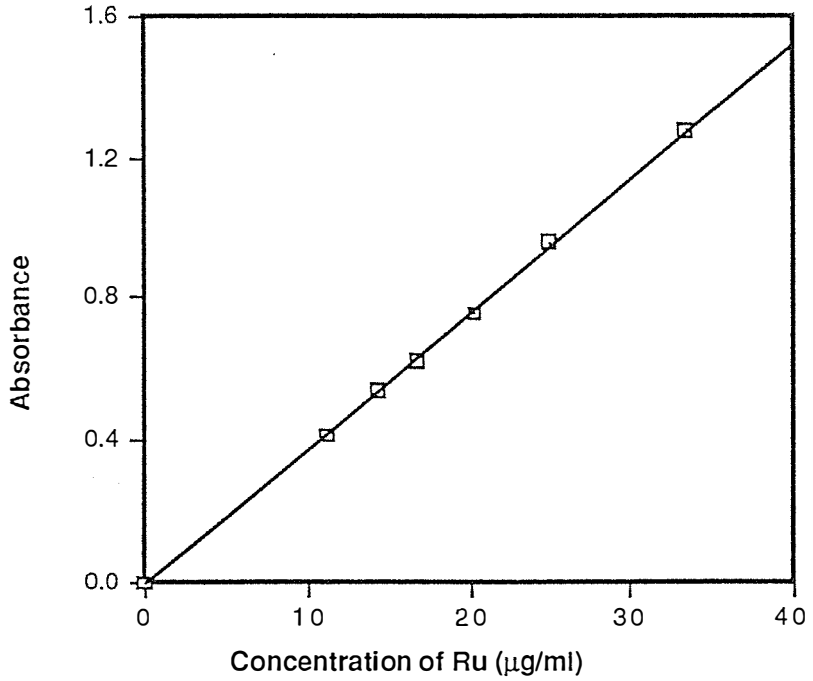

Figure 3.4 Calibration Curve for the Determination of Ru in Chloroform

Variation of absorbance, with the concentration of Ru in a 1:1 mixture of chloroform and acetone. The absorbances were detertermined using u.v.-vis. molecular absorption spectrophotometry at a wavelength of 444 nm. The absorbing species is formed when acetone is added to a solution containing RuO_4 in chloroform.

For a column of resin of height, h, and cross-sectional area, A, the volume of eluant, V, needed to elute an analyte element is given by the formula,

$$V = h \times A \times (i + K_D).$$

The symbol i, represents the fractional interstitial space (usually *ca.* 0.5) in the packed column. If $K_D > 100$ this term becomes insignificant and the equation simplifies to,

$$V = h \times A \times K_D.$$

If h is 5 cm, and A is 0.75 cm^2, then V for Pt is 1,800 cm^3, and V for Pd is 1,200 cm^3.

3.1 (b) Elution Trial

To test the feasibility of separating Pt and Pd iodide complexes from other metals in geological samples, an experiment was carried out using PTC-1 standard ore.

A 2% PTC-1 solution was prepared (see Section 2.7). Then 5 ml of this solution was mixed with 0.5 ml of 10% KI solution; unfortunately a precipitate formed. The addition of more iodide solution (1 ml of 100% KI solution) caused the precipitate to dissolve. Then the analyte solution was passed through a column of Bio-Rad AG 1-X8 resin (h = 5 cm, and A = 0.75 cm^2).

The column was washed with 2 mol/l HCl. Eluant fractions were collected and these were monitored for K, Cu, Ni, and Fe by F-AAS. Elution curves for these metals are shown in Figure 3.5. The initial fractions contained very high concentrations of K, Cu, Ni, and Fe. These concentrations were well outside the linear sections of the F-AAS response curves. However, no attempt was made to dilute the solutions. This was because the aim of the experiment was to determine how much eluant was required to elute most of the K, Cu, Ni, and Fe; this does not require the metal concentrations in the initial fractions to be known.

Figure 3.5 shows points (marked with arrows) on the elution curves where the metal concentrations drop to 1 μg/g. After 18 ml of solution have passed

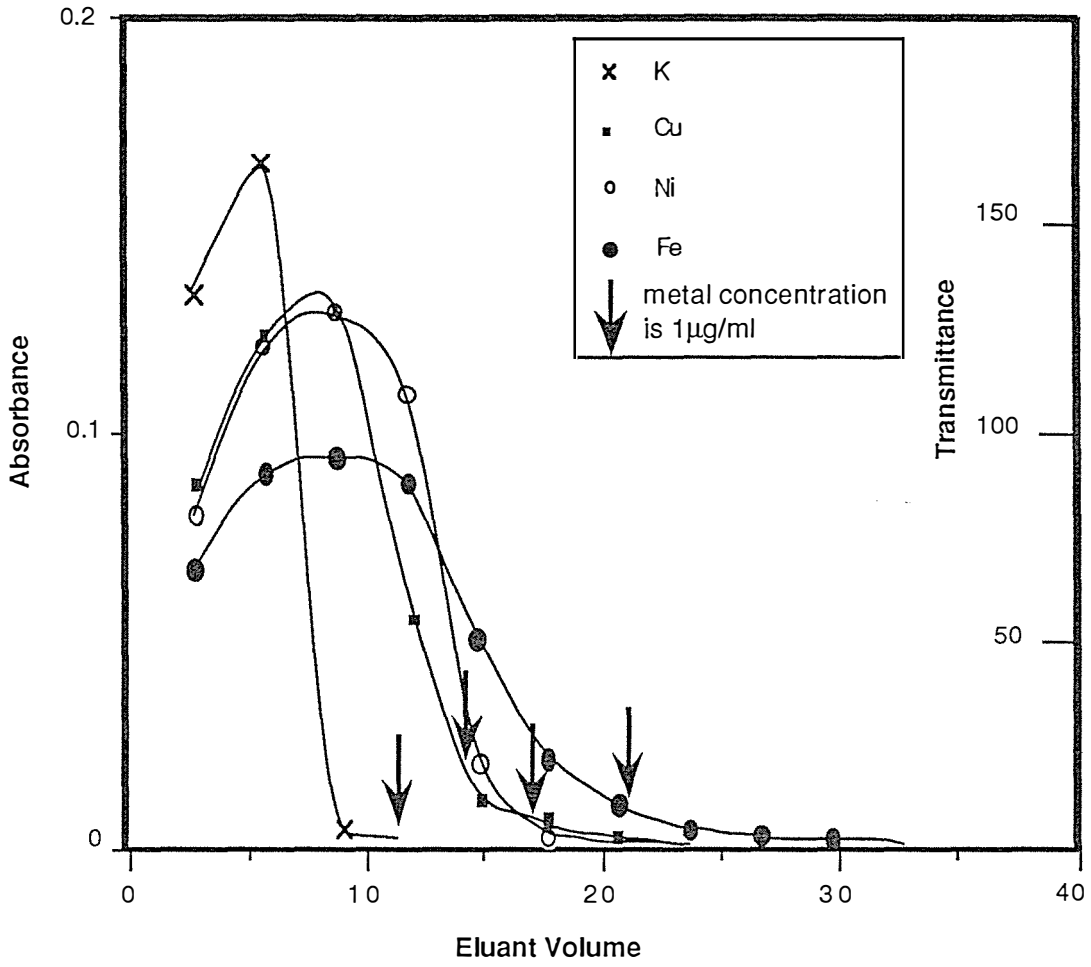

Figure 3.5 Elution Curves for PTC-1 Constituents from Anion Exchange Resin

Plot of absorbance (and transmittance) for four metals in eluant fractions, as determined by F-AAS (and F-AES), versus volume of solution eluted from a column of Bio-Rad AG 1-X8 resin. The inital sample solution which passed through the column was a mixture of a 2% PTC-1 solution and a KI solution. Then a 2 mol/l HCl solution (eluant) was passed through the column. Arrows indicate where the concentrations of metals in the eluant have fallen to 1 µg/g. Absorbances were determined for Cu, Ni, and Fe, by F-AAS. Transmittances were determined for K, by F-AES.

through the column the K, Cu, Ni, and Fe concentrations in the eluant have all dropped below 2 μg/ml.

3.1 (c) Replicate Determinations of Platinum and Palladium in PTC-1

Replicate determinations of platinum and palladium in PTC-1 were performed. The following steps describe the process used to perform each determination:

(1). Equilibrate some Bio-Rad AG 1-X8 resin with a solution of 1% KI in 2 mol/l HCl.
(2). Use the resin to prepare an ion exchange column of height 5 cm and cross-sectional area of 0.75 cm^2.
(3). Add 1 ml of 100% KI solution to 5 ml of 2% PTC-1 solution, to give 6 ml of analyte solution.
(4). Pass the analyte solution through the resin.
(5). Wash the column with 2 mol/l HCl until 18 ml of eluant has been collected.
(6). Place the resin in a Pyrex beaker and dry the resin in an oven at 100 °C.
(7). Ash the resin at 500 °C in a muffle furnace.
(8). Dissolve the ash with 5 ml of aqua regia.
(9). Boil the aqua regia until only approximately 1.5 ml of solution remains.
(10). Take 0.5 ml of solution and dilute it five fold with 6 mol/l HCl. Analyse the dilute solution for Pd using GF-AAS.
(11) Take some of the undiluted analyte solution and determine its Pt content using GF-AAS. The furnace program used for Pt determinations in aqueous solutions is given in subsection 2.0 (e).

In all, one reagent blank and eleven sample determinations were performed. The results are shown in table 3.0. Including blank subtraction, a value of 10.4 μg/g was obtained for the concentration of Pd in PTC-1, with a standard deviation of 1.8 μg/g. The recommended concentration value is 12.7 μg/g. The precision and accuracy of the technique are too poor for it to be used to analyse geological samples for Pd. The results for Pt were much lower than the recommended value, indicating the high iodide concentration required to prevent precipitation may have suppressed the absorption of Pt by the resin.

TABLE 3.0 REPLICATE DETERMINATIONS OF PLATINUM AND PALLADIUM IN PTC-1 BY GF-AAS

Sample Number	Mass of the Analyte Solution (g)	Volume of the Analyte Solution (ml)	Absorbance Reading for Pd in Diluted (5x) Solution	Concentration of Pd in Diluted (5x) Analyte Solution (μg/ml)	Mass of Pd in Undiluted Analyte Solution (μg)	Concentration of Pd in PTC-1 (μg/g)	Absorbance Reading for Pt	Concentration of Pd in Analyte Solution (μg/ml)	Mass of Pt in Analyte Solution (g)	Concentration of Pt in PTC-1 (μg/g)
1	1.414	1.288	0.212	0.197	1.27	12.7	0.201	0.179	0.231	2.3
2	1.687	1.536	0.133	0.123	0.95	9.5	0.057	0.051	0.078	0.8
3	1.600	1.457	0.174	0.102	1.18	11.8	0.067	0.060	0.087	0.9
4	1.930	1.758	0.114	0.106	9.3	9.3	0.070	0.063	0.110	1.1
5	1.845	1.680	0.129	0.119	1.00	10.0	0.117	0.105	0.180	1.8
6	2.130	1.940	0.153	0.142	1.38	13.8	0.085	0.076	0.147	1.5
7	1.970	1.794	0.117	0.108	0.97	9.7	0.046	0.041	0.074	0.7
8	1.951	1.777	0.115	0.106	0.94	9.4	0.680	contamination	—	—
9	1.733	1.578	0.159	0.147	1.16	11.6	0.096	0.068	0.135	1.4
10	1.864	1.698	0.138	0.128	1.09	10.9	0.071	0.063	0.108	1.1
11	1.896	1.727	0.134	0.124	1.07	10.7	0.058	0.052	0.089	0.9
blank										
mean results						10.8				1.2

3.2 SOLVENT EXTRACTION OF A RHODIUM CHELATE COMPLEX

3.2 (a) Studies of Extraction from Pure Solutions

Ryan [71] found Rh could be extracted from HCl solutions into chloroform after the formation of Rh chelate complexes with substituted 2-mercaptothiazole compounds. Diamantatos [72] used 2-mercaptobenzothiazole (2MBT) to extract Rh and Ir into chloroform. In a later paper Diamantatos described a separation scheme involving the use of 2-mercaptobenzothiazole to extract Rh and Ir into MIBK from HCl solutions [73]. The author reported that following the addition of 2MBT, it was necessary to heat the acid solutions to effect complex formation.

An attempt was made to extract Rh and Ir from a pure 6 mol/l HCl solution, using the 2MBT/MIBK system. While 100 % extraction was achieved for Rh, only 69 % extraction was achieved for Ir. No further investigation into the extraction of Ir was carried out because this element is easily determined by NAA, and because even if matrix separation was achieved, Ir determinations in boundary clays would not be possible using our GF-AAS instrumentation (the technique is not sufficiently sensitive for Ir).

An experiment was conducted to determine the effect that varying the acid concentration of the aqueous phase, has on the distribution coefficient for Rh extraction. For the extractions, 0.005 g of 2MBT was added to 25 µg of Rh in each HCl solution. The results of the experiment are plotted in Figure 3.6. The values of K_D were calculated using the following formula:

$$K_D = \left(\frac{Mi}{Mf} - 1\right) x \left(\frac{Va}{Vo}\right)$$

Mi is the mass of Rh in the aqueous phase before extraction.
Mf is the mass of Rh in the aqueous phase after extraction.
Va is the volume of the aqueous phase.
Vo is the volume of the organic phase.

The strongest extraction occurred where the HCl concentration in the aqueous phase was 6 mol/l. This was the strongest acid concentration used in the trial.

Higher acid concentrations were not used because this increases the solubility of the MIBK in the aqueous phase [74].

Obviously the degree of complex formation has a major bearing on the degree of extraction. This is influenced by the heating time. It was found that at least 50 minutes of heating is required to achieve maximum Rh extraction. A heating time of 60 minutes was chosen for subsequent analyses to ensure maximum extraction. Curiously Diamantatos [73] found full extraction occurred after only 15 minutes of heating.

3.2 (b) Extraction from a Geological Matrix

Diamantatos [73] used the 2MBT/MIBK extraction system to facilitate the determination of Rh in Cu-Ni converter matte. In his scheme, most of the base metals in the matte were removed by dissolution with HCl, followed by filtering.

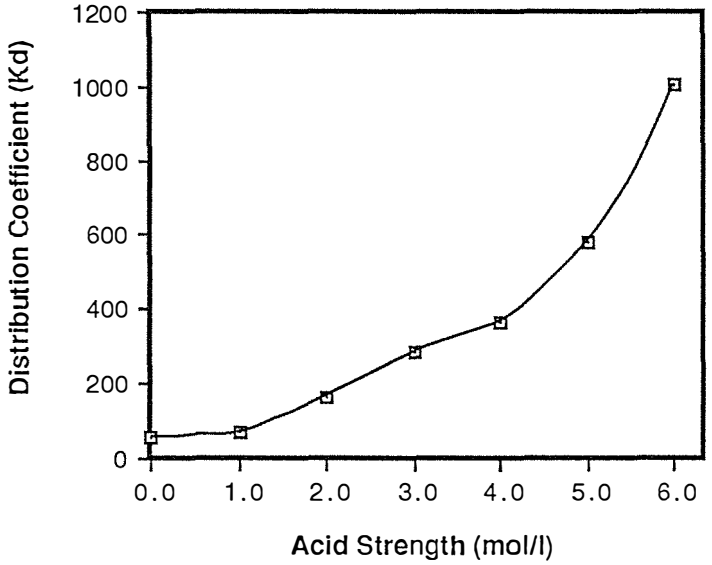

Figure 3.6 Optimization of Acid Concentration for Rh Extraction

Variation of the distribution coefficient with acid strength, for Rh extraction from HCl solutions, into MIBK. The extractions involved using 2-mercaptobenzothiazole (2MBT) as a chelating reagent. For each extraction, 5 ml of an HCl solution containing 5 µg/ml of Rh, was mixed with 0.5 ml of a 1% solution of 2MBT in ethanol. The mixing was performed in test-tubes. Each tube was then placed in boiling water for one hour. Then 5 ml of MIBK was added to each tube, and the aqueous and organic phases were equilibrated for ten minutes to allow extraction to occur. Determinations of the masses of Rh remaining in the aqueous phases, after equilibration, were performed by GF-AAS using the 343.5 nm absorbance line.

The insoluble PGM were then filtered off for further processing. As mentioned in subsection 3.0 (c), a procedure such as this is not suitable for the determination of the PGM in K/T boundary sediments. This is because there is no guarantee that the PGM can be filtered off when they are in nan ogram quantities. At these levels the PGM may be soluble, or form colloidal aggregations which may pass through the filter.

The determination of Rh in PTC-1 standard ore, using the 2MBT/MIBK extraction system, was attempted without using an initial HCl dissolution and filtration step. A 1% PTC-1 solution was produced (see Section 2.7). Then 5 ml of this solution was added to a test-tube along with 0.5 ml of 2MBT. As before, the tube was placed in boiling water for an hour to allow complex formation. This was followed by the usual equilibration with MIBK. This procedure was performed for five aliquots of the PTC-1 solution. Unfortunately Rh was not found in any of the five MIBK phases. This was probably due to the scavenging of the 2MBT ligand by other metals in the solution.

Subsequent determinations of Rh in PTC-1 were performed with higher levels of 2MBT. A large excess of 2MBT can lead to the formation of a precipitate which does not completely dissolve during the extraction with MIBK. So, it was necessary to have a level of 2MBT in the extractions which would allow Rh to be extracted into the organic phase, but not cause the formation of a precipitate.

When 0.02 g of 2MBT is used in an extraction involving 5 ml volumes of PTC-1 solution and MIBK, no precipitate remains after equilibration, and the subsequent analysis of the MIBK phase for Rh indicates that PTC-1 has a Rh abundance of 0.74 μg/g. This value is significantly higher than the recommended value of 0.62 μg/g.

The MIBK phase (after extraction) exhibited a deep orange colour. This indicated that high concentrations of other metals had been co-extracted with the Rh. Thus the high results for Rh could have been due to matrix effects. Determinations of Rh in the MIBK phase using standard additions, gave a more credible result; PTC-1 was determined to have a Rh abundance of 0.67 μg/g. This result represents the mean result of ten determinations having a relative standard deviation of 6.6 %.

Toluca (iron) meteorite has microgram quantities of the PGM contained within a simpler matrix than PTC-1. An attempt to determine Rh in Toluca, without standard additions, was successful; replicate determinations gave abundances of 1.1, 1.0, and 1.0 μg/g which compare well with the value of 1.1 ± 0.1 μg/g determined by Nichiporuk and Brown [75], and 1.28 μg/g determined by Ryan et al [76]. The procedure used to determine Rh in Toluca meteorite was as follows:

(1). Accurately weigh about one gram of meteorite shavings into a Teflon beaker.
(2). Add 10 ml of HNP mixed acid solution (see Section 2.7) to the beaker, and evaporate to dryness on a sandbath.
(3). Repeat step (2).
(4). Add 16 ml of aqua regia to the beaker and evaporate down to about 5 ml of solution on a sandbath.
(5). Shake the remaining 5 ml of acid solution with 5 ml of MIBK. Separate the phases and retain the aqueous phase (raffinate) for further processing. This step removes most of the Fe from the aqueous solution.
(6). Add the raffinate to a 100 ml volumetric flask, and make it up to the mark with 6 mol/l HCl. Shake the flask.
(7). Take an aliquot of 2 ml from the volumetric flask, and place it in a test-tube with 1 ml of 1 % 2MBT/ethanol solution. Place the tube in boiling water for an hour.
(8). Cool the tube to room temperature. Add 1 ml of MIBK to the tube and mix the phases for ten minutes.
(9). Following equilibration, determine Rh in the MIBK phase by GF-AAS.

Two Flaxbourne River K/T boundary samples were analysed for Rh. A full description of the Flaxbourne River K/T boundary sequence is given in Chapter 6. The two samples chosen, were the samples containing the highest Ir abundances. Sample (A) was removed from the interval -2 to -1 cm below the boundary. Sample (B) was removed from the interval 0 to +1 cm above the boundary. Each sample was analysed three times using a modification of the procedure used for Toluca meteorite. For the boundary samples, step (6) of the procedure was deleted, and step (5) was altered so that the acid solution was evaporated down to 2 ml. Standard additions were not used. This is because the most abundant base metal constituents of PTC-1 (Fe,Cu,Ni) should not cause

interference problems with boundary sediment Rh determinations; the concentrations of Cu and Ni in boundary clays are generally less than 1% of their concentrations in PTC-1 and Fe is removed anyway.

Both sets of analyses gave extremely poor precision. For (A) the results were 5.2, 3.7, and 4.5 ng/g; for (B) they were 1.0, 2.3, and 2.9 ng/g. Due to the imprecision of the results, no meaningful conclusions could be drawn from the data. Further investigations may lead to refinements in the method that would allow it to be applied to boundary sediments.

3.3 THE DDTU/MIBK SOLVENT EXTRACTION SYSTEM

Jones *et al* have reported an extraction system for the PGM involving the S-(1-decyl)-N,N- diphenyl isothiouronium (DDTU) ligand [77]. They investigated the extraction of various PGM ions from HCl solutions into a 5% solution of DDTU in diisobutylketone (DIBK). Their choice of DIBK as the organic solvent was made because they consider it to be the best solvent for direct determinations by F-AAS. They noted that DDTU is also soluble in MIBK. So, the extraction system could also be used with this solvent.

Extractions of Rh^{3+}, Pd^{2+}, and Pt^{4+} ions were investigated using the DDTU/MIBK system. These oxidation states were chosen because they are the most likely states to occur in a rock solution under oxidising conditions. The extractions were performed from a range of HCl solutions into a 5% solution of DDTU in MIBK. Distribution coefficients for the extractions were calculated. The method used to determine the distribution coefficients was the same as that used for the 2MBT/MIBK system (see subsection 3.2 (a)). The analyses of the aqueous phases were performed by F-AAS. Table 3.1 lists the distribution coefficients for the extractions.

The levels of extraction achieved for Rh and Pt were too low to warrant further investigation of the system for these elements. The distribution coefficients for Pd, indicate that the DDTU/MIBK extraction system could be used in a separation scheme to facilitate the determination of Pd in geological materials. However this was not pursued because the APDC/MIBK system offers superior levels of extraction for this element.

Table 3.1 Distribution Coefficients for the Extraction of Rhodium (3+),Palladium (2+),and Platinum (4+) from HCl Solutions into a DDTU/MIBK Solution

Hydrochloric Acid Strength (mol/l)	Distribution Coefficient (KD)		
	Rh^{3+}	Pd^{2+}	Pt^{4+}
2.0	18	76	28
3.0	11	55	26
4.0	5	49	20
5.0	2	49	9
6.0	0	16	8

The extraction of Ru, Os, and Ir with the DDTU/MIBK system, was not investigated; Jones *et al* showed the extraction efficiencies for these elements were too low to use in separation schemes where a concentration enrichment is required. The poor sensitivity of GF-AAS for Os and Ir would prevent their determination in boundary sediments, even if they could be separated from the bulk geological matrix.

3.4 THE APDC/MIBK SOLVENT EXTRACTION SYSTEM

3.4 (a) Introduction

The analytical significance of ammonium pyrrolidine dithiocarbamate (APDC), as a ligand for metal complexes extractable into methyl isobutyl ketone (MIBK), was first suggested by Malissa and Schoffmann [78]. Following this early report, numerous other workers employed extraction of APDC-metal complexes into organic solvents (usually MIBK) for the determination of trace elements in brines [79], and seawater [37]. There have however, been very few examples of the use of the APDC extraction system for samples other than natural waters, although there has been a report of its use at pH 2.4 for determining heavy metals in fish samples [80] and for precipitation at pH 3 of heavy metals directly onto a graphite furnace preparatory to electrothermal atomic absorption analysis [81].

Although extraction of metal-APDC complexes from aqueous solutions in the pH range 2-14 has been considered the standard procedure, it has not

previously been appreciated that some of these complexes can be extracted from strongly acidic solutions (which are essential to make solutions of geological materials).

An initial experiment indicated that Pd is greatly extracted from 2 mol/l HCl into MIBK, when APDC is used as a chelating agent. This indicated the possibility that other metals — including other PGM— would extract as APDC complexes from strong acid solutions.

The extraction of PGM into MIBK from a range of HCl and HNO_3 solutions, was investigated. Acid concentrations up to 6 mol/l were used. Concentrations above 6 mol/l cannot be used for solvent extraction because of the increased miscibility of the MIBK with the aqueous phase. Also, experiments were carried out to see if the PGM are extracted from HCl solutions into MIBK (without the use of APDC) as their chloro-complexes. Strong extraction of these would indicate that extraction where APDC was present, might also be due to the chloro-complexes.

3.4 (b) Experimental

The extractability of PGM-APDC complexes was determined by equilibrating equal volumes of organic or aqueous phases, and determining the concentrations of the metal ions in the aqueous phases before and after equilibration. When extraction was not excessively great, it was possible to carry out these determinations by F-AAS. When extraction was very great, so that the residual metal concentrations in the aqueous phases were very small, determinations of the metal concentrations were performed by GF-AAS.

Extractions were carried out on 5 ml aliquots of three sets of solutions prepared as follows:

(1). Solutions of 0, 0.5, 1.0, 2.0, 3.0, 4.0, 5.0, and 6.0 mol/l HCl.
(2). As for (1) but with addition of 0.01 g APDC to each aliquot.
(3). HNO_3 solutions of the same strength as (1) and with the addition of 0.01 g APDC to each aliquot.

The original metal ion concentrations in the aqueous phases ranged from 10-200 µg/ml, depending on the analytical sensitivity of the metals concerned. The

oxidation state of each metal was chosen to represent the most likely state expected to be found in a rock solution prepared under oxidising conditions (e.g. Pt^{4+} rather than Pt^{2+}). This was in order to approximate the actual conditions likely to be encountered in the course of the silicate rock analysis.

3.4 (c) Extraction Results and Discussion

Figure 3.7 shows the percentage extraction into MIBK of six PGM ions as a function of concentrations of mineral acids, with and without addition of APDC. Table 3.2 gives values of the distribution coefficient (K_D) for the extraction of each ion from 2 mol/l solutions of HNO_3 and HCl with and without addition of APDC. An acid strength of 2 mol/l is the minimum strength required for a stable rock solution.

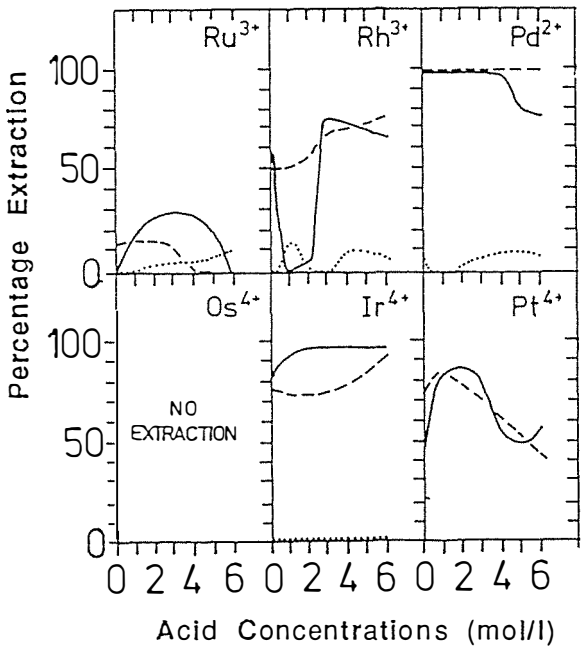

Figure 3.7 Curves for the Extraction of PGM Complexes into MIBK
Variation of extraction of PGM species into MIBK from hydrochloric and nitric acid solutions, with and without addition of APDC; (——) HNO_3 + APDC; (-----) HCl + APDC; (·····) HCl only.

Table 3.2 Values of K_D for the Extraction of PGM Ions into MIBK from Acid Solutions with and without APDC

Ion	Aqueous Phase for Extraction		
	2 mol/l HCl	2 mol/l HCl with APDC	2 mol/l HNO_3 with APDC
Ir^{4+}	<0.01	3.00	24
Os^{4+}	<0.01	<0.01	<0.01
Pd^{2+}	0.05	8000	—
Pt^{4+}	<0.01	3.50	3.00
Rh^{3+}	0.04	1.40	0.06
Ru^{3+}	0.01	0.17	0.40

None of the PGM exhibited strong extraction from HCl into MIBK when APDC is not present. The ions, Pt^{4+} and Os^{4+} showed no extraction under these conditions. The ions, Ru^{3+}, Rh^{3+}, Pd^{3+}, and Ir^{4+} showed only slight extraction. Therefore the anionic chloro-compounds do not readily form extractible ion association complexes with cationic species in solution. Extractions involving APDC varied greatly depending on the element involved, the type of acid used in the aqueous phase, and the acid concentration. The ions mentioned in Figure 3.7 can be divided into three classes as follows:

(1). Ions which did not extract under any of the conditions tested.
(2). Ions which were extracted, but where extraction was not high enough for the method to be used in a solvent extraction scheme.
(3). Ions whose extraction was high enough under some of the conditions tested to allow the method to be used as a solvent extraction system for those ions.

The only ion in class (1), is Os^{4+}. The Ru^{3+} ion is in class (2); extraction of Ru^{3+} into MIBK never exceeds 30% under any of the conditions tested. The ions Rh^{3+}, Ir^{4+}, Pt^{4+}, and Pd^{2+} fall into class (3). All these ions have extractions of at least 70% under some of the conditions tested. The highest extraction of Rh^{3+} (76%) occurs from HCl at 6 mol/l concentration. The highest extraction for Pt^{4+} (86%) occurs from 2 mol/l HNO_3. The highest extraction of Ir^{4+} (96%) occurs from 6 mol/l HNO_3. For these elements it would be possible to achieve essentially complete extraction with two or more separate operations.

The extraction of Pd^{2+} is virtually 100% from all the HCl concentrations tested. In fact K_D for the extraction from 2 mol/l HCl into MIBK, is about 6000; it is about 3000 for the extraction from 6 mol/l HCl. Any extraction system where the values for K_D are so great, offers the potential for considerable concentration enrichment of the extractable element.

An example of this is the extraction of Pd^{2+} from say 10 ml of 2 mol/l HCl, into 1 ml of MIBK. For this extraction $K_D = 8000$.

$$\%E = \frac{K_D.R.100}{K_D.R + 1} = \frac{8000 \times 0.1 \times 100}{8000 \times 0.1 + 1} = 99.88\%$$

%E is the percentage extraction
R is the organic/aqueous phase volume ratio
Vo is the volume of the organic phase
So, the percentage of the total mass extracted is 99.88% with a ten fold concentration enrichment.

CHAPTER FOUR

THE QUANTIFICATION OF PALLADIUM IN GEOLOGICAL MATERIALS

4.0 INTRODUCTION

To determine Pd in geological samples by GF-AAS the analyte must be separated from potential chemical interferences. Solvent extraction can be used to achieve this.

In Chapter Three it was reported that Pd, as an APDC chelate complex, extracts strongly into MIBK from 3 mol/l HCl. Unfortunately this does not ensure that Pd will extract strongly from rock solutions with the same system.

A rock solution is a complex matrix. The high solids content of such a solution, can lead to the formation of a precipitate when such an extraction is attempted. If this happens, some of the analyte may be incorporated in the precipitate, and fail to be extracted into the organic phase. Other factors may prevent the satisfactory quantification of Pd in a rock solution. Interfering elements may be co-extracted during solvent extraction. Technical problems, associated with GF-AAS, can make it difficult to achieve reproducible results.

It is necessary to check that the proposed analytical method is suitable for determining Pd in geological materials. This can be done by using the method to quantify Pd in a suitable geological standard such as PTC-1 [82].

4.1 DETERMINATION OF PALLADIUM IN PTC-1

4.1 (a) Initial Investigation

A 1% PTC-1 solution was prepared (see Section 2.7). An initial attempt to extract Pd from the solution was only partially successful; the level of Pd detected in the MIBK extractant was much lower than expected. A brown precipitate was formed when APDC was added to the extraction mixture, and it remained after equilibration. Pd was probably incorporated in the precipitate.

PTC-1 contains 9.42% Ni and 5.14% Cu by weight [82]. Both elements form stable complexes with APDC in HCl solutions [83]. It is likely that Ni, and Cu, APDC complexes made up the bulk of the brown precipitate.

4.1 (b) Extraction as a Function of APDC Concentration

The degree of extraction, was found to be a function of the level of APDC present in the extraction mixture. This relationship is shown in Figure 4.0. The figure was constructed from data obtained for a series of extractions.

Figure 4.0 is divided into three sections. In section (1), there is not enough APDC to allow maximum extraction. In this section the degree of extraction increases with increasing APDC levels. In section (2), the APDC levels are sufficient to allow maximum extraction. In section (3), the degree of extraction declines as the levels of the chelate in the extraction mixture increase. In this section alone, a

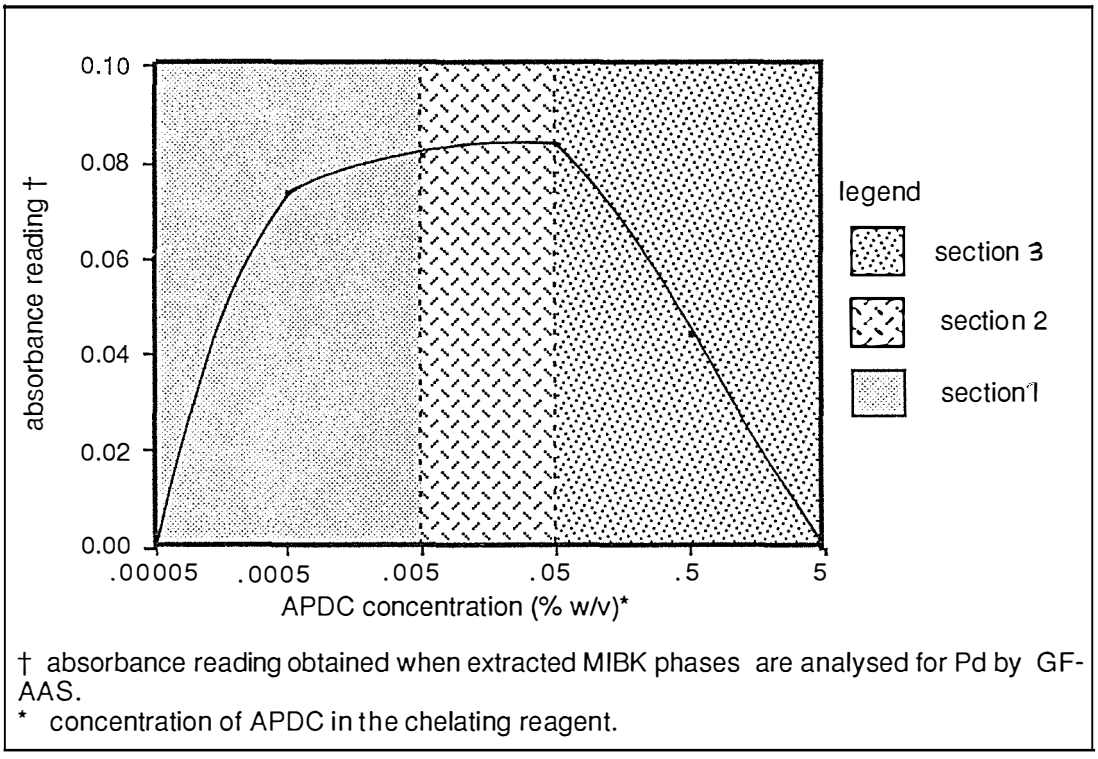

† absorbance reading obtained when extracted MIBK phases are analysed for Pd by GF-AAS.
* concentration of APDC in the chelating reagent.

Figure 4.0. Effect of APDC Levels on Extraction
Curve representing the relationship between the degree of Pd extraction (from a PTC-1 solution into MIBK), and the concentration of APDC in the chelating reagent. The degree of extraction is shown in terms of absorbances obtained when the MIBK extractant is analysed for Pd, by GF-AAS. Each extraction involved, 1 ml of chelating reagent, 3 ml of 1% PTC-1 solution, and 3 ml of MIBK; equilibration was achieved by shaking this mixture for ten minutes. Determinations of Pd in the MIBK phases, were were performed by GF-AAS, using the 247.6 nm absorbance line; 3µl furnace dryings were used.

brown precipitate forms. The amount of the precipitate increases with increasing APDC levels. The decline in extraction in this section, is probably due to an increasing proportion of the available Pd being incorporated in the precipitate.

Complexes are in equilibrium with the free ligand (L), and metal (M). The general expression (excluding charges) for this equilibrium is:

$$M + nL \rightleftharpoons ML_n$$

In PTC-1 solution, there are several metal ions which can complex with the pyrrolidine dithiocarbamato (PDC^-) ligand. Therefore, there are several competing equilibria. The solvent extraction of Pd, in this instance, is probably due to the following equilibrium (see Section 4.3):

$$Pd^{2+} + 2\,PDC^- \rightleftharpoons Pd(PDC)_2$$

The stability constant for this equilibrium, is greater than those for equilibria involving Cu and Ni metal ions; otherwise, Cu and Ni ions would scavenge the available PDC and prevent much of the Pd in solution from being complexed.

When the level of PDC in solution exceeds the amount required to complex all the Pd, PDC complexes of other elements form in significant concentrations. Once the concentrations of these complexes reach saturation point in solution, precipitation occurs.

4.1 (c) Replicate Determinations of Pd in PTC-1

A chelating reagent with a 0.05% (w/v) APDC concentration, was found to allow maximum Pd extraction under the conditions used for Figure 4.0. This reagent concentration was chosen for 14 replicate determinations of Pd in PTC-1. In each determination 3ml of PTC-1 solution, 1 ml of 0.05% APDC reagent, and 3ml of MIBK were equilibrated for ten minutes. Then the MIBK phase was analysed, by GF-AAS, to determine the concentration of Pd in the phase. So 14 concentration values were obtained. From the mean of these values, the abundance of Pd in PTC-1 standard ore, was calculated to be 12.44 μg/g. This compares to a recommended value of 12.70 μg/g [82], giving a relative error of only 2%. The precision for the analyses was 5.2%.

4.1 (d) Conclusions

The standard reference ore, PTC-1, has higher levels of the base metals (such as Fe, Ni, and Cu) than most geological materials. So, matrix effect problems make PTC-1 more difficult to analyse than most geological materials. The analytical method used, gave a value for Pd in PTC-1, which is only 2% less than the recommended value. This method should therefore be suitable for determining Pd in most geological materials. To further check the method, a PGM ore sample from the Canadian Arctic was analysed. The sample was found to contain 18.5 μg/g Pd. This differed by only 6.5% from the value reported by Lee [84].

4.2 PALLADIUM AT THE K/T BOUNDARY

The APDC/MIBK extraction system that was used to determine Pd in PTC-1 (see Section 4.1 (c)), was used to determine Pd in K/T boundary sediments. A full description of the analytical scheme used to determine Pd abundances in boundary clays, is given in Section 4.3.

A series of samples spanning the K/T boundary at the Flaxbourne River site, in New Zealand, were analysed. Table 4.0 shows the concentration of Pd in each of the samples. There is a spike of elevated Pd concentration at the boundary. In the next chapter these data are compared with the corresponding Ir data, and they are discussed with respect to the K/T boundary debate.

Table 4.0 Palladium Abundances Across the Flaxbourne River Sequence

Era	Cretaceous			Tertiary			
Sample Position	-2 to -5 cm	-2 to -1 cm	-1 to 0 cm	0 to +1 cm	+1 to +2 cm	+2 to +3 cm	+3 to +6 cm
Pd Content (ng/g)	1.1	8.9	4.5	11.5	3.1	3.0	2.6

Several other boundary materials were available to be analysed. These materials were boundary clays from; Woodside Creek, in New Zealand; Stevns Klint, in Denmark; Browny Butte, in the Raton Basin of the United States; and Bottacione, near Gubbio in Italy.

The clay layer collected from Woodside Creek was about 8 mm thick [28]. This layer was divided in half to give sections (A) and (B). Section (A) covers that half of the clay layer which is contiguous with the late Danian limestone. Section (B) covers the rest of the clay layer. The other boundary materials were not subdivided. The Pd abundances in the materials were determined. These are shown in Table 4.1. Where Ir abundances are known for the samples, they have been included in the table.

Table 4.1 Boundary Clay Ir and Pd Abundances

Boundary Clay	Pd Concentration (ng/g)	Ir* Concentration (ng/g)	Ir/Pd abundance ratio
Brownie Butte	12	_	_
Gubbio	5	_	_
Stevns Klint	14	_	_
Woodside Creek (A)	37	54	1.5
Woodside Creek (B)	15	26	1.7
Flaxbourne River (-2→ -1cm)	9	12	1.3
Flaxbourne River (0→ +1cm)	12	16	1.3

* Ir values determined by INAA at Los Alamos (see Section 2.3)

For comparison, the two Flaxbourne River samples with the highest Pd contents have been included in the table. The Ir/Pd abundance ratios for the Woodside Creek and Flaxbourne River samples are similar, ranging from 1.3 to 1.7. Assuming these elements are of asteroidal origin , the asteroid may have had a lower Ir/Pd abundance ratio than these data indicate; Pd has greater mobility than Ir under leaching conditions so during the 65 million years since the deposition of the sediments, some fractionation may have occurred.

Few data are available on the background levels of Pd in sedimentary rocks. The lowest concentration of Pd detected in a sample from the Flaxbourne river

sequence, was 1.1 ng/g. It is reasonable to take *ca.* 1 ng/g as the upper limit for the background concentration of Pd in sedimentary rocks. On this basis all the boundary materials listed in Table 4.1 have anomalous Pd concentrations.

4.3 THE EXTRACTABLE PALLADIUM COMPLEX

The analytical scheme given in Section 4.4 uses aqua regia to dissolve the Pd. The chlorine in this acid medium ensures elemental Pd is oxidised. The most important oxidation state for Pd is the +2 state. In HCl solution, Pd^{2+} exists as the $[PdCl_4]^{2-}$ species. When APDC is added to the solution, chloride ions are displaced from the coordination sphere of the metal ion to be replaced by PDC ligands. Kellner [85] gives the PDC complex of Pd^{2+} as having the molecular formula, $Pd(PDC)_2$, with a square planar geometry as is depicted below:

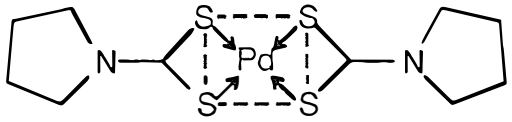

Based on infra-red spectra, Kellner [85] suggested this complex is stabilised by electron delocalisation represented by the following resonance structures:

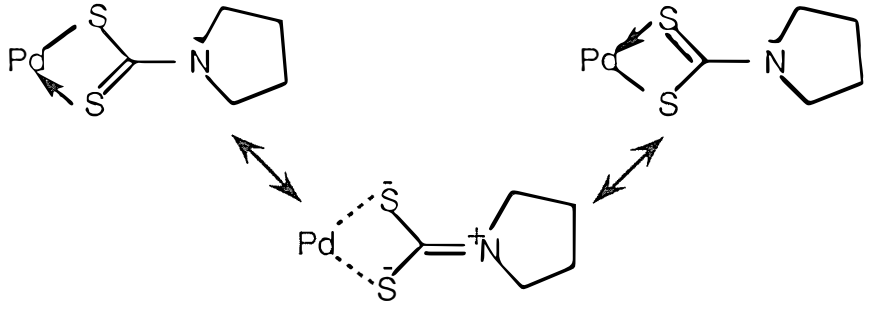

Because $Pd(PDC)_2$ is charge neutral, no ion association is required to facilitate extraction into an organic phase from HCl.

4.4 METHOD USED TO QUANTIFY PALLADIUM IN SEDIMENTS

The method used was as follows:

(1). Digest 1 g of finely powdered rock in a 25 ml Teflon beaker with 10 ml of a 1:1:1 mixture of HNO_3, HCl, and $HClO_4$. Heat over a sandbath until fumes of $HClO_4$ have disappeared.
(2). Add 16 ml of aqua regia and evaporate down to about 3ml over the same sandbath.
(3). Add 16 ml of 6 mol/l HCl and again evaporate down to about 3 ml.
(4). Shake with an equal volume of MIBK for about five minutes in a graduated centrifuge tube. Centrifuge to separate the phases and remove the organic layer with a pasteur pipette.
(5). Dilute the aqueous layer with an equal volume of water and 1 ml of 0.05% APDC in water. Then add 0.35 ml of MIBK and shake for about ten minutes and again centrifuge.
(6). Remove some of the MIBK for GF-AAS determination of its Pd content.
(7). Determine Pd in the MIBK using the GBC System1000 instrument (see subsection 2.0 (d) (ii)). Use ten 3 µl sample dryings onto the furnace using the heating cycle conditions given in Table 2.0.

CHAPTER FIVE

THE FLAXBOURNE RIVER CRETACEOUS/TERTIARY BOUNDARY SEQUENCE: A CASE STUDY

5.0 INTRODUCTION

A sedimentary sequence was sampled from the newly discovered K/T boundary site at Flaxbourne River, in New Zealand.

The record of changes occurring across a K/T boundary section can be obscured by processes such as weathering, bioturbation, and tectonic activity. Fortunately, the Flaxbourne River section is well preserved. It also has one of the most complete K/T boundary sections known. These factors make this an ideal section to examine for evidence of the bolide impact proposed by the impact theory (see Section 1.1).

As will be shown, lithological, palaeontological, and geochemical studies of the Flaxbourne River section indicate that a sudden catastrophic event occurred at the end of the Cretaceous geological period. As an alternative to the impact theory, it has been suggested that massive volcanism may have led to the deposition of the Ir rich layer found at K/T boundary sites world-wide [86][87]. This suggestion will be examined in the light of the analyses performed on samples from the Flaxbourne River section.

5.1 SITE LOCATION

The Flaxbourne River K/T boundary site, is in NZMS Quadrangle P29 (1:50,000), some 4 km southeast of the settlement of Ward, in the Marlborough province of New Zealand's South Island (see Figure 5.0). The locality lies near the mouth of the Flaxbourne River, within the belt of moderately and completely deformed upper Cretaceous and Paleogene limestone, which more or less parallels the coast for about 20 km, from the Ure River to Cape Campbell [88]. Other K/T boundary localities were previously described about 5 km away at Needles Point, and 2 km away at Chancet Rocks [89][90][91].

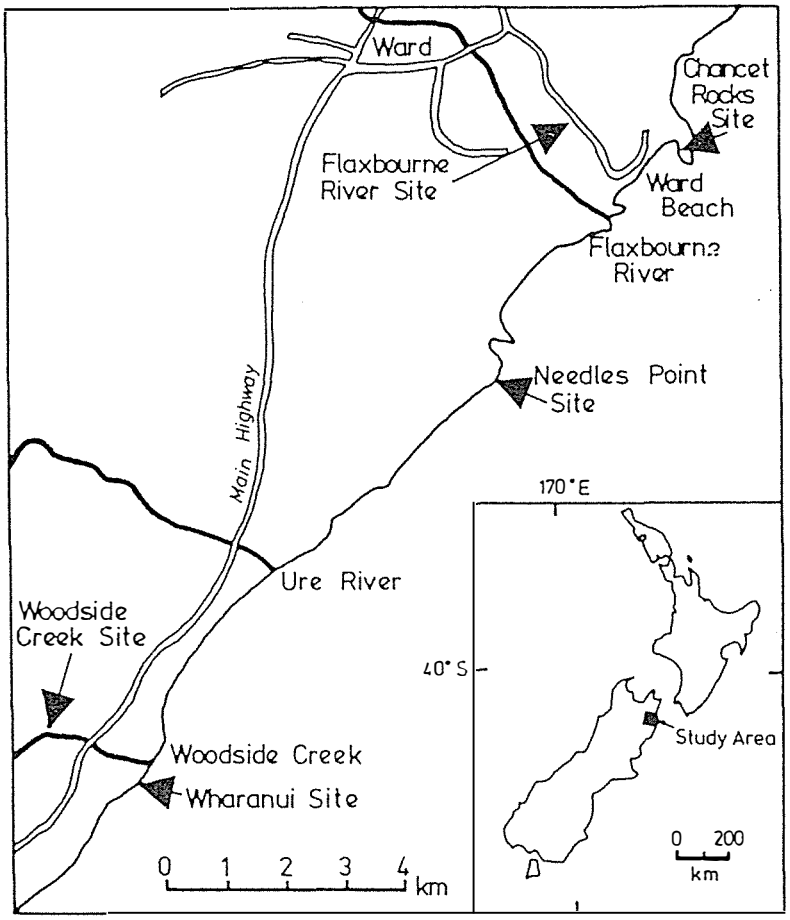

Figure 5.0 Location Map Showing the Flaxbourne River K/T Boundary Site in Relation to Other Sites in the Area

5.2 LITHOLOGY

Lithologically, the Flaxbourne River K/T boundary section is similar to the nearby Chancet Rocks section [89][90]. The essential difference between the two sites is that at Chancet Rocks the lowest few cm of the boundary interval, including the boundary clay, is usually missing owing to marine errosion of the relatively soft boundary unit, and infilling of the resultant cleft with sediment.

Figure 5.1 shows the area where sampling was carried out. The boundary section has been exposed by limestone quarrying, making it readily accessible for sampling. A closer view of the boundary is shown by Figure 5.2. The hammer head lies against the dark boundary clay. To the left of the clay lie Tertiary sediments, to the right Cretaceous.

Figure 5.1 The Flaxbourne River K/T Boundary Section

Figure 5.2 The Boundary Clay and Surrounding Sediments

A diagram of the section, in the form of a stratigraphic column, is given in Figure 5.3. The figure lists and describes nine lithologic units which can be identified in the section we sampled. The most interesting lithological changes occur in units adjacent to, and including the boundary layer (i.e. units 3-5).

Unit three is a 2-5 cm layer of soft off-white marl. This unit is not well represented at Chancet Rocks. The transition from unit 3 to unit 4 (the boundary clay) is very sharp. This transition is made particularly distinct by the sharp contrast in the colouration of the two units; the clay layer is a dark grey colour. The lower half of this layer is made up of very finely divided material, with a much lower carbonate level than the marl of unit 3. This merges into the upper half where the clay is interspersed with limestone lenses. The average depth of the boundary clay is 20 mm.

The transition from unit 4 to unit 5 is also quite sharp. The soft boundary clay gives way to a hard calcareous mudstone which is about 8 mm thick. A similar unit occurs at Chancet Rocks where it is of comparable thickness.

The boundary clay has a starkly different lithology from the zones which sandwich it. How could it have formed? There are two possibilities:

(1). The clay may have formed as a result of redissolution of carbonates in limestones and calcareous mudstones, which contain fine detrital material.
(2). The clay may have formed as a result of a sudden, drastic, change in oceanic conditions which altered the accumulation rates of the various sedimentary components. A major decrease in carbonate deposition would leave the detrital component to aggregate on the ocean floor, thereby forming the clay. Washout of atmospheric dust from a large bolide impact would dramatically increase the amount of detrital material available to form a pelagic clay.

Because the clay layer/Cretaceous marl interface is very sharp and shows no signs of errosion, the second of the two possibilities mentioned above is the one most likely to have formed the boundary layer.

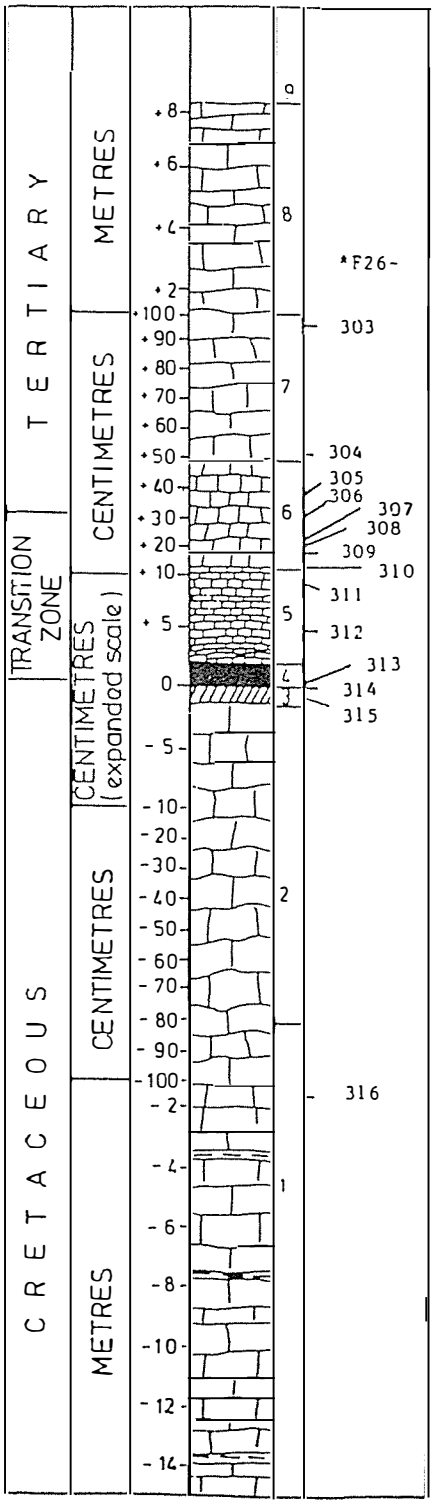

9. Limestone, massive, grey to maroon with "sponge" fossils.

8. Limestone, medium bedded, yellow-green.

7. Limestone, thick bedded, brownish weathering (18%)

6. Calc. mudstone, thin bedded, greyish green, argillaceous (28%)

5. Calc. mudstone, thin bedded, internally laminated, dark grey (39%)

4. Clay, dark grey to black (26-36%).

3. Marl, soft, off-white. Blankets irregularities on surface of underlying bed (52%)

2. Limestone, thick bed, brownish grey, hard (60%)

1. Limestone, thin to medium bedded, brownish grey, hard, with thin marly partings.

Base of exposure

Figure 5.3 Stratigraphic Column at the Flaxbourne River K/T Boundary Site

Values in parentheses are % $CaCO_3$

5.3 BIOSTRATIGRAPHY

Biostratigraphy enables the approximate age of a geological rock to be determined. Because of this, it is useful in locating and confirming the position of a K/T boundary. It can also provide evidence of environmental conditions at the time of deposition.

The position of the K/T boundary at the Flaxbourne River site was confirmed using biostratigraphy. In all, 14 samples were examined from selected positions across the sequence. These are labeled F26303-F26314 in Figure 5.3 and Table 5.0. A survey of the foraminifera in the samples, revealed the sequence to be exceptionally complete.

The sequence can be divided into the four zones shown in Table 5.0. Zone (i) contains late Cretaceous bathyal fauna in abundance. Zone (ii) begins with a boundary clay containing an Ir anomaly. As with Zone (i), it contains late Cretaceous species but the specimens are greatly reduced in size and abundance. Zone (iii) contains the first specimens of early Tertiary foraminifera. In Zone (iv), the variety and abundance of the foraminifera is reminiscent of the pre-anomaly zone, yet the specimens are all new early Tertiary forms.

A similar pattern of faunal changes across the K/T boundary sequence has been observed at other sites. In fact, Smit and Romein proposed a standard palaeontological K/T boundary sequence after studying ocean drill core samples as well as samples from land based sites [33]. All the zones of this sequence can be recognised at Flaxbourne River.

Clearly there is a faunal discontinuity at the K/T boundary contiguous with the lithological discontinuity. The pattern of faunal change points to a sudden catastrophic change in environmental conditions at the boundary, which is compatible with the impact theory.

Table 5.0 Biostratigraphic Zones Resolved from the Flaxbourne River K/T Boundary Sequence

Era	Biostratigraphic Zone	Standard Zone Equivalent†	Sample Number(s)	Lithological Unit(s)	Foraminifera	Comments
Tertiary	Zone (iv), or Early Tertiary Zone,	*Globorotalia pseudobulloides* Zone (P1c).	F26303 to F26304.	Units 7-8.	*Globoconusa daubjergensis* and undetermined *Globigerina*, *Globorotalia*, and *Chiloguembelina* species.	The variety and abundance of foraminifera are much greater than in zone (iii). Benthics make up about 1% of all the specimens.
	Zone (iii), or Tertiary Pioneers Zone.	*Globigerina eugubina* Zone (P1a and P1b).	F26305.	Upper Unit 6.	*Globigerina* cf. *fringa*, and others.	First appearance of Tertiary foraminifera species.
	Zone (ii), or Cretaceous Survivors Zone.	*Guembelitria cretacea* Zone (Po).	F26314 to F26316.	Units 4-6.	*Guembelitria cretacea*, *Heterohelix globulosa*, *H.* cf. *punctulata*, *Globigerinalloides volutus*, *Nuttalides tholus*, and others.	Cretaceous foraminifera species of much lower size and abundance than in zone (i). Benthics make up about 10% of all specimens in this post boundary zone.
Cretaceous	Zone (i), or Late Cretaceous Zone.	*Abathomphalus mayaroensis* Zone (M3).	F26315 to F26316.	Units 1-3.	*R. pustulata*, *Heterohelix globulosa*, *H.* cf. *punctulata*, *Glodigerinelloides volutus*, *Hedbergella monmouthensis*, and others.	Typical Late Cretaceous foraminifera species. Benthics makeup <1% of specimens.

†See reference [33]

5.4 GEOCHEMISTRY

5.4 (a) Collection and Storage of Sedimentary Material for Elemental Analysis

Material was taken from 26 different subsections of the of the boundary sequence spanning stratigraphic positions through -60 cm to +72 cm, with continuous sampling between -17 cm and +39 cm. The material from each subsection was ground to -100 mesh and stored in sealable plastic bags. A tungsten carbide concentric ring grinder was used to grind the samples.

5.4 (b) Elemental Determinations

(i) Determinations by Inductively Coupled Plasma Atomic Emission Spectroscopy (ICP-AES).

The sedimentary material was processed to produce solutions made up with 2 mol/l HCl (therefore suitable for analysis). These solutions were subsequently analysed by ICP-AES (see Section 2.1 for instrumental details). Concentration values for Al, B, Ca, Cu, Fe, K, Mg, Mn, Ni, P and Sr were obtained.

The processing of the sedimentary material was performed as follows:

(1). 0.5 g of each sample was placed in a polypropylene beaker over a waterbath.
(2). 5 ml of 1:1 HF/HNO_3 was added to each mixture to digest the contents.
(3). The resulting solution was evaporated to dryness.
(4). 10 ml of 2 mol/l HCl was added to each beaker to redissolve the residue.
(5). The solution was then poured into a storage container and made up to 25 ml with 2 mol/l HCl.

(ii) Determinations by Neutron Activation Analysis (NAA)

A portion of the ground material from each of the 26 subsections was sent to Los Alamos for NAA determinations. The elements Co, Cr, As, Ce, Sb, Sc, Th, and U, were determined directly in powdered rock samples by INAA; Ir was determined by RNAA. Both methods have been described by Orth *et al* [92]. Figure 5.4 illustrates the two approaches with a scheme. The RNAA method for Ir involves sample dissolution with 1:1:1 HF/HNO_3/$HClO_4$ mixed acid solution, followed by absorption of Ir on an ion exchanger.

(iii) Determinations by Graphite Furnace Atomic Absorption Spectroscopy (GF-AAS)

The levels of Pd in subsections of the Flaxbourne River sequence are taken from work reported in Section 4.2. The analytical procedure is described there also.

5.4 (c) Data Presentation

The elemental abundance data for the Flaxbourne River sequence were adjusted to convert them to a carbonate-free form. The resulting values are shown in Table 5.1. Carbonate-free data are necessary because this ensures elemental anomalies observed in the data are not merely the result of redissolution of the carbonates. A study by Orth *et al* of the Ordovician/Silurian boundary sequence underlines the importance of this measure [92]. An Ir anomaly was detected at this boundary but the authors concluded it was not the result of a large meteorite impact, as the anomaly disappears when the data are expressed on a carbonate-free basis.

The important features of the data given in Table 5.1, can be quickly recognised when they are presented in graphical form. The histograms of the Ir and Pd data given in Figure 5.5 illustrate well the strong enrichment that occurs for these elements at the K/T boundary. Do significant trends and anomalies occur for the other elements? Figure 5.6 shows how mean elemental

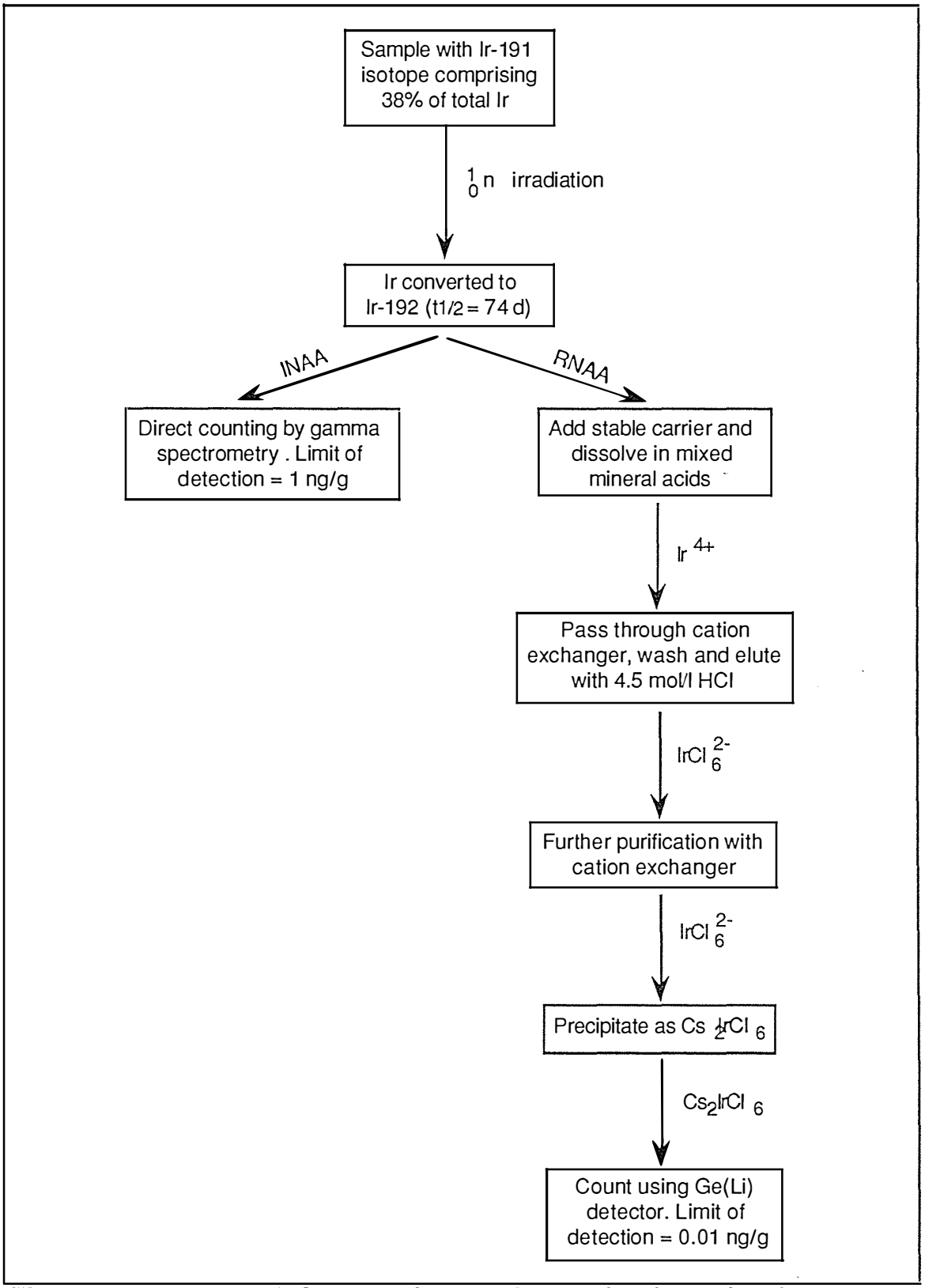

Figure 5.4 Analytical Scheme for the Determination of Ir by Neutron Activation Analysis

Table 5.1 Elemental Abundances at the Flaxbourne River K/T Boundary Sequence

Values are in µg/g unless otherwise stated, and except for $CaCO_3$ are on a decalcified basis. The K/T boundary lies in the interval 0 to +1 cm.

Position cm	Al %	As	B	$CaCO_3$ %	Ce	Co	Cr	Cu	Fe %	Ir ng/g	Pd ng/g	K	Mg	Mn	Ni	P	Sb	Sc	Sr	Th	U	Zn
-60 to -50	0.09	1.0	700	56	22.5	8.1	82	<20	0.45	0.19		1900	1400	4390	<20	510	0.5	3.8	1170	1.3	0.7	90
-22 to -17	0.78	1.8	600	49	19.6	7.5	135	30	0.39			1300	1100	2650	<20	450	1.1	2.7	930	1.6	1.5	<20
-17to -22	1.44	3.0	1100	69	54.4	18	21	65	0.80			2900	3600	5780	40	770	0.5	6.1	2050	1.3	1.4	110
-9 to -8	1.51	3.2	900	67	44.9	41	23	30	0.76	0.57		2100	3400	5440	<30	730	1.1	6.9	1930	1.6	2.1	110
-8 to -5	2.59	9.6	2700	71	65.6	63	37	85	1.21			5200	10200	6210	<40	1400	2.6	9.9	2200	4.0	4.3	240
-5 to -2	3.93	11.5	4400	81	115.3	69	55	80	1.83	2.4	5.8	8600	16400	10480	80	2180	3.5	18.0	3650	7.3	6.3	450
-2 to -1	3.38	30.9	2400	41	55.8	170	140	140	1.27	20	15.1	5800	7400	1610	160	1010	5.4	13.0	670	4.8	3.2	360
-1 to 0	3.14	10.6	1900	62	70.7	150	52	65	1.18	7.4	11.8	5200	7900	3540	90	1300	2.5	15.0	1410	4.9	3.7	330
0 to +1	4.93	29.8	2000	26	51.3	270	130	260	2.09	21	15.5	8100	10600	880	280	680	5.5	13.9	380	9.2	3.1	730
+1 to +2	3.14	3.4	1300	36	42.4	91	47	110	1.18	2.1	4.8	6200	7400	1340	80	790	1.4	8.0	660	4.8	1.4	370
+2 to +3	3.72	14.0	4100	32	45.3	110	56	140	1.46	8.3	4.4	6600	7900	1100	130	730	3.7	10.7	570	5.1	1.9	360
+3 to +6	2.44	4.6	3000	45	35.0	69	38	100	0.94	5.3	4.7	4600	6200	1250	50	610	1.4	7.9	580	4.0	1.4	310
+6 to +8	2.96	6.1	1600	43	53.9	79	34	190	1.39	1.0		5800	8000	1910	110	790	1.9	8.7	740	5.2	1.2	380
+8 to +9	2.94	5.1	1900	37	46.1	69	21	170	1.19			6400	7700	1510	240	760	1.6	7.7	620	4.2	1.4	230
+9 to +12	4.17	7.5	1500	33	67.1	54	37	190	1.46	1.2		6600	10800	1190	120	1340	2.5	14.9	470	6.7	2.2	270
+12 to +13	6.08	10.0	2100	34	54.7	52	36	240	2.13			12200	13600	1370	150	990	2.8	13.9	560	8.2	1.6	190
+13 to +15	4.19	6.1	2500	30	44.0	48	41	150	1.78			7800	9500	1140	100	600	1.9	12.0	420	8.6	1.4	160
+15 to +21	3.58	3.8	1000	26	28.3	18	27	140	1.42			7400	9100	950	70	510	1.3	9.2	390	5.8	1.1	110
+21 to +23	3.12	3.9	1900	23	28.6	15	21	65	1.24			6400	6600	850	50	440	1.0	8.9	360	4.6	0.9	120
+23 to +26	3.65	3.5	1200	26	35.1	17	34	55	1.35	0.36		7400	10600	880	70	500	1.0	10.0	410	5.6	1.0	120
+26 to +28	3.63	3.0	1200	24	30.4	19	44	80	1.32			7300	8900	860	70	520	0.9	9.8	370	6.4	1.1	110
+28 to +33	2.73	3.0	900	30	37.1	25	41	35	0.98			5200	6900	820	40	400	0.7	7.3	310	4.7	1.0	110
+33 to +36	3.92	5.7	1900	29	40.6	20	30	55	1.75			7700	10200	1120	80	770	1.1	10.7	440	6.4	1.1	120
+36 to +39	3.44	5.5	1100	20	37.5	22	28	20	1.31			6900	7700	750	40	460	1.2	9.8	300	5.0	1.0	80
+48 to +52	2.88	3.0	500	17	34.8	14	27	20	0.96	0.23		5900	8100	540	30	270	0.8	7.6	250	5.0	1.0	80
+70 to +72	3.08	1.8	800	19	64.3	17	27	25	1.23	0.21		7400	9000	680	40	1230	0.5	8.6	340	5.0	1.1	<20

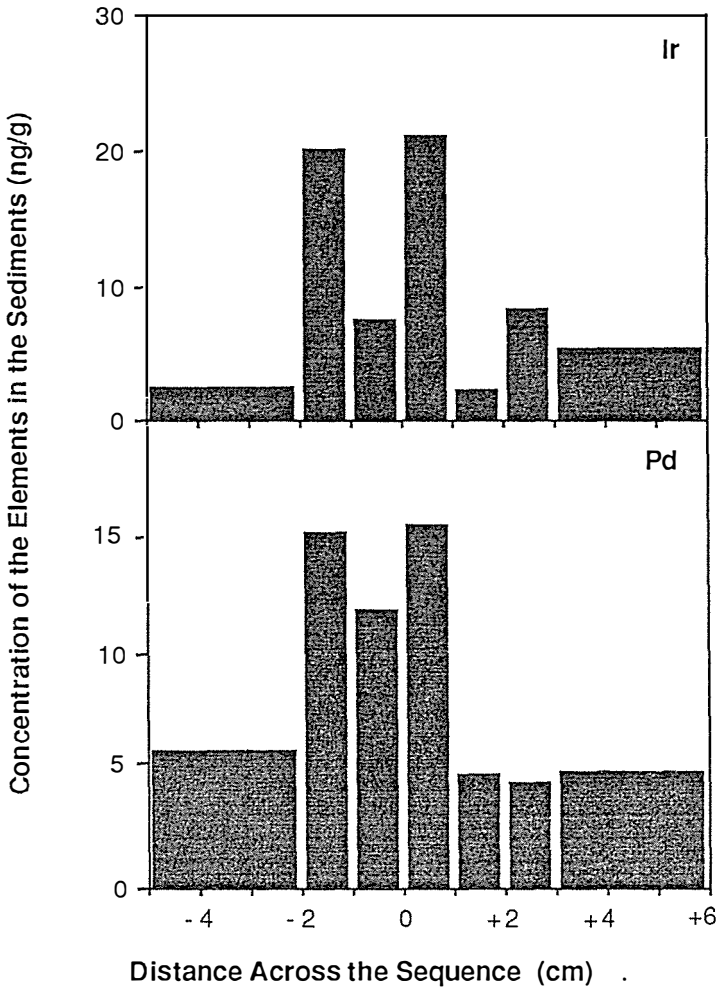

Figure 5.5 Iridium and Palladium Abundances in the Vicinity of the K/T Boundary

Concentrations of Ir and Pd in contiguous samples taken from the Flaxbourne River K/T boundary Sequence. The palaeontological K/T boundary occurs at 0 cm on the horizontal scale. Enrichment is observed for both Ir and Pd in the vicinity of the boundary. The concentration values are on a $CaCO_3$ free basis.

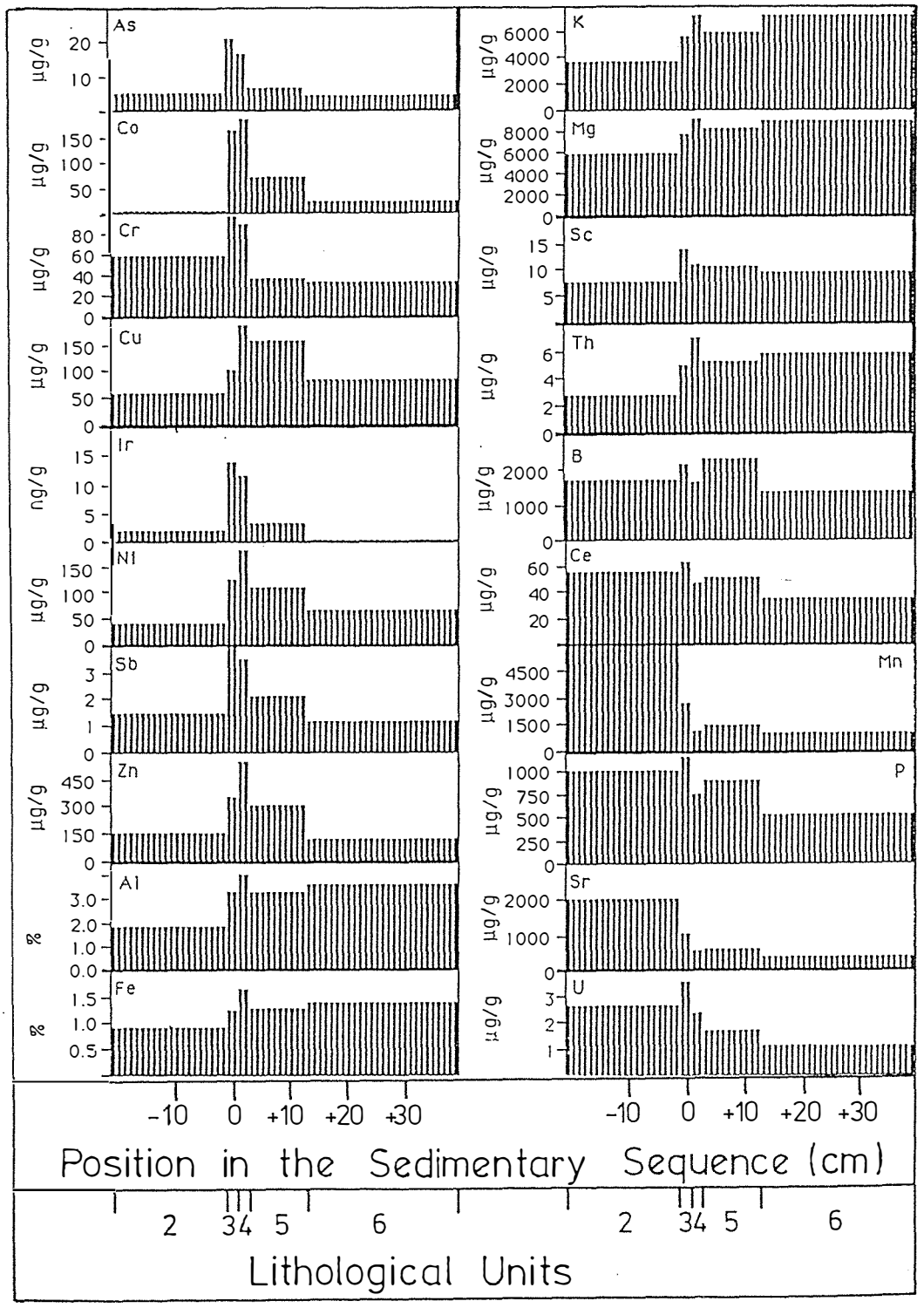

Figure 5.6 Mean Elemental Abundances in Lithological Units of the Flaxbourne River K/T Boundary Sequence

The abundances are expressed on a decalcified basis.

abundances vary between different lithologic units and highlights some striking differences in the geochemistries of the units.

The first grouping of elements in this figure contains As, Co, Cr, Cu, Ni, Sb, and Zn. These elements show an enrichment in the vicinity of the boundary (concomitant with that of Ir and Pd) and then return to their previous levels. The elements Cr, Co, and Ni are depleted in crustal rocks relative to meteorites like their fellow siderophiles, Ir and Pd. Therefore some of the excess of these elements at the boundary may be derived from a meteoritic source. The other four elements (all chalcophiles) in the first grouping of figure 5.6, do not have significantly higher concentrations in meteorites than in crustal rocks. The source of their enrichment at the K/T boundary must be terrestrial.

In the next grouping, the elements Al, Fe, K, and Mg, are enriched at the boundary but remain at high levels in the Tertiary sediments. These elements are found in high levels in aluminous clays. It is probable that the K/T event led to a lasting change in sedimentation patterns leading to an increase in aluminous clay deposition.

The last four elements (Mn, P, Sr, and U) show a marked decrease in the Tertiary sediments. This may be an artefact of calculating the elemental abundances on a carbonate free basis, which is only valid if the elements concerned are present in the clay fraction. It is likely the aforementioned elements are part of the carbonate fraction. If this is so, the histograms are erroneous.

The greatest error would occur for sediments with the highest carbonate contents. Why is this so? A high level of carbonate in a sample would supply a high level of Mn, P, Sr, and U to be detected and then be erroneously attributed to the clay fraction. The error is then exaggerated by calculation to a carbonate free basis, because an enrichment factor is used. To make matters worse, the enrichment factor increases with increasing carbonate content. The observed decrease of Mn, P, Sr, and U levels in the Tertiary sediments may simply reflect a decrease in the carbonate content of the sediments.

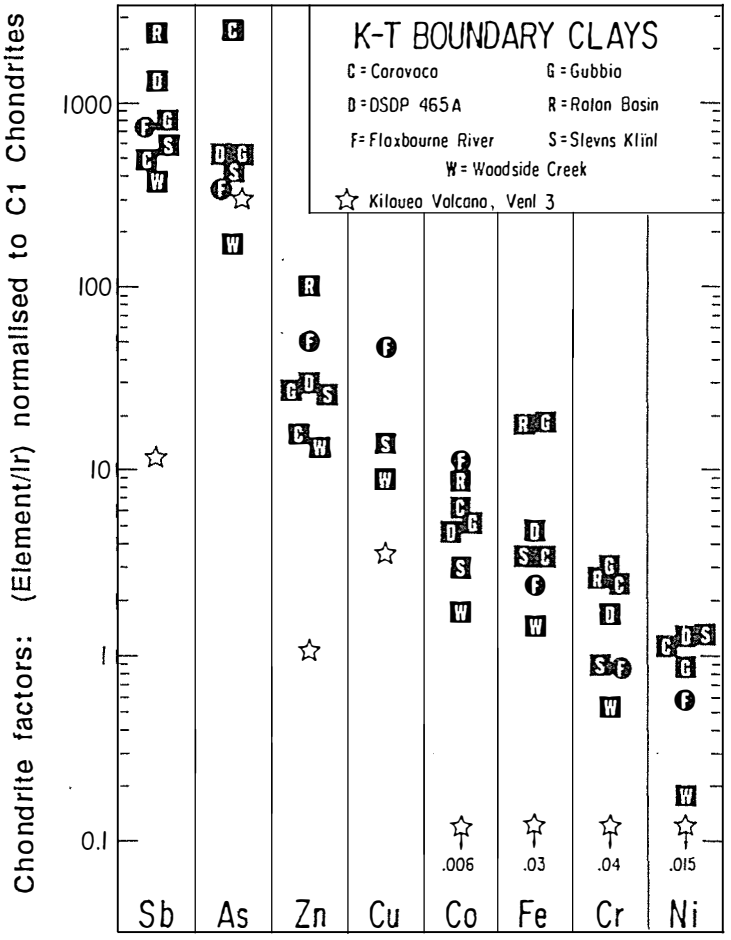

Figure 5.7 Chondrite Factors for Eight Elements in Boundary Clays and Volcanic Emissions

Elemental ratios in K/T boundary clays and Kilauea Volcano emissions normalised to Ir and C1 chondrite. The normalised elemental ratios are termed 'chondrite factors'.

5.4 (d) Origin of Enrichments

The greatest enrichment at the boundary occurs for Ir. It is difficult to explain how the steady state Ir contribution (detrital material and micrometeorites) could be concentrated to provide this level of enrichment. Besides, comparisons of Os isotope ratios in boundary clays and Mn-nodules, indicate the steady state contribution is not the source of PGM enrichments at the boundary [31][93].

Assuming the Ir at the boundary is of chondritic (stony meteorite) origin, can the other elements with strong enrichments at the boundary have come from the same source? To answer this question it is helpful to refer to Figure 5.7. This figure was constructed with information given in Table 5.2.

Table 5.2 Elements Enriched at the K/T Boundary: Abundances (decalcified basis) and Ratios

Element or Ratio	Boundary clays (whole section)*							Potential Sources				
	FR	WC	GB	DS	CV†	SK	RB	CRUST[a]	MANTLE[b]	OCEAN[c]	C1 CH.[d]	KILAUEA[e]
As (µg/g)	22	40	19	34	374	83	—	1.8	0.1	$2x\ 10^{-3}$	1.93	—
Co (µg/g)	190	104	48	77	230	146	54	25	91	$2x10^{-6}$	502	—
Cr (µg/g)	75	168	148	146	474	225	86	100	1,970	$3x10^{-4}$	2,640	—
Cu (µg/g)	195	134	—	—	—	167	—	55	31	$1.2x10^{-4}$	124	—
Fe (%)	1.54	3.36	6.50	2.97	4.87	6.40	4.20	5.0	6.18	$4x10^{-9}$	19.0	—
Ir (ng/g)	16	58	9	i6	36	47	6	0.2	3.4	—	481	—
Ni (ng/g)	208	228	177	461	946	1,370	—	75	1,610	$4.8X10^{-4}$	11,000	—
Sb (ng/g)	4.1	7.3	2.5	7.3	6.0	9.4	5.0	0.2	0.03	$2X10^{-4}$	0.162	—
Zn (ng/g)	540	505	166	318	374	810	400	70	63	$3.9X10^{-4}$	312	—
Cu/Sb	48	18	—	—	—	18	—	280	520	0.6	764	233
Zn/As	24	13	9.0	9.4	1.0	9.8	—	38	630	0.2	162	0.56
Zn/Sb	131	69	66	44	62	86	80	350	1,030	2	1,920	177
As/Sb	5.4	5.5	7.4	4.6	62	8.8	—	9	3	10	11.9	314
Ni/Ir	13,000	3,930	19,700	28,800	26,300	29,100	—	375,000	474,000	—	22,800	343
Cr/Ir	4,600	2,800	16,400	9,000	13,150	4,770	—	500,000	578,000	—	5,494	230
Ni/Cr	2.8	1.4	1.2	3.2	2.0	6.1	—	0.75	0.82	1.6	4.15	1.5
Ni/As	9.5	5.7	9.3	13.6	2.5	16.5	—	42	16,000	0.24	5,680	0.3
Fe/Ni	74	147	367	64	51	47	—	666	38	0.08	17.4	30

*FR- Flaxbourne River (this thesis)
GB - Gubbio (references [94] [4])
CV - Caravaca (reference [95])
DS - DSDP 465A (reference [159])
RB - Raton Basin (reference [30])
SK - Stevns Klint (reference [95])
WC - Woodside Creek (reference [28]))

†Mean of three layers in boundary clay.

a. Reference [36].
b. References [96] [97] [98] [99]
c. Reference [100].
d. C1 Chondrites. Reference [101].
e. Reference [102].

The vertical axis of Figure 5.7 gives normalised concentration values (chondrite factors). The chondrite factor for an element in a material, is calculated by normalising the element concentration to Ir, and then normalising the resulting ratio to C1 chondrites. Ir is used as the normalising element because it is the most clearly meteoritic element.

Chondrite factors for eight elements, in various boundary clays, are plotted in the figure. Most factors for Ni and Cr in the clays are close to unity. Therefore, the Ni/Ir and Cr/Ir ratios for boundary clays are close to chondrite ratios. This is consistent with the hypothesis that Ni and Cr anomalies in boundary clays (including Flaxbourne River clay) are of meteoritic origin. The levels of Fe and Co in the clays would appear to be too high to be attributed solely to a meteoritic source; the excess contribution probably comes from the crustal rock portion of the impact ejecta.

The chondrite factors for the four chalcophiles mean these elements must have been derived almost entirely from terrestrial reservoirs. Possible reservoirs are included in Table 5.3, which gives a mass balance for the chalcophiles at the Flaxbourne River K/T boundary site. As Kyte *et al* pointed out, anoxic ocean conditions following an impact, would aid the scavenging of chalcophiles from the water column [103]. Ejecta dust particles would have provided ideal surfaces for the chalcophiles to precipitate onto.

Table 5.3 Mass Balance for the Chalcophiles in the Flaxbourne River Boundary Clay

Element		As	Sb	Cu	Zn
Boundary clay	($\mu g/cm^2$)	51	9	396	1240
Ocean mass required	(kg/cm^2)	25	47	3300	3200
Crustal mass required	(g/cm^2)	20	36	5.8	14
Mantle mass required	(g/cm^2)	510	300	13	20

NB - global abundance of boundary clay is 2-5 g/cm^2. Values in this table were calculated by multiplying elemental abundances (not on decalcified basis) by the density of the clay (2.3 g/cm^3).

The elements As and Sb, could easily have been derived from the ocean. To supply all the As at the Flaxbourne River K/T boundary , 25 kg of seawater would be needed for every cm^2 of the seafloor. This corresponds to a water column of 250 m. For Sb the value is 47 kg/cm^2 corresponding to a water

column of 470 m. Both these depths seem reasonable in terms of the observed faunal assemblages.

The ocean depths required to supply Cu and Zn seem impossibly great. All the Cu and Zn at the boundary could be supplied by 6-15 g of crustal rock per cm^2 of the ocean floor. This is greater than the global abundance of the boundary clay (2-5 g/cm^2), for an assumed thickness of 1-2 cm and a density of 2.5 g/cm^3. So, if crustal rock is to supply the required Cu and Zn, it must be rock with greater than average concentrations of these elements.

Some of the Sb and As at the boundary may be derived from crustal rock. Theoretically the oceanic contribution for the elements can be determined by examining their levels in Raton Basin boundary material (continental sediments); any As or Sb at this site must be derived from sources other than the ocean. No As values have been determined for this site, and the Sb levels at the boundary are only slightly higher than the unusually high background (reflecting local rather than global conditions).

5.4 (e) The Volcanic Source Proposal

Opponents of the impact theory have suggested a volcanic source for the elemental anomalies found at the K/T boundary. In particular, they point to the volcanic activity which formed the Deccan Traps in India [86][87].

Chemical analyses of basaltic rocks indicate that the Ni/Ir and Cr/Ir ratios in mantle material are much higher than in boundary clays (see Table 5.2). This appears to preclude a mantle source for the K/T boundary anomalies. However Zoller *et al* reported that Ir can be greatly enriched in volcanic aerosol emissions, compared to basaltic rocks [104]. This report was based on studies of emissions from Kilauea Volcano in Hawaii. The authors suggest that Ir in the emissions is in the form of the volatile IrF_6 compound. This type of Ir enrichment has not been observed for other volcanos and is probably due to an unusually high F/Cl ratio which is indicative of a very deep magma source [104].

Officer and Drake suggested that if the Deccan Traps volcanism was of the deep magma variety, it would have supplied enough Ir to explain the K/T boundary anomaly [34]. Let us examine this claim. According to Olmez *et al* about 0.3 % of the Ir in the magma would have been degassed [102]. Using this value, they calculate the aerosol Ir emission from the Deccan Traps magma would have been about $3x10^{10}$ g. In their calculations, they assume this magma to have the same Ir concentration as Kilauea magma (0.32 ng/g). This assumption was unnecessary as Morgan had determined the average Ir value in five samples of Deccan Basalt to be 0.006 ± 0.001 ng/g [105]. Using this value, the gaseous Ir emission reduces to about $6x10^{8}$ g. This is only about 0.1% of the Ir which was deposited at the boundary [103][106].

Anomalously high levels of Pd were found at the Flaxbourne River K/T boundary. Unfortunately no work has been done to determine if Pd is enriched in volcanic aerosol emissions relative to magma. Indeed, none of the PGM have been determined in these emissions except Ir. It would be useful to be able to compare the relative abundances of the PGM in volcanic emissions and boundary clays.

Figure 5.7 shows that the chondrite factors for elements in Kilauea emissions are dissimilar to those for boundary clays, arsenic excepted. As only 0.1% of the required Ir can be supplied by volcanism, the situation is the same for arsenic.

In summary, the geochemical data for the Flaxbourne River K/T boundary sequence (and other sites) indicate that volcanism of the Kilauea type was not responsible for the elemental anomalies found in boundary clays.

5.5 CONCLUSION

The unusual trace element composition of the clay layer at the Flaxbourne River K/T boundary is best explained by the impact theory. This view is reinforced by the lithological and palaeontological evidence for the sequence.

Acknowledgement

I would like to thank Professor Edward Anders of the University of Chicago for assisting with the interpretation of the elemental data.

FINAL DISCUSSION

An Ir enrichment is found at the K/T boundary at sites around the world, implying a linkage with the faunal and floral extinctions which define the boundary. If the extinctions and Ir deposition were due to a large asteroid impact, other PGM should be enriched in boundary sediments.

A method was developed to allow the determination of Pd in geological samples. The method used GF-AAS for the determinations. Geological samples were dissolved using a mixed acid attack. Then Pd was extracted from acid solution into MIBK to remove it from the presence of base metals which would interfere with its determination. The Pd was extracted as an APDC chelate complex.

The method was successfully used to determine Pd in a certified geological standard. Then the method was used to determine Pd in a suite of samples from the Flaxbourne River K/T boundary site in New Zealand. An enrichment of Pd was found in the vicinity of the boundary contiguous with the Ir enrichment (determined by RNAA). Boundary clays from several other sites were analysed and found to contain anomalously high levels of Pd.

A survey of elemental abundances for 20 elements across the Flaxbourne River sequence revealed that elements other than the PGM have distinctive enrichments at the K/T boundary. These elements are As, Co, Cr, Cu, Ni, Sb, and Zn. Of these, Co, Cr, and Ni are siderophile elements which are sufficiently abundant in meteorites to have been derived from that source; As, Cu, Sb, and Zn in the boundary clay must be of terrestrial origin. The Ni/Ir and Cr/Ir abundance ratios for the Flaxbourne River K/T boundary clay suggest a meteoritic rather than a volcanic source for the siderophile elements at the boundary. Deccan Traps volcanism could only have supplied about 0.1% of the global Ir fluence observed at the boundary. The elemental composition of K/T boundary materials is best explained by the impact theory rather than its volcanic competitor.

It is now over a decade since the impact theory was first proposed. Elemental analysis of K/T boundary sediments has produced substantial evidence in favour of the theory. Other areas of scientific research have also produced evidence favouring the impact theory rather its volcanic counterpart. Of particular importance was the discovery of shock quartz grains, containing multiple lamellae, in boundary sediments [107]. In late 1988 a major conference on the

K/T boundary controversy was held at Snowbird in Utah. A considerable portion of the discussion at the conference was devoted to the shock quartz evidence [108]. Only large meteorite impacts and nuclear explosions are known to produce multiple lamellae shock features. Volcanic eruptions do not produce sufficient pressures to produce such features [108].

Other exotic components to K/T boundary clays have been reported. High concentrations of soot have been found at the boundary and have been attributed to global wildfires caused by an impact [18]. In 1989, Zhao and Bada [109] reported the presence in a boundary clay of two amino acids which are exceedingly rare on earth but which are major amino acids in carbonaceous chondrites.

With the impressive list of evidence in favour of the impact theory it seems only a matter of time before it becomes firmly woven into the fabric of geological orthodoxy.

LIST OF REFERENCES

[1] Silver L.T. Introduction *Geol. Soc. Am. Special Paper* **190,** xiii (1982).

[2] Hartmann W.K., Strom R.G., Weidchilling S.J., Balsins K.R., Woronow A., Dence M.R., Grieve A.F., Diaz J., Chapman C.R., Shoemaker E.M. and Jones K.L. *Basaltic volcanism on terrestrial planets, chapter 8* : Pergamon Press (New York) p. 1049 (1982).

[3] Alvarez L.W. Experimental evidence that an asteroid impact led to the extinction of many species 65 million years ago. *Proc. Natl. Acad. Sci.* **80,** 627 (1983).

[4] Alvarez L.W., Alvarez W., Asaro F. and Michel H.V. Exraterrestrial cause for the Cretaceous-Tertiary extinction. *Science* **208,** 1095 (1980).

[5] Alvarez L.W., Alvarez W., Asaro F. and Michel H.V. Experimental evidence in support of an extraterrestrial trigger for the K-T extinctions. *Eos Trans.* AGU **60,** 734 (1979).

[6] Goldschmidt V.M., *Geochemistry: Oxford Clarendon Press* p. 731 (1954).

[7] Brooks R.R. Analytical chemistry and the dinosaurs. *Can. J. Chem.* **65,** 1033 (1987).

[8] Strong C.P., Brooks R.R., Wilson S.M., Reeves R.D., Orth C.J., Mao X., Quintana L.R., and Anders E. A new Cretaceous/Tertiary boundary site at Flaxbourne River, New Zealand: Biostratigraphy and geochemistry. *Geochim. et Cosmochim. Acta* **51,** 2769 (1987).

[9] *Encyclopaedia Britannica, Micropaedia* 15th edition, p. 320.

[10] Gault D.E. and Sonett C.P. Laboratory simulation of pelagic asteroidal impact: Atmospheric injection, benthic topography, and the surface wave radiation field. *Geol. Soc. Am. Special Paper* **190,** 69 (1982).

[11] O'Keefe J.D. and Ahrens T.J. Impact flows and crater scaling on the moon. *Phys. Earth Planet. Int.* **16,** 341 (1978).

[12] Lewis J.S., Watkins G.H., Hartman H. and Prinn R.G. Consequences of major impact events on earth. *Geol. Soc. Am. Special Paper* **190,** 215 (1982).

[13] Emiliani C., Kraus E.B. and Shoemaker E.M. Sudden death at the end of the Mesozoic. *Earth Planet. Sci. Lett.* **55,** 317 (1981).

[14] Rampino M.R. and Stothers R.B. Flood basalt volcanism during the last 250 million years. *Science* **241,** 663 (1988).

[15] Wolbach W.S., Gilmour I. and Anders E. Major wildfires at the Cretaceous/Tertiary boundary. In: *Global Catastrophies in Earth History. Geol. Soc. Am. Special Paper.* (1989)

[16] Bourgeois J., Hansen T.A., Wiberg P.L., Kauffmann E.G. A tsunami deposit at the Cretaceous-Tertiary boundary in Texas. *Science* **241,** 567 (1988).

[17] Toon O.B., Pollack J.B., Ackerman T.P., Turco R.P., McKay C.P., Liu M.S. Evolution of an impact-generated dust cloud and its effects on the atmosphere. *Geol. Soc. Am. Special Paper* **190,** 187 (1982).

[18] Wolbach W.S., Lewis R.S., Anders E. Cretaceous extinctions: Evidence for wildfires and search for meteoritic material. *Science* **230,** 167-170 (1985).

[19] Wolbach W.S., Gilmour I., Anders E., Orth C.J. and Brooks R.R. A global fire at the Cretaceous-Tertiary boundary. *Nature* **334,** 665-669 (1988).

[20] Venkatesen M.I. and Dhal J. Organic geochemical evidence for global fires at the Cretaceous/Tertiary boundary. *Nature* **338,** 57 (1989).

[21] Wolbach W.S., Lewis R.S., Anders E., Grady M.M., Pillinger C.T., Brooks R.R., Orth C.J. and Gilmore J.S. Carbon isotopes and iridium at two Cretaceous-Tertiary (K-T) boundary sites in New Zealand. *Meteoritics* **21,** 541 (1986).

[22] Crutzen P.J. Acid rain at the K/T boundary. *Nature* **330,** 108 (1987).

[23] Prinn R.G. and Fegley B. Bolide impacts acid rain and biospheric traumas at the Cretaceous-Tertiary boundary. *Earth Planet. Sci Lett.* **83,** 1 (1987).

[24] Gilmour I. and Guenther F. The global Cretaceous-Tertiary fire: Biomass or fossil carbon? *Global catastrophies in Earth history.* Snowbird, UT: Lunar Planet. Inst., pp. 60-61 (1988).

[25] Officer C.B. and Drake C.L. The Cretaceous-Tertiary transition. *Science* **219,** 1383 (1983).

[26] Alvarez L.W., Alvarez W., Asaro F. and Michel H.V. The end of the Cretaceous: sharp boundary or gradual transition? *Science* **223,** 1183 (1984).

[27] Rampino M.R. A non-catostrophist explanation for the Ir anomaly at the Cretaceous/Tertiary boundary. *Geol. Soc. Am. Special Paper* **190,** 445 (1982).

[28] Brooks R.R., Reeves R.D., Yang X.H., Ryan D.E., Holtzbecher J., Collen J.D., Neall V.E. and Lee J. Elemental anomalies at the Cretaceous-Tertiary boundary, Woodside Creek, New Zealand. *Science* **226,** 539 (1984).

[29] Kent D.V. Asteroid extinction hypothesis. *Science* **211,** 648 (1981).

[30] Orth C.J., Gilmore J.S., Knight J.D., Pillmore C.L., Tschudy R.H., and Fassett J.E. An iridium abundance anomaly at the palynological Cretaceous-Tertiary boundary in northern New Mexico. *Science* **214,** 1341 (1981).

[31] Lichte F.E., Wilson S.M., Brooks R.R., Reeves R.D., Holzbecher J., Ryan D.E. New method for the determination of osmium and its isotopes applied to a New Zealand Cretaceous/Tertiary boundary shale. *Nature* **322,** 816 (1986).

[32] Luck J.M. and Turekian K.K. Osmium-187/osmium-186 in manganese nodules and the Cretaceous-Tertiary boundary. *Science* **222,** 613 (1983).

[33] Smit J. and Romein A.J.T. A sequence of events across the Cretaceous-Tertiary boundary. *Earth Planet. Sci. Lett.* **74,** 155 (1985).

[34] Officer C.B. and Drake C.L. Terminal cretaceous environmental events. *Science* **227,** 1161-1166 (1985).

[35] Kerr R.A. Searching land and sea for the dinosaur killer. *Science* **237,** 856 (1987).

[36] Mason B.H. and Moore C.B. *Principles of geochemistry, 4th edition*: Wiley (1982).

[37] Brooks R.R., Presley B.J. and Kaplan I.R. APDC-MIBK extraction system for the determination of trace elements in saline waters by atomic absorption spectrophotometry. *Talanta* **14,** 809 (1967).

[38] Walsh A. Application of atomic absorption to chemical analysis. *Spectrochim. Acta* **7,** 108 (1955).

[39] Price W.J. *Spectrochemical analysis by atomic absorption:* Heyden p. 29 (1979).

[40] L'vov B.V. Analytical use of atomic absorption spectra. *Spectrochim. Acta* **17,** 761 (1961).

[41] Massman H. Comparison of atomic absorption and atomic fluorescence in graphite curvettes. *Spectrochim. Acta* **23B**, 215 (1968).

[42] *Chemical Abstracts* Catalytic properties of diluted layers of Pd-Rh absorption catalysts. vol. **77,** 79917a (1972).

[43] *Snell-Ettre encyclopaedia of industrial chemical analysis:* Interscience. **vol 8**, p. 140 (1974).

[44] Fassel V.A. Conception, birth, and development of three new successful analytical concepts. *J Assoc. Off. Anal Chem.* **67,** 212 (1984).

[45] Date A.R. An introduction to inductively coupled plasma source mass spectrometry. *Trends Anal. Chem.* **2,** 225 (1983).

[46] Morrison G.H. and Freiser H. *Solvent extraction in analytical chemistry:* Wiley. p. 6 (1966).

[47] Fischer W. Separation of inorganic mixtures by partition: Determination of arsenic and germanium after separation by solvent extraction. *Angew. Chem.* **66,** 165 (1954).

[48] Green M. and Kafalas J.A. Preparation and isolation of carrier free As^{74} from germanium cyclotron targets. *J. Chem. Phys.* **22,** 760 (1954).

[49] Margerum D.W. and Banks C.V. Spectrophotometric determination of iron in vanadium, chromium, manganese, nickel, and zinc. *Anal. Chem.* **26,** 200 (1954).

[50] Braun R.D. *Introduction to chemical analysis:* McGraw-Hill Book Company. p. 361 (1985).

[51] Vogel A.I. *Vogel's textbook of quantitative inorganic analysis, fourth edition:* Longman. p. 161 (1983).

[52] Kallmann S. Analytical chemistry of the precious metals. *Anal. Chem.* **vol. 56** no. 9 (1984).

[53] Van Loon J.C. Analytical chemistry of the noble metals. *Pure and Appl. Chem.* **49,** 1495 (1977).

[54] Bugbee E.E. *A textbook on fire-assaying:* Wiley (New York). 3rd edition (1940).

[55] Beamish F.E. and Van Loon J.C. *Analysis of noble metals. Overview and selected methods.* Academic Press, New York (1977).

[56] Robert R.V.D., van Wyk E. and Palmer R. Concentration of the noble metals by a fire-assay technique using nickel sulphide as the collector. *Nat. Inst. Metall., Repub. S. Afr. Rep.* No. 1371 (1971).

[57] Date A.R. and Gray A.L. Progress in plasma source mass spectrometry. *Spectrochim. Acta* **38B,** 29 (1983).

[58] Longerich H. ICP-MS interferences. Personal communication (1987).

[59] Kraus K.A. and Nelson F. Separation of elements by anion exchange. *Proc. Internl. Conf. Peaceful Use. Atom. Energy* vol **7,** 113 (1956).

[60] Marhenke E.R.R. and Sandell E.B. Spectrophotometric determination of traces of palladium after coprecipitation with tellurium. *Anal. Chim. Acta* **28,** 259 (1963).

[61] Korkisch J. *Modern methods for the separation of rarer metal ions:* Pergamon Press p. 546 (1969).

[62] Wilson S.M. Osmium as an indicator of extraterrestrial material Cretaceous/Tertiary boundary sediments. *B.Sc.(Hons) Thesis, Massey University* (1985).

[63] Sauerbrumn R.D. and Sandel E.B. Ionization constants of osmic (VIII) acid. *J. Am. Chem. Soc.* **75,** 4170 (1953).

[64] Meadows J.W.T. and Matlack G.M. Radiochemical determination of ruthenium by solvent extraction and preparation of carrier free ruthenium activity. *Anal. Chem.* **34,** 89 (1962).

[65] Sandell E.B. *Colorimetric determination of traces of metals:* Interscience (New York) (1959).

[66] Killick R.A. and Morris D.F.C. The determination of traces of ruthenium in samples of platinum by neutron activation analysis. *Talanta* **9,** 139 (1962).

[67] Belew W.L., Wilson G.R. and Corbin L.T. Spectrophotometric determination of ruthenium by thiocyanate. *Anal. Chem.* **33,** 886 (1961).

[68] Pearson R.G. Hard and soft acids and bases. *J. Am. Chem. Soc.* **85,** 3533 (1963).

[69] Faye G.H. and Inman W.R. A scheme for the separation of platinum, palladium, rhodium and iridium by solvent extraction. *Anal. Chem.* **35,** 985 (1963).

[70] Schlesinger H.I. and Palmateer R.E. Studies on complex ions-III. The relative stabilities of halogenoplatinates. *J. Am. Chem. Soc.* **52,** 4316 (1930).

[71] Ryan D.E. The separation of small amounts of the platinum metals. 1. The colorimetric determination of rhodium and its separation from iridium. *Can. J. Chem.* **39,** 2389 (1961).

[72] Diamantatos A. A new solvent extraction scheme for the separation of platinum, palladium, rhodium, and iridium. *Anal. Chim. Acta* **67,** 317 (1973).

[73] Diamantatos A. A solvent-extraction scheme for the determination of platinum, palladium, rhodium, iridium and gold in platiniferous materials. *Anal. Chim. Acta* **131,** 53 (1981).

[74] Naidu S.D. The determination of gold in vegetation and its application in specific problems in biogeochemistry. *M.Sc. Thesis, Massey University* (1985).

[75] Nichiporuk W. Brown H. The distribution of platinum and palladium metals in iron meteorites and in the metal phase of ordinary chondrites. *J. Geophys. Res.* **70,** 459 (1965).

[76] Ryan D.E., Holzbecher J., Brooks R.R. Rhodium and osmium in iron meteorites. *Chemical Geology* **85,** 295 (1990).

[77] Jones E. A., Warshawsky A., Dixon K., Nicolas D.J. and Steel T.W. The Group extraction of the noble metals with s-(1-decyl)-N,N'-diphenylisothiouronium bromide and their determination in the organic extract by atomic-absorption spectrometry. *Anal. Chim. Acta* **91,** 257 (1977).

[78] Malissa H. and Schoffmann E. Uber die verwendung von substituierten dithiocarbamaten in der mikroanalyse. III. *Mikrochim. Acta* **1,** 187-202 (1955).

[79] Sprague S. and Slavin W. Detection limits in analytical atomic absorption spectrophotometry. *At. Absorpt. Newsl.* **3,** 11 (1964).

[80] Okuno I., Whitehead J.A. and White R.E. Flameless atomic absorption determination of heavy metals in whole fish samples. *J. Assoc. Off. Anal Chem.* **61,** 664 (1978).

[81] Nichols J.A. and Woodriff R. Coprecipitation of heavy metals directly in graphite curvettes for furnace atomic absorption spectrometry. *J. Assoc. Off. Anal Chem.* **63,** 500 (1980).

[82] McAdam R.C., Sutarno, Moloughney P.E. Noble-metals-bearing sulphide concentrate PTC: its characterisation and preparation for use as a standard reference material. *Department of Energy, Mines, and Resources, Ottawa. Technical Bulletin* TB 176.

[83] Brooks R.R., Hoashi M., Wilson S.M. and Zhang R.Q. Extraction into methyl isobutyl ketone of metal complexes with ammonium pyrrolidine dithiocarbamate formed in strongly acid media. *Anal. Chim. Acta* **217,** 165 (1989).

[84] Lee B.S. The determination of Pt and Pd in soils and vegetation by electrothermal atomic absorption spectrometry. *B.Sc. (Hons) Thesis, Massey University* (1987).

[85] Kellner R. Beitrag zum problem der bandenverschiebungen in den I.R.-spektren von diathyl-und tetramethylendithio-carbamidaten. *Anal. Chim. Acta* **63,** 277 (1973).

[86] McLean D.M. Flood basalt volcanism and global extinction at the Cretaceous-Tertiary transition. Paper presented at the 148th national meeting of the American Association for the Advancement of Science (1982).

[87] Turekian K.K. Potential of $^{187}Os/^{186}Os$ as a cosmic versus terrestrial indicator in high iridium layers of sedimentary strata. *Geol. Soc. Am. Special Paper* **190,** 243 (1982).

[88] Lensen G.J. Sheet 16 Kaikoura. *Geol. Map.* N. Z. 1: 250000. D.S.I.R., Wellington.

[89] Brooks R.R., Strong C.P., Lee J., Orth C.J., Gilmore J.S., Ryan D.E. and Holzbecher J. Stratigraphic occurance of iridium anomalies at four Cretaceous-Tertiary boundary sites in New Zealand. *Geology* **14,** 727-729 (1986).

[90] Strong C.P. Cretaceous-Tertiary boundary at Chancet Rocks Scientific Reserve, Northeast Marlborough. *N. Z. Geol. Surv. Rec.* **3,** 47 (1984).

[91] Strong C.P. Cretaceous-Tertiary boundary at Needles Point, Northeast Marlborough. *N. Z. Geol. Surv. Rec.* **8,** 82 (1985).

[92] Orth C.J., Gilmore J.S., Quintana L.R. and Sheehan P.M. Terminal Ordovician extinction: Geochemical analysis of the Ordovician/Silurian boundary, Anticosti Island, Quebec. *Geology* **14,** 433 (1986).

[93] Luck J.M., Turekian K.K. Osmium-187/osmium-186 in manganese nodules and the Cretaceous-Tertiary boundary. *Science* **222,** 613 (1983).

[94] Smit J. and Ten Kate W.G.H.Z. Trace element patterns at the Cretaceous-Tertiary boundary—Consequences of a large impact. *Cret. Res.* **3,** 307 (1982).

[95] Kyte F.T., Smit J. and Wasson J.T. Siderophile interelement variations in Cretaceous-Tertiary boundary sediments from Caravaca, Spain. *Earth Planet. Sci. Lett.* **73,** 183 (1985).

[96] Anderson D.L. Chemical composition of the mantle. *J. Geophys. Res.* **88,** B41 (1983).

[97] Jagoutz E., Palme H., Baddenhausen H., Blum K., Cendales M., Dreibus G., Spettle B., Lorenz V. and Wanke H. The abundance of major, minor, and trace elements in the earth's mantle as derived from primative ultramafic rocks. *Proc. Lunar Planet. Sci. Conf. 10th,* 2031 (1979).

[98] Morgan J.W., Wandless G.A., Petrie R.K. and Irving A.J. Composition of the earth's upper mantle II: volatile trace elements in upper mantle xenoliths. *Proc. Lunar Planet. Sci. Conf. 11th,* 213 (1980).

[99] Morgan J.W., Ultramafic xenoliths: clues to Earth's late accretionary history. *J. Geophys. Res.* **91,** 12,373 (1986).

[100] Quinby-Hunt M.S. and Turekian K.K. Distribution of elements in seawater. *Eos* **64,** 130 (1983).

[101] Anders E. and Ebihara M. Solar-system abundances of the elements. *Geochim. Cosmochim. Acta* **46,** 2363 (1982).

[102] Olmez I., Finnegan D.L., Zoller W.H. Iridium emissions from Kilauea volcano. *J. Geophys. Res.* **91,** 653 (1986).

[103] Kyte F.T., Zhou Z. and Wasson J.T. Siderophile-enriched sediments from the Cretaceous-Tertiary boundary. *Nature* **288,** 651 (1980).

[104] Zoller W.H., Parrington J.R. and Phelan Kotra J.M. Iridium enrichment in airbourne particulates from Kilauea volcano: January 1983. *Science* **222,** 1118 (1983).

[105] Morgan J.W. Lunar crater glasses and high magnesium australites: Trace element volatilisation and meteoritic contamination. *Proc. Lunar Planet. Sci. Conf. 9th,* 2713 (1978).

[106] Alvarez W. Toward a theory of impact crisis. *Eos* **67,** 649 (1986).

[107] Bohor B.F.,Foord E.E., Modreski P.J., and Triplehorn D.M. Mineralogic evidence for an impact event at the Cretaceous-Tertiary boundary. *Science* **224,** 867 (1984).

[108] Kerr R.A. Huge impact is favored K/T boundary killer. *Science* **242,** 865 (1988).

[109] Zhao M. and Bada J.L. Extraterrestrial amino acids in Cretaceous/Tertiary boundary sediments at Stevns Klint, Denmark. *Nature* **339,** 463 (1989).

[110] Morrison G.H. and Freiser H. *Solvent extraction in analytical chemistry:* Wiley. p. 8 (1966).

[111] Long G.L. and Winefordner J.D. Limit of detection: A closer look at the IUPAC definition. *Anal. Chem.* **55,** 712A (1983).

[112] "Nomenclature, symbols, units, and their usage in spectrochemical analysis—II," *Spectrochim. Acta B* **33B,** 242 (1978).

[113] "Nomenclature, symbols, units, and their usage in spectrochemical analysis—III," *Spectrochim. Acta B* **33B,** 248 (1978).

APPENDICES

APPENDIX I

THERMODYNAMIC DERIVATION OF THE DISTRIBUTION LAW

The following derivation was taken from reference [110]. The derivation relates to the equilibrium distribution of a solute between two liquid phases. Equilibrium is attained at constant temperature and pressure when the chemical potentials (Φ) of the solute in each phase are equal. Thus

$$\Phi_1 = \Phi_2 \quad \text{(E1)}$$

where the subscripts 1 and 2 refer to the respective solvent phases. Substituting the suitable expressions for Φ, we next have

$$\Phi_1^o + RT \ln m_1 + RT \ln \gamma_1 = \Phi_2^o + RT \ln m_2 + RT \ln \gamma_2 \quad \text{(E2)}$$

where Φ^o represents the chemical potential of solute in a hypothetical ideal 1 molal solution, m, the solute concentration in molality , and γ, the molal activity coefficient. From this we may obtain an expression for the molal distribution coefficient, K_D

$$K_D \equiv \frac{m_1}{m_2} = \frac{\gamma_1}{\gamma_2} e^{-(\Phi_2^o - \Phi_1^o)/RT} \quad \text{(E3)}$$

In this equation the Φ^o's represent constants provided the presence of the solute does not significantly effect the mutual solubilities of the two solvents. If this condition is met, equation E3 may be written as

$$K_D \equiv \frac{m_1}{m_2} = \frac{\gamma_1}{\gamma_2} \times K' \quad \text{(E4)}$$

where K' is a constant for the system at constant temperature. Variation in the distribution coefficient (K_D) can be seen to result from variations in the activity coefficients for each of the phases. When solute concentration is very low, the activity coefficients approach unity and the value of K_D can be regarded as constant.

APPENDIX II

LIMITS OF DETECTION

In terms of concentration, the limit of detection for an analytical technique is the lowest concentration value that can be determined to be statistically different from the analytical blank. There are several approaches to determining whether such a value is statistically different from the blank. Winefordner and Long have reviewed the various methods for determining limits of detection, including the following two treatments [111].

The IUPAC Method

IUPAC states that $x_L = \overline{x}_B + k.s_B$ (E1)

x_L, is the limit of detection in terms of an instrumental reading.
$\overline{x}_B$, is the mean of the blank instrumental readings.
s_B, is the standard deviation of the blank instrumental readings.
k, is the factor chosen in accordance with the desired confidence level.

If k=2, then the probability that a sample reading greater than x_L, is just a random fluctuation of the blank, is 2.3%. If k=3, then this probability falls to 0.14%. IUPAC recommend k=3 be used as the level of confidence [112][113].

For many analytical techniques a concentration value (c) can be derived from an instrumental reading (x) by using a calibration curve. A linear relationship between x and c is described by the relationship:

$$x = m.c + i \quad (E2)$$

This is the equation for the line (calibration curve) with a slope of m and an intercept of i, shown below:

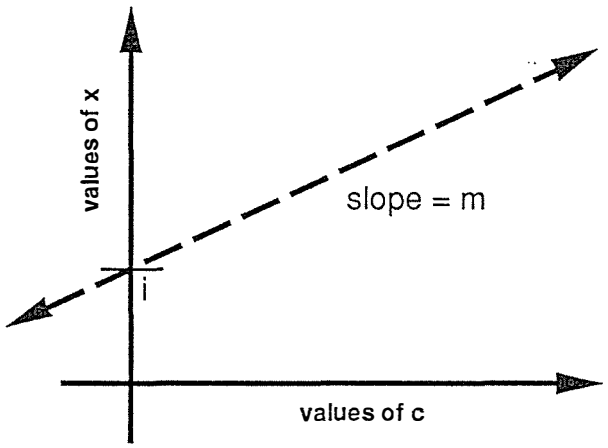

Rearranging E2 gives: $c = \frac{x - i}{m}$ (E3)

Where c is the limit of detection in terms of concentration (c_L), this equation becomes :

$$c_L = \frac{x_L - \bar{x}_B}{m} \quad (E4)$$

Substituting E1 into E4 gives:

$$c_L = \frac{k.s_B}{m} \quad (E5)$$

So the limit of detection can be calculated once the standard deviation of the blank readings, and the slope of the calibration curve have been determined.

The Propagation of Errors Method

The equation E3, relates concentration values (c) to instrumental readings (x).

$$c = \frac{x - i}{m} \quad (E3)$$

With the propagation of errors approach, the uncertainty in a concentration value is derived not only from uncertainty in the value of the instrumental reading, but also from uncertainty in the slope (m) and the intercept (i) of the calibration curve. The contribution of each term to the total error may be found by taking the first derivative of c with respect to each term.

$$s_c^2 = \left(\frac{dc}{dx}\right)^2 .s_x + \left(\frac{dc}{di}\right)^2 .s_i^2 + \left(\frac{dc}{dm}\right)^2 .s_m^2 \quad (E6)$$

Taking the designated derivatives and the square root gives:

$$s_c = \left[\left(\frac{1}{m}\right)^2 .s_x^2 + \left(\frac{-1}{m}\right)^2 .s_i^2 + \left(\frac{i - x}{m^2}\right)^2 .s_m^2 \right]^{1/2} \quad \text{(E7)}$$

Finally, combining the like terms yields:

$$s_c = \frac{\left[s_x^2 + s_i^2 + \left(\frac{i - x}{m}\right)^2 .s_m^2 \right]^{1/2}}{m} \quad \text{(E8)}$$

The value s_c gives a measure of the uncertainty in a designated concentration value. One example of this, is the uncertainty ($s_{c(blank)}$) which pertains to a mean analytical blank value ($\overline{c}_B$), when it is expressed in terms of concentration.

$$s_{c(blank)} = \frac{\left[s_B^2 + s_i^2 + \left(\frac{i - \overline{x}_B}{m}\right)^2 .s_m^2 \right]^{1/2}}{m} \quad \text{(E9)}$$

Usually blank subtraction is performed. If so, $\overline{x}_B = 0$ and E9 simplifies to:

$$s_{c(blank)} = \frac{\left[s_B^2 + s_i^2 + \left(\frac{i}{m}\right)^2 .s_m^2 \right]^{1/2}}{m} \quad \text{(E10)}$$

Equation E1 states that: $x_L = \overline{x}_B + k.s_B$ (E1)

Usually blank subtraction is performed. If so, this equation simplifies to:

$$x_L = k.s_B \quad \text{(E11)}$$

The concentration value equivalent to E11 is:

$$c_L = k.s_{c(blank)} \quad \text{(E12)}$$

$$= k.\frac{\left[s_B^2 + s_i^2 + \left(\frac{i}{m}\right)^2 .s_m^2 \right]^{1/2}}{m}$$

Equation E12 is analogous to equation E5 (which is used for the IUPAC method). To determine the parameters required to calculate $s_{c(blank)}$, instrumental readings must be taken for a range of analyte concentrations (including analytical blank readings). Twenty readings for each concentration

chosen, should ensure $s_{c(blank)}$ relates to a normal distribution. Table AII gives the statistical expressions required to calculate m, i, s_B, s_i, and s_m.

Table AII Statistical Expressions Required to Determine s_c

$$m = \frac{\left(n\sum_{j=1}^{n} c_j x_j\right) - \left\{\left(\sum_{j=1}^{n} c_j\right)\left(\sum_{j=1}^{n} x_j\right)\right\}}{\left(n\sum_{j=1}^{n} c_j^2\right) - \left(\sum_{j=1}^{n} c_j\right)^2}$$

$$i = \left(\frac{\sum_{j=1}^{n} x_j}{n}\right) - m\left(\frac{\sum_{j=1}^{n} c_j}{n}\right)$$

$$s_{cc} = \left(\sum_{j=1}^{n} c_j^2\right) - \frac{\left(\sum_{j=1}^{n} c_j\right)^2}{n}$$

$$s_{xx} = \left(\sum_{j=1}^{n} x_j^2\right) - \frac{\left(\sum_{j=1}^{n} x_j\right)^2}{n}$$

$$s_{cx} = \left(\sum_{j=1}^{n} c_j x_j\right) - \frac{\left(\sum_{j=1}^{n} c_j\right)\left(\sum_{j=1}^{n} x_j\right)}{n}$$

$$s = \left(\frac{s_{xx} - m.s_{cx}}{n-2}\right)^{1\backslash 2} \qquad s_m = \frac{s}{(s_{cc})^{1\backslash 2}} \qquad s_i = \frac{\left(\sum_{j=1}^{n} c_j^2\right)^{1/2}}{(n s_{cc})^{1\backslash 2}}$$

APPENDIX III

ABBREVIATIONS

2MBT	2 mercaptobenzothiazole
AAS	atomic absorption spectroscopy
APDC	ammonium pyrrolidine dithiocarbamate
DDTU	S-(1-decyl)-N,N'-diphenylisothiouronium
F-AAS	flame atomic absorption spectroscopy
F-AES	flame atomic emission spectroscopy
GF-AAS	graphite furnace atomic absorption spectroscopy
HNP	1:1:1 mixture of concentrated HF, HNO_3, and $HClO_4$
ICP-AES	inductively coupled plasma atomic emission spectroscopy
ICP-MS	inductively coupled plasma source mass spectrometry
INAA	instrumental neutron activation analysis
IUPAC	International Union of Pure and Applied Chemistry
K/T	Cretaceous/Tertiary
MIBK	methyl isobutyl ketone
NAA	neutron activation analysis
PDC^-	pyrrolidine dithiocarbamato ligand
PGM	platinum group metal or platinum group metals
POEM	propagation of errors method of determining limits of detection
PTC-1	platinum ore flotation concentrate (certified reference material)
RNAA	radiochemical neutron activation analysis

PUBLICATIONS ARISING FROM THIS THESIS

Strong C.P., Brooks R.R., Wilson S.M., Reeves R.D., Orth C.J., Mao X., Quintana L.R., and Anders E. A new Cretaceous/Tertiary boundary site at Flaxbourne River, New Zealand: Biostratigraphy and geochemistry. *Geochim. et Cosmochim. Acta* **51,** 2769 (1987).

Brooks R.R., Hoashi M., Wilson S.M. and Zhang R.Q. Extraction into methyl isobutyl ketone of metal complexes with ammonium pyrrolidine dithiocarbamate formed in strongly acid media. *Anal. Chim. Acta* **217,** 165 (1989).

Wilson S.M., Hoashi M., Brooks R.R. and Reeves R.D. A method for the quantification of bismuth and palladium in geological materials including Cretaceous-Tertiary boundary clays. *Chemical Geology* **75,** 305 (1989).